Planktonic foraminifera as signal carriers in paleoceanography: from modern biology to proxy application in the western South Atlantic

Dissertation

zur Erlangung des

Doktorgrades in den Naturwissenschaften (**Dr. rer. nat.**)

im Fachbereich Geowissenschaften

der Universität Bremen

vorgelegt von

Igor Martins Venancio Padilha de Oliveira

– Gutachter –

Prof. Dr. Michael Schulz

Prof. Dr. Gert-Jan Reichart

Tag des Prüfungskolloquiums

11. Juli 2017

-Versicherung an Eides Statt-

Ich, _____
(Vorname, Name, Anschrift, ggf. Matr. -Nr.)

versichere an Eides Statt durch meine Unterschrift, dass ich die vorstehende Arbeit selbständig und ohne fremde Hilfe angefertigt und alle Stellen, die ich wörtlich dem Sinne nach aus Veröffentlichungen entnommen habe, als solche kenntlich gemacht habe, mich auch keiner anderen als der angegebenen Literatur oder sonstiger Hilfsmittel bedient habe, und die zu Prüfungszwecken beigelegte elektronische Version der Dissertation mit der abgegebenen gedruckten Version identisch ist.

Ich versichere an Eides Statt, dass ich die vorgenannten Angaben nach bestem Wissen und Gewissen gemacht habe und dass die Angaben der Wahrheit entsprechen und ich nichts verschwiegen habe.

Die Strafbarkeit einer falschen eidesstattlichen Versicherung ist mir bekannt, namentlich die Strafandrohung gemäß § 156 StGB bis zu drei Jahren Freiheitsstrafe oder Geldstrafe bei vorsätzlicher Begehung der Tat bzw. gemäß § 161 Abs. 1 StGB bis zu einem Jahr Freiheitsstrafe oder Geldstrafe bei fahrlässiger Begehung.

_____ _____

Ort, Datum Unterschrift

Acknowledgements

This PhD project was funded by CNPq (National Counsel of Technological and Scientific Development-Brazil) and the study was funded through the DFG Research Center/Cluster of Excellence "The Ocean in the Earth System", the REKLIM (Regionale Klimaänderungen) project and the Brazilian projects "PALEOCEANO" and "ASPECTO" funded by CAPES (Coordination for the Improvement of Higher Education Personnel-Brazil).

First, I would like to Dr. Stefan Mulitza for his support and supervision during my PhD. I am also very grateful to Prof. Michal Kucera and Prof. Michael Schulz for their ideas and constructive comments. Also thanks Dr. Aline Govin who hosted me in France during my research stay and helped me with fruitful scientific discussions. I am especially grateful to Prof. Ana Luiza S. Albuquerque, without her encouragement and support this thesis would not have been written.

I would especially like to thank my family, my girlfriend and friends who helped me in this journey through constant support and motivation. This project would not be possible without them.

During my PhD, I also made friends in the MARUM that helped me daily. Among these, I would like especially to thank Dr. Ines Voigt for sharing thoughts about science and life with me.

I also would like to thank everyone from MARUM and GLOMAR who helped me in a certain part of my stay in Bremen.

Abstract

Proxies derived from planktonic foraminifera shell chemistry and assemblage composition allowed to assess past changes in surface hydrography. However, the usefulness of these planktonic foraminifera proxies relies on the understanding of their biology and species-specific environmental preferences. Despite the importance of these evaluations regarding foraminiferal biology, informations about the species reproductive cycle, calcification depth and seasonal fluxes still not well constrained. Therefore, this thesis focuses on the assessment of planktonic foraminiferal biology (e.g. reproduction and calcification depth) and on paleoceanographic application of proxies derived from these organisms in marine archives located at the western South Atlantic, which is a key region due to the presence of boundary currents that transport heat to high latitudes.

The first step was to investigate short-term dynamics in the foraminiferal fluxes using high-resolution (3-7 days) sediment trap samples from a mooring located at the southeastern Brazilian coast (**Chapter 2**). For the first deployment (3-days resolution), we found evidence of synchronized shell fluxes of four planktonic foraminifera species (*Globigerinoides ruber, Trilobatus sacculifer, Neogloboquadrina dutertrei* and *Orbulina universa*). Using periodic regression analysis on this series, we show that the maximum shell flux occurs approximately 4-6 days after the full moon. These findings support the idea of synchronized reproduction in planktonic foraminifera linked to lunar cycles. However, the periodic regression results for the other deployments and for the entire dataset suggest that the period of the reproductive cycle cannot be strictly synchronous with the phases of the moon during each month. We also point out that an exogenous factor, instead of an endogenous biologic clock, may be the trigger for this synchronized reproductive behavior and that the variable expression of such factor between months leads to uneven peak spacing. Thus, we conclude that planktonic foraminifera shell fluxes and consequently carbonate export to the seafloor is influenced by lunar periodicity.

Since the fossil record represents an integration of foraminiferal flux patterns, which can have large seasonal variations, it becomes necessary to assess the magnitude of the seasonality in the planktonic foraminiferal shell fluxes. In addition, planktonic foraminiferal species may record conditions at different depths, which can be assessed by estimating their calcification depths.

Thus, both types of information may improve interpretations of foraminifera-based proxies in the sedimentary record. Therefore, as a second step, we used sediment trap samples from the same mooring to estimate calcification depths and the influence of the seasonal component on calcification depths, as well as in the foraminiferal fluxes (**Chapter 3**). We analyzed shell fluxes and oxygen isotopic composition of six planktonic foraminifera species (*Globigerinoides ruber* pink, *Globigerinoides ruber* white, *Trilobatus sacculifer*, *Orbulina universa*, *Neogloboquadrina dutertrei*, *Globorotalia menardii*). Our results revealed the presence of significant seasonal component on the shell fluxes of *G. ruber* white and *N. dutertrei* and in the calcification depths of all species, except *O. universa* and *T. sacculifer*. Moreover, estimated calcification depths for *N. dutertrei* and *G. menardii* appear to track the depth of the thermocline in the region, whereas the calcification depth of the remaining species corresponds to mixed layer conditions. We also compared our trap samples with recent sediments and observed higher values in oxygen-isotopic composition in the sediments, which we explained by the presence of specimens with a secondary layer of calcite in the sediment samples. Based on our findings, we also proposed the use of the difference between the oxygen isotopic composition of *G. ruber* pink and *N. dutertrei* as a proxy for reconstructing stratification. These results provide new estimations of shell flux seasonality and calcification depths, which can be used prior to proxy application or for further interpretation of the fossil record.

The last chapter (**Chapter 4**), as the appendices, of this thesis has as focus the application of foraminifera-based proxies in sediment cores located in the western South Atlantic. The dynamics of the atmosphere and surface ocean circulation in the tropical areas can influence the global distribution of heat and moisture, thus contributing to set the global climate. To gain a better understanding of these relevant processes, we used high-resolution records of major elemental ratios (e.g. Fe/Ca) and interspecific oxygen isotopic composition of planktonic foraminifera from two cores located off northeastern Brazil. The aim was to investigate millennial-scale changes in precipitation, subsequently terrigenous input to the ocean, over northeastern Brazil and surface circulation in the western equatorial Atlantic since the Last Interglacial (129 ka). Our Fe/Ca records are unprecedented since they reveal the influence of Dansgaard-Oeschger cycles in the fluvial discharge and consequently in the precipitation in this region. Furthermore, the interspecific isotopic composition of planktonic foraminifera ($\Delta\delta^{18}O_{dut\text{-}rub}$) showed pronounced millennial and glacial-interglacial changes in stratification in the western equatorial Atlantic, which can be explained by two different modes (zonal and meridional) of thermocline variability. The shoaling of the thermocline during millennial-scale stadials was associated with the zonal mode, caused by a decrease in the strength of the southeast trade winds and a weakening of the South Equatorial Current (SEC) transport. However, the shoaling of the thermocline in our site during

glacial stages or cold substages of marine isotope stage 5 was linked to the meridional mode, caused by more zonal and intense trade winds with the presence of a strong and prolonged North Equatorial Countercurrent (NECC). These thermocline modes were associated to variations in the trade winds, which are in turn modulated by meridional sea surface temperature gradients. Our data also allow the differentiation between Heinrich and DO stadials in terms of the magnitude of the changes in upper stratification and runoff in the western equatorial Atlantic, with stronger responses occurring during Heinrich stadials than during DO stadials.

Zusammenfassung

Planktische Foraminiferen tragen wesentlich zum Fossilieninhalt in marinen Sedimenten bei. Zeitliche Veränderungen in der isotopen-geochemischen Zusammensetzung ihrer fossilen Gehäuse dienen als wichtiger Proxy bei der Rekonstruktion mariner Paläoumweltbedingungen. Dennoch ist bislang nur wenig bekannt über die Reproduktionszyklen planktischer Foraminiferen, sowie über die jeweiligen Kalzifizierungstiefen der verschiedener Foraminiferenarten und deren Einfluss auf die paläoklimatischen Interpretationen.

Daher befasst sich der erste Teil der Dissertation (**Kapital 2**) mit kurzfristigen Änderungen in den Reproduktionsraten von planktischen Foraminiferen und damit einhergehender Sinkraten (Foraminiferen-Fluss) in Abhängigkeit vom Mondzyklus. Aufschlüsse liefern dabei zeitgeschaltete Sediment-Fallen vor der Küste Südostenbrasiliens, die in einer Folge vorgegebener Sammelintervalle (3 bis 7 Tage) Partikel, darunter auch planktische Foraminiferen, in der Wassersäule auffangen. Bei unserem ersten Einsatz (3-Tage-Auflösung) fanden wir Hinweise auf synchronisierte Sinkraten von vier planktischen Foraminiferenarten (*Globigerinoides ruber, Trilobatus sacculifer, Neogloboquadrina dutertrei* und *Orbulina universa*). Mit Hilfe einer periodischen Regressionsanalyse zeigen wir, dass der Foraminiferen-Fluss innerhalb eines Monats nicht homogen und kontinuierlich verläuft, sondern etwa 4 bis 6 Tage nach dem Vollmond ein Maximum aufzeigt. Diese Ergebnisse stützen daher die Vermutung einer synchronisierten Reproduktion von planktischen Foraminiferen in Abhängigkeit vom Mondzyklus. Im Unterschied dazu deuten die Ergebnisse der anderen Einsätze (5 bis 7-Tage-Auflösung) auf einen Fortpflanzungszyklus hin, der nicht (strikt) synchron mit den Phasen des Mondes verläuft. Eine mögliche Erklärung dafür ist, dass ein exogener Faktor anstelle eines endogenen („biologische Uhr“) der Auslöser für das Fortpflanzungsverhalten darstellt, und dass der jeweils variable Einfluß eines solchen Faktors zu ungleichen Maximal-Reproduktionen zwischen den Monaten führt.

Saisonale Effekte können auch Einfluss auf die Flussraten planktischer Foraminiferen nehmen. Zudem wandern planktische Foraminiferen während ihrer Ontogenie in der Wassersäule auf und ab (Kalzifizierungstiefe). Im zweiten Teil der Dissertation (**Kapitel 3**) haben wir daher die Sediment-Fallenproben aus dem Untersuchungsgebiet verwendet, um die saisonalen Abhängigkeiten der Flussraten, als auch die Kalzifizierungstiefen der planktischer Foraminiferen zu bestimmen, und damit deren Einfluss auf die isotopen-geochemische Zusammensetzung der Foraminiferengehäuse abzuschätzen. Dafür wurden die Flussraten und die Sauerstoff-Isotopenzusammensetzung ($\delta^{18}O$) von sechs planktonischen Foraminiferenarten (*Globigerinoides*

ruber (rosa), *Globigerinoides ruber* (weiß)*, Trilobatus sacculifer, Orbulina universa, Neogloboquadrina dutertrei, Globorotalia menardii*) untersucht. Unsere Ergebnisse zeigen eine signifikante saisonale Komponente in den Flussraten von *G. ruber* (weiß) und *N. dutertrei*, sowie in den Kalzifizierungstiefen aller Arten, abgesehen von *O. universa* und *T. sacculifer*. Interessanterweise spiegeln die Kalzifizierungstiefen für *N. dutertrei* und *G. menardii* die Tiefe der Thermokline wider (~100m), während die Kalzifizierungstiefen der verbleibenden Arten den Bedingungen der oberen Mischschicht (< 50m) entsprechen. Daher kann der Unterschied in der Sauerstoff-Isotopenzusammensetzung von *N. dutertrei* und *G. ruber* (rosa) ($\Delta\delta^{18}O_{dut\text{-}rub}$) als Proxy zur Rekonstruktion der oberflächennahen Statifizierung im Ozean (Variationen in der Thermokline) verwendet werden. Auch zeigen die Sediment-Fallenproben im Vergleich mit Oberflächensedimentproben aus dem Untersuchungsgebiet deutlich niedrigere Werte in der Sauerstoff-Isotopenzusammensetzung der untersuchten planktischen Foraminiferen, was auf eine vermehrte Anwesenheit von planktischer Gehäuseschalen mit einer sekundären Kalzitschicht im Sediment hinweist.

Der letzte Teil (**Kapital 4**) der Dissertation befasst sich mit der isotopen-geochemischen Untersuchung planktischer Foraminiferen als Proxy zur Rekonstruktion mariner Paläoumweltbedingungen. Sowohl die Dynamik der Atmosphäre als auch der ozeanischen Oberflächenwasserzirkulation in den tropischen Gebieten beeinflussen die globale Wärme- und Feuchtigkeitsverteilung und tragen daher im starken Maße zur Entwicklung des globalen Klimas bei. Zum besseren Verständnis der hierbei relevanten Prozesse untersuchen wir die klimatischen Veränderungen im Bereich des westlichen Äquatorialatlantiks während der letzten 130 000 Jahre. Mit Hilfe hochauflösender sedimentologischer und isotopen-geochemischer Befunde aus marinen Sedimentkernen vom oberen Kontinentalhang Nordostbrasiliens untersuchen wir kurzfristige spätquartäre Klimaschwankungen im westlichen Äquatorialatlantik. Die Sedimentation entlang des oberen Kontinentalhangs von Nordostbrasilien wird durch den Eintrag von terrigenem Material vom angrenzenden Festland maßgeblich geprägt. Signifikante Änderungen im fluvialen Sedimenteintrag deuten auf erhöhte Niederschlagsraten auf dem Festland während der Kältephasen der Dansgaard-Oeschger-Zyklen hin. Schwankungen in der Sauerstoff-Isotopenzusammensetzung planktischer Foraminiferen verweisen auf ausgeprägte zeitliche Variationen in der oberflächennahen Statifizierung des westlichen Äquatorialatlantiks, die durch zwei verschiedene Modi der Thermoklinenvariationen (*zonaler* und *meridionaler Modus*) beschrieben werden können. Die Änderungen der Thermoklinentiefe werden dabei im Allgemeinen durch Variationen der Innertropischen Konvergenzzone und der damit verbundenen Passatwindzirkulation, und die damit verbundenen Variationen in der Oberflächenwasserzirkulation bedingt. Der *meridionale* Modus beschreibt das Abflachen der Thermokline während der letzten Kaltzeit und während der Kältepha-

sen innerhalb der letzten Warmzeit und steht mit einer Intensivierung der Windzirkulation und einer Zunahme des Nordäquatorialen Gegenstroms (NECC) in Verbindung. Hingegen beschreibt der *zonale Modus* das Abflachen der Thermokline während der Heinrich Stadiale und kann durch eine Abschwächung des Südost-Passats sowie durch eine Abschwächung des Südäquatorialstroms (SEC) erklärt werden. Zahlreiche paläozeanographische Studien im Nordatlantik weisen auf eine Abschwächung der thermohalinen Zirkulation während dieser Zeitabschnitte hin. Es ist daher wahrscheinlich, dass neben der direkten Kopplung über die tropische Atmosphäre auch Veränderungen der großskaligen Meridionalzirkulation eine wesentliche Rolle für Thermoklinenvariationen im westlichen äquatorialen Atlantik spielen.

Table of Contents

Chapter 1. Introduction

1.1. Motivation

A comprehensive understanding of the factors that control the Earth's climate is crucial for future projections. One way of acquiring such knowledge is to investigate past natural variability in the compartments of the Earth's climatic system. The ocean is one of the most important of these compartments, since it plays an essential role in the storage and distribution of heat around the world (Rahmstorf, 2002). Therefore, paleoceanographic reconstructions can improve our understanding of the system, by revealing the past variations that occurred in the ocean and its consequences to global climate.

Paleoceanographic reconstructions are based on the interpretation of proxies, which have specific relationships with environmental parameters. The quality of the information provided by a proxy relies on our comprehension of factors that can influence its final signature. In paleoceanography, many robust and reliable proxies are derived from planktonic foraminifera, for example by their fossil assemblages or chemical composition of their calcite shells (e.g. Kucera, 2007). Planktonic foraminifera are organisms widely distributed in the ocean and with an outstanding preservation potential. However, several studies have shown that planktonic foraminifera species have distinct ecological preferences (e.g. Boltovskoy et al., 1996; Žarić et al., 2005) life cycle durations (Bijma et al., 1990a) and live at different depths (e.g. Ortiz et al., 1995; Rebotim et al., 2017). Therefore, assessments of species-specific depth habitats, as well as on how temporal changes in environmental parameters may influence differently each species and a better understanding of their life cycle, becomes crucial for a reliable interpretation of proxies recorded by these organisms. Despite the importance of such evaluations, these parameters are still not well constrained in the present, which hampers the improvement of climate reconstructions. This study focuses on the assessment these aspects (e.g. reproduction, calcification depths and seasonality) regarding planktonic foraminifera biology, as well as in the application of proxies derived from these organisms in marine archives in regions where reconstructions are still scarce and lack appropriate temporal resolution.

1.2. Modern planktonic foraminifera

Planktonic foraminifera are unicellular marine protists surrounded by a calcite shell. There are about 50 morphospecies of planktonic foraminifera (Schiebel and Hemleben, 2005), where many of them comprise different genotypes, which are denominated cryptic species (Kucera and Darling, 2002). Planktonic foraminifers represent only a minor percentage of the existing marine zooplankton (Hemleben et al., 1989), but can constitute a significant part of the total calcite budget in the oceans. As part of the group of marine zooplankton, planktonic foraminifers are passively transported by water masses and their buoyancy is controlled by cytoplasmatic structures called fibrillary bodies (Hemleben et al., 1989). Planktonic foraminifera show distinct trophic behaviors and species living in the photic zone often harbor algal symbionts (Hemleben et al., 1989; Kucera, 2007). As pointed out by Kucera (2007), this symbiotic relationship can be an advantage in oligotrophic environments, where nutriens are scarce and light is abundant. However, in these oligotrophic waters, planktonic foraminifera abundances are low (25-50 specimens/m^3), whereas a number of their shells (>600 specimens/m^3) can be found in temperate or polar regions (Schiebel and Hemleben, 2005).

Due to the low population densities of these organisms, one might expect the presence of adaptive strategies in their reproduction cycle, in order to enhance the chances of successful fertilization and survival (Hemleben et al., 1989; Schiebel and Hemleben, 2005). Among these strategies, is the release of a large number of gametes, from 200,000 to 400,000 gametes (Schiebel and Hemleben, 2005), and synchronization of their life cycle both in space and time (Kucera, 2007). Evidence of synchronized reproduction was found in culture experiments (Spindler et al., 1979), in plankton tows studies (Bijma et al., 1990a) and in sediment trap time series (Kawahata et al., 2002; Lončarić et al., 2005; Jonkers et al., 2015) and was linked to lunar periodicities. Although the mechanism (endogenous or exogenous) for lunar reproductive cycles remains unknown, it seems to be a common feature in planktonic foraminifera species (Jonkers et al., 2015). In addition, the release of gametes may occur at species-specific depths, which planktonic foraminifers achieve by vertical migration through the water column (Schiebel and Hemleben, 2005). After gamete fusion, shell growth develops by sequential addition of chambers (Kucera, 2007) and growth rate, as well as the abundance of juveniles, depends on the environmental conditions (Schiebel and Hemleben, 2005; Lombard et al., 2009).

Specific ecological preferences of different planktonic foraminifera species influence their vertical and latitudinal distribution across the oceans. The species of

planktonic foraminifera can be devided into five main assemblages or provinces: tropical, subtropical, temperate, subpolar and polar (Bé and Tolderlund, 1971). These latitudinal provinces can be mainly explained by the fact that planktonic foraminifera are linked to water column parameters, where temperature is exerting a major control (Morey et al., 2005). Planktonic foraminifera species appear to have distinct optimal temperature ranges for growth and survival (Bijma et al., 1990b; Žarić et al., 2005; Lombard et al., 2009), which finally defines their abundances (Kucera, 2007). However, temperature is not solely controlling the distribution of planktonic foraminifera species. As pointed out by Schiebel and Hemleben (2005), at a regional and seasonal scale, the availability of food can be predominant and affect the species distribution. This factor is especially important on species that do not host symbionts, consequently relying more on primary productivity. Therefore, as a result of increase nutrient concentration or food availability, the abundance of opportunistic species (*Globigerina bulloides and Globigerinita glutinata*) increases, showing a fast response to productivity changes (Schiebel and Hemleben, 2005; Kucera, 2007).

Water column parameters not only exert control on the abundance of planktonic foraminifera, but also on their diversity and depth habitat. In high latitudes, at low temperature ranges, the diversity of planktonic foraminifera is low and assemblages on these regions are dominated by *Neogloboquadrina pachyderma* (Schiebel and Hemleben, 2005). Towards lower latitudes, diversity increases together with stratification, probably due to an increase of vertical niches (Kucera, 2007). Consequently, vertical niche separation of species is more marked in tropical areas compared to polar regions, where the water column is less stratified (Schiebel and Hemleben, 2005). Therefore, species-specifc depth habitats of planktonic foraminifera reflect vertical structure of water column properties, where each species may maintain a certain depth habitat according to their ecological preferences. This relation is confirmed by several studies using stratified plankton tows (Bé and Tolderlund, 1971; Ortiz et al., 1995; Field, 2004).

Since the water column properties can change through time, due to seasonal variations for example, the relative abundances of planktonic foraminifera species will also vary according to their preferences. This is exemplified by several time series generated by sediment trap studies, where sucessions of planktonic foraminifera species occur as a result of a changing environment (Sautter and Thunell, 1989; Conan and Brummer, 2000; Eguchi et al., 2003; Lin, 2014). These temporal changes in the planktonic foraminifera assemblages will be recorded in marine sediments, which can be interpreted as integration of multiple flux

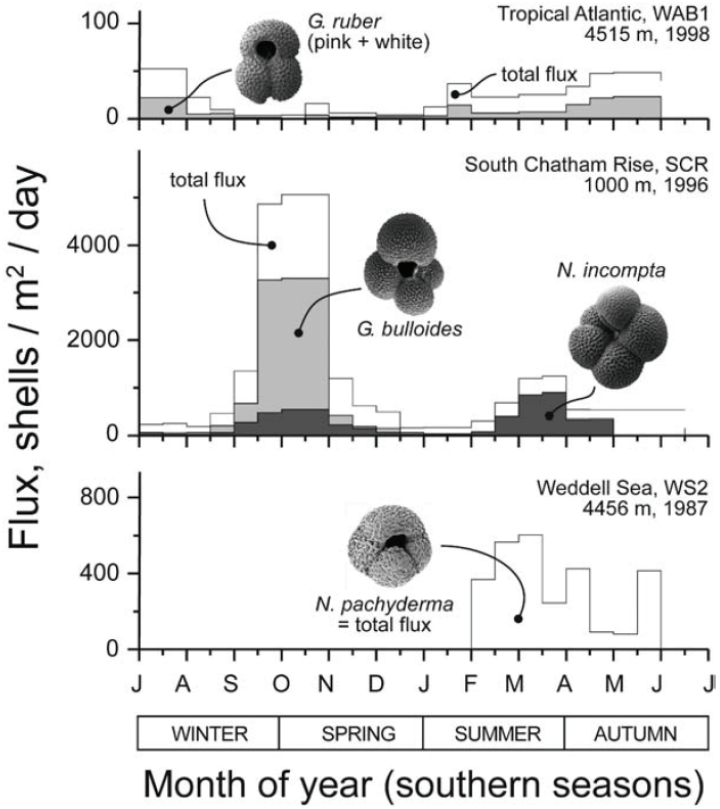

Figure 1. . Examples of foraminiferal shell flux patterns from sediment traps located at polar, temperate and tropical regions. The fluxes are derived from the compilation made by Žarić (2005) and the figure was extracted from Kucera (2007).

patterns, due to distinct temporal-scale changes, and may be biased towards a certain period (or season), rather than reflect the annual condition, for example (King and Howard, 2003). Therefore, in tropical or subtropical oceans where seasonality is less pronounced, fluxes are more characterized by a steady rain of foraminiferal shells, while at polar or temperate regions seasonal peaks in the fluxes of species are predominant (Schiebel and Hemleben, 2005; Kucera, 2007; Figure 1).

Planktonic foraminifera shell fluxes observed in sediment trap studies consist, in general, of empty shells that sink towards the seafloor after gametogenesis or death (Schiebel and Hemleben, 2005). The sinking velocity of the shells differ depending on their shape, weight and size, where in general small shells sink slowly (100 m day^{-1}) and the large ones sinking faster (1,500 m day^{-1}) (Takahashi and Bé, 1984; Schiebel and Hemleben, 2005). For that reason, planktonic foraminiferal assemblages are biased towards large shells, since the smaller shells are more exposed to dissolution (Schiebel and Hemleben, 2005). Moreover, the fast-sinking specimens are less susceptible to expatriation (Berger, 1970; Kucera, 2007). Thus, these after-death processes and other post-depositional factors (e.g. bioturbation) can

alter the final fossil assemblage, affecting the interpretation of paleoceanographic records.

1.3. Planktonic foraminiferal proxies in paleoceanography

Several proxies in paleoceanography are derived from planktonic foraminifera due to their potential to preserve information of the water column conditions. These proxies can be linked to the physical structure of the shell (ex. morphology and preservation), to the relative or absolute abundances of species and to the geochemical composition of the shells. The species composition in a foraminiferal assemblage is one of the most common proxies and contains substantial information about the past environmental conditions of the ocean (Kucera, 2007). One simple approach is to look for key species that can indicate the environmental state. For example, studies have shown that the abundances of *Globigerina bulloides* can be used as an indicator of upwelling intensity (Naidu et al., 1996; Black et al., 1999; Conan et al., 2002). Another way is to group the species and analyze them as assemblages, which provides a more robust approach (Kucera, 2007). In this case, one example is the study by Peeters et al. (2004), where the authors reconstruct past changes in the Agulhas leakage using a typical faunal composition associated with the regional currents. Estimations of environmental parameters can also be achieved using the faunal composition, by applying transfer functions, which was developed by Imbrie and Kipp (1971), and/or other statistical approaches such as the modern analog technique (Hutson, 1980) or the artificial neural networks (Malmgren and Nordlund, 1997). However, these tecniques assume that a certain environmental parameter have a major effect on the assemblage composition, and that the functions, which describe this relation, are calibrated to the target parameter (Kucera, 2007). In addition, the relationship between target environmental parameter and the proxy must remain through time, which is more unlikely the further a reconstruction goes through geological time.

Another source of proxies is the morphology or physical structure of planktonic foraminiferal shells. For example, studies dealing with shell weight or density (Barker and Elderfield, 2002; Marshall et al., 2013; Johnstone et al., 2014) have shown that these features can provide information about the state of the carbonate system. Barker and Elderfield (2002) shown that variations in planktonic foraminifera shell weight are related to changes in the ambient carbonate ion concentration on glacial-interglacial time scale.

Besides the useful information derived from planktonic foraminifera species composition and physical structure of their shell, the chemical composition of foraminifera shells is the main source of proxies, which enabled paleoceanographers to made

major discoveries in this field of research. One of the most used chemical proxies is the stable isotopic composition, mainly oxygen and carbon, from their calcite shells. The use of oxygen isotopes in calcite shells as a proxy for paleotemperature is based on the early works of Urey (1947) and Epstein (1953). By using oxygen isotopes in planktonic foraminifera derived from marine sediments covering the late Pleistocene, Emiliani (1955) was able to reconstruct the ocean conditions, revealing the existence of several glacial and interglacial stages in the Earth history, naming them marine isotope stages. Later, Shackleton (1967) demonstrated that oxygen isotopic composition in foraminifera is influenced by global ice volume changes, which was not previously considered by Emiliani as a major effect. These works are the basis for the use of oxygen isotopes in foraminifera as a proxy in paleoceanography.

After these scientific breakthroughs, other studies showed that the interpretation of stable isotopic composition in planktonic foraminifera might not be straightforward. For example, for the interpretation of oxygen isotopes ($\delta^{18}O$) in planktonic foraminifera as a proxy for temperature, one must take into account all the processes related to the isotopic composition of seawater ($\delta^{18}Osw$) and "vital effects", which may cause foraminifera not to calcify in thermodynamic equilibrium with the seawater (Ravelo and Hillaire-Marcel, 2007). For example, species that have symbionts may present lower values of $\delta^{18}O$, relative to equilibrium, due to higer calcification rates (Ravelo and Fairbanks, 1992; Spero, 1992). Besides the effects of photosynthesis by the symbionts (Ravelo and Hillaire-Marcel 2007), carbonate ion concentrations (Spero et al., 1997) and gametogenic calcification (Duplessy et al., 1981) may also cause disequilibrium effects. Carbon isotopic compostion ($\delta^{13}C$) in planktonic foraminifera, which can be used as a proxy for changes in productivity or in the carbon cycle, is also affected by photosynthesis and respiration of the symbionts, and the effect in the final isotopic signature is even stronger. These symbiotic processes have the potential to affect the microenvironment of the foraminifera, influencing their carbon pool and final carbon isotopic composition (Zeebe et al., 1999).

Besides these factors, knowledge about the seasonality and depth of calcification of planktonic foraminifera species needs to be understood in order to make a robust interpretation of their stable isotopic compostition (Ravelo and Hillaire-Marcel, 2007). This is supported by Kucera (2007), who pointed out that the interpretation of geochemical proxies in planktonic foraminifera relies on the detailed knowledge of the biology of these organisms. Regarding the seasonal effect, one must understand the timing of deposition of the foraminifera shells in

the studied site. If it is constant through the year, the signal recorded in a sample represents the annual average, but if short-term peaks characterize the deposition during a certain season, the signal deviates from the annual mean. In a simple model, Mix (1987) demonstrated that the temperature recorded by foraminifera depends on the annual temperature cycle and on the frequency of occurrence of the species (Figure 2) This idea was further corroborated by a study using a more complex global model (Fraile et al., 2009). Therefore, proxies from paleoceanographic records can reflect the seasonal signals, which can be species-specific and may vary spatially. Consequently, a crucial assessment of the calcification depth of planktonic foraminifera must also be made in order to interpret their geochemical proxies. Several studies have demonstrated that species may calcify in different depths (Farmer et al., 2007; Wejnert et al., 2013). Therefore, for understanding the depth level that a given proxy derived from planktonic foraminifera reflects, it is necessary to know the depth range where their calcite was built. Such knowledge can be used to reconstruct the stratification of the water column by taking planktonic foraminifera species that calcify at different depths (Mulitza et al., 1997).

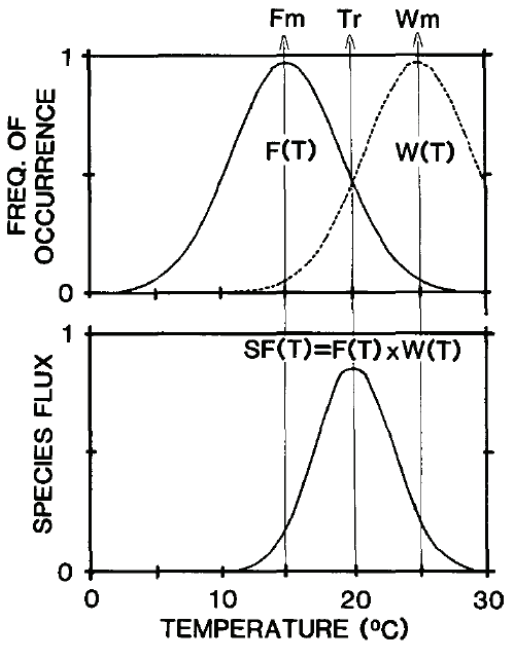

Figure 2. The model derived from the study of Mix (1987) showing that the temperature preferences from a species (Ft) and the range of temperatures available (Wt) defines the recorded temperature (SFt). The figure was extracted from Mix (1987).

Therefore, paleoceanographic studies using foraminifera-based proxies must consider these factors prior to interpretation of the records. Moreover, seasonality as well as calcification depth may not only change for each species, but also may vary according to the location (latitudinal) and hydrography of the studied site. Thus regions that lack this kind of assessments need to be investigated, which is one of the main objectives of this thesis.

1.4. Western boundary currents in the South Atlantic

The western boundary currents are located at the western edge of the ocean

basins and flow towards the high latitudes transporting heat, nutrients and carbon (Atkinson, 2010). Since these currents carry warm waters, they affect not only the region where they are flowing, but can also have an influence in the global merional heat transport and climate (Imawaki et al., 2013). Examples of these currents in the western South Atlantic are the Brazil Current (BC) (Figure 3) and the North Brazil Current (NBC). Both currents derive from the bifurcation of the South Equatorial Current (SEC) around 10°S in the Brazilian margin (Peterson and Stramma, 1991).

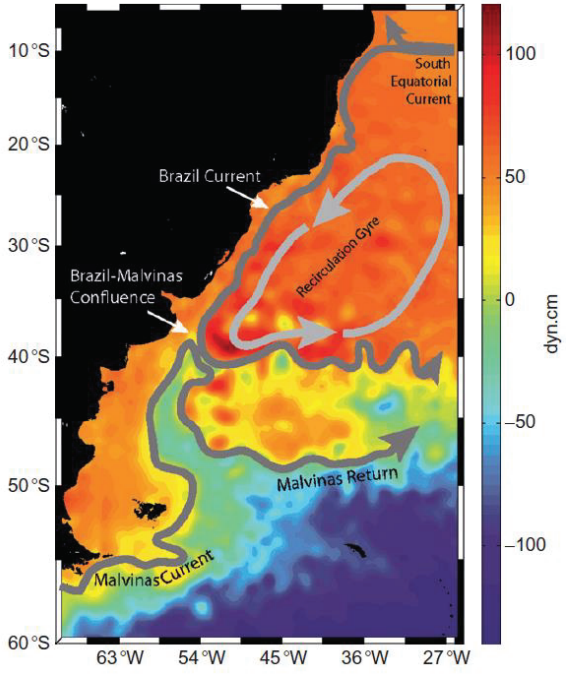

Figure 3. Dynamic topography (dyn.cm) for the western South Atlantic and the main current circulation of that area. Figure extracted from Imawaki et al. (2013).

The BC is a mid-latitude current flowing southward as a part of the South Atlantic subtropical gyre. Transport of the BC initiates with 4 Sv, being enhanced (up to 20 Sv) during its pathway along the Brazilian margin due to the presence of anticyclonic recirculation cells (Peterson and Stramma, 1991; Garzoli, 1993). Mesoscale dynamics linked to BC transport (meanders and eddies) influences the circulation of shelf areas along the coast and may even trigger upwelling events associated to subsurface intrusions of the South Atlantic Central Water (SACW) (Campos et al., 2000; Silveira et al., 2000). Several studies have shown a close connection between the BC transport and upwelling intensity along the coast, showing significant biogeochemical changes driven by the relationship between shelf circulation and the BC dynamics (Diaz et al., 2012; Albuquerque et al., 2014; Cordeiro et al., 2014).

The NBC, also referred as North Brazil Undercurrent (NBUC) south of 5°S (Stramma et al., 1995), is a northward-flowing current, which transports heat to the North Atlantic as part of the upper limb of the Atlantic meridional overturning circulation (AMOC) (Johns et al., 1998; Imawaki et al., 2013). Near 5° S, the NBUC has a transport around 15 Sv (Schott et al., 1995). Towards the equator, the NBC transport increases (up to 32 Sv) due to the surface inflow of SEC branches (Schott et al., 1993; Johns et al., 1998). After crossing the equator, around 6°N, the surface waters from the NBC retroflect eastwards (from June to Jan-

uary) into the North Equatorial Countercurrent (NECC) (Schott et al., 1998; Johns et al., 1998). During this process of retroflection, the interhemispheric heat transport is influenced by the presence of eddy shedding (or rings) derived from the NBC/NECC zone, and may contribute up to a third of the total transport (Johns et al., 1993; Fratantoni et al., 1995; Schott et al., 1998; Goni and Johns, 2001). The activity of the NECC is also closely linked to the position of the Intertropical Convergence Zone (ITCZ), intensifying when the ITCZ is at its northernmost position and becoming weak when the ITCZ is further south (Garzoli and Richardson, 1989; Fonseca et al., 2004).

Despite the relevance of these western boundary current systems (North Brazil Current and Brazil Current) transporting heat poleward, they are still lacking high-resolution paleoceanographic reconstructions and modern assessments of the relationship between proxies and environmental variables. Therefore, it becomes important to investigate these systems and generate new datasets, which can elucidate and improve our understanding of the global climate.

1.5. Research objectives

The main objective of this thesis is to improve the understanding on the biology of planktonic foraminifera (e.g. reproduction and depth habitat) and to apply proxies derived from these organisms in marine archives in the western South Atlantic in order to assess past changes in the water column stratification.

The specific objectives of this thesis are related to the following questions, which are grouped regarding planktonic foraminifera biology (A1-4) and the application of foraminifera-based proxies (B1-2):

A1. Is synchronization with lunar phases a feature present in planktonic foraminifera reproductive cycle?

A2. What is the magnitude of the seasonal component in foraminiferal fluxes in the tropical western South Atlantic?

A3. At what depth range do different planktonic foraminifera species calcify in the tropical western South Alantic?

A4. Is this calcification depth changing seasonally?

B1. How can these assessments about biology and ecology of planktonic foraminifera help the interpretation of foraminifera-based proxies in marine archives?

B2. What are the informations that we can derive from paleoceanographic records using planktonic foraminifera proxies in the western South Atlantic? Are these informations relevant for understanding global climate changes?

The questions are addressed in different chapters (manuscripts) in this thesis. The chapter 2 deals with question (A1) regarding

evidence for synchronized reproductive cycles in the southwestern Atlantic. The chapter 3 deals with questions (A2-4), where estimates of the calficifation depths and the magnitude of seasonal component are shown for several planktonic foraminifera species. Chapter 4 and appendices (1-2) are related to the application of planktonic foraminifera proxies to several marine sediment cores in the western South Atlantic, thus being linked to the final questions (B1-2).

1.6. Paleoceanographic proxies

1.6.1. Planktonic foraminifera census data

Identification and counting of planktonic foraminifera species is a common method in paleoceanography and determination of their assemblage typically involves the counting of 300-500 specimens in random sub-samples of the size fraction >150μm (Kucera, 2007). However, analyzed size fraction can vary and the use of other size fractions, for example >125μm, can provide more information about the foraminiferal assemblage (Al-Sabouni et al., 2007). These size fractions were established as standards, since small adults or juveniles of foraminifera are difficult to identify (Kucera, 2007). In sediment trap or plankton tow studies is also common to count the entire sample (Rigual-Hernández et al., 2012; Davis et al., 2016). In the sediment trap samples used in this study the count of the entire sample was performed, in order to estimate changes in foraminiferal fluxes related to seasonality and to reproductive cycles.

1.6.2. Oxygen isotopes

The stable oxygen isotope ratio of foraminiferal shells ($\delta^{18}O$) is one of the most used proxies for paleoceanography. Oxygen has three stable isotopes ^{16}O, ^{17}O and ^{18}O. Their abundance are variable with ^{16}O being the most abundant on Earth with 99.76% and the other two ^{17}O and ^{18}O showing small percentages of 0.04% and 0.2%, respectively. Most of the studies use the ratio $^{18}O/^{16}O$ in a sample and compare this with the same ratio in a known standard to obtain a value of $\delta^{18}O$, following the equation:

$$\delta^{18}O = \frac{^{18}O/^{16}O_{sample} - {}^{18}O/^{16}O_{standard}}{^{18}O/^{16}O_{standard}} \times 1000$$

Therefore, $\delta^{18}O$ values are given in units per thousand (‰). Various standards are used in laboratories, all are calibrated to an international reference standard. In the case of $\delta^{18}O$ in carbonate samples, the reference standard is the Vienna PeeDee Belemnite (VPDB). In order to determine the $\delta^{18}O$ values of foraminifera shells, the samples need to be dissolved at a given temperature in orthophosphoric acid to produce CO_2 (Ravelo and Hillaire-Marcel, 2007). The oxygen isotopic composition is then measured in the CO_2, which has no offset or a known isotopic offset (Ravelo and Hillaire-Marcel, 2007). Inside a mass spectrometer, this CO_2 gas is then ionized in a vacuum chamber by electron bombarding, and the ions are subse-

quently accelerated under high voltage, being afterwards splitted by magnetic fields into streams of different isotope ratio that generate electrical currents in the detectors (Pearson, 2012). The ratio of the currents is proportional to the isotopic ratio of the sample, and by alternating the sample with the standards the isotope ratio can be calculated (Pearson, 2012).

The $\delta^{18}O$ values of planktonic foraminifera reflect the oxygen isotopic compostion of the seawater ($\delta^{18}O_{sw}$) in which they calcified, with the offset between $\delta^{18}O$ of the calcite and $\delta^{18}O_{sw}$ depending on the temperature of the water, assuming a thermodynamic equilibrium between calcite and seawater (Ravelo and Hillaire-Marcel, 2007). As previously mentioned in this thesis, the $\delta^{18}O$ in planktonic foraminifera can be used as proxy for paleotemperature (Bemis et al., 1998), for stratification (Mulitza et al., 1997), ocean circulation (Wilson et al., 2011) and also for estimation of surface salinity (Schmidt et al., 2004) when coupled with elemental ratios (Mg/Ca) measured in the same calcite shell. In this study, $\delta^{18}O$ of multispecies of foraminifera where analyzed in order to estimate their calcification depths, isotopic flux-weighted exported to the seafloor and ocean stratification.

1.6.3. Major element analysis

The development of X-ray fluorescence (XRF) core scanners made it possible to analyze the chemical composition of sediments and to reconstruct climate changes on short-term time scales (seasonal or millennial scales). Examples of high-resolution paleocliamtic time series generated by this method are extensive (Haug et al., 2001; Mulitza et al., 2008; Govin et al., 2014; Zhang et al., 2015). Besides, XRF core scanners allow a nondestructive, continuous and fast analysis of several elements (Tjallingii et al., 2007).

XRF core scanners measure the chemical composition of the elements present in the sediments as intensities, in total counts or counts per second, being both proportional to the chemical concentrations of the elements (Tjallingii et al., 2007). However, potential problems of this method can arise depending on pore space, water content and heterogeneities present on sediment archives (Röhl and Abrams, 2000; Tjallingii et al., 2007).

In this study, we used the XRF Core Scanner II (Avaatech Serial No. 2) at the MARUM, University of Bremen. The scanner is able to analyze several elements from Aluminum to Uranium. Detector and source of X-rays are oriented in a 45° angles with the sediment surface and the scanner can irradiate in intervals equal or even below 1 cm, if dimensions are changed (Tjallingii, 2007). The system detects the emission line energies of the X-ray irradiated samples, as their frequency over a predefined measure time as intensities, which are proportional to

the elemental concentrations (Tjallingii, 2007). Using this approach was possible to obtain information about changes in continental terrigenous input to the ocean in a marine sediment core investigated by this thesis.

1.7. Outline

This thesis is presented in the form of manuscripts (case studies) that are published (chapter 2 and appendices 1-2), under review (chapter 3) or in preparation for international journals. This includes three manuscripts as first author (chapters 2-4) and two as a co-author (appendices 1-2), as follow:

Chapter 2. Planktonic foraminifera shell fluxes from a weekly resolved sediment trap record in the southwestern Atlantic: Evidence for synchronized reproduction.

Igor M. Venancio, Daniel Franco, Andre L. Belem, Stefan Mulitza, Michael Siccha, Ana Luiza S. Albuquerque, Michael Schulz, Michal Kucera.

Published in *Marine Micropaleontology*

This study presents results from sediment traps deployed in the southwestern Atlantic. Planktonic foraminiferal fluxes were analyzed from four different species collected by a double-set of traps at 50 and 100 m depth. Due to the high-resolution of the sampling (3-7 days), it was possible to assess the influence of the reproductive cycle of these species on their final shell fluxes. Results showed evidence for synchronized reproduction, predominantly in the first deployment that has 3-days sampling integration.

Contribution: The study was designed by I. Venancio and M. Kucera. I. Venancio counted and identified the planktonic foraminifera species. A. Belem analyzed the physical oceanographic data. I. Venancio interpreted the data and wrote the manuscript with contributions from the co-authors.

Chapter 3. Calcification depths of planktonic foraminifera from the southwestern Atlantic derived from oxygen isotope analyses of sediment trap material

Igor M. Venancio, A. L. Belem, T. P. Santos, D.O. Lessa, A. L. S. Albuquerque, S. Mulitza, M. Schulz, M. Kucera.

Under review in *Marine Micropaleontology*

This manuscript presents an estimation of the magnitude of seasonality on the foraminiferal fluxes and calcification depths of six planktonic foraminifera species. Foraminiferal fluxes and oxygen isotopic composition were used in order to evaluate the flux-weighted $\delta^{18}O$ values for each species, which were then compared with top cores. The study also provides an assessment of the influence of expatriation on the dataset.

Contribution: The study was designed by I. Venancio and M. Kucera. I. Venancio, T. Santos and D. Lessa counted and identified

the planktonic foraminifera species. I. Venancio picked the planktonic foraminifers for stable isotopic analysis and performed the estimations of calcification depths. A. Belem analyzed the physical oceanographic data. I. Venancio interpreted the data and wrote the manuscript with contributions from the co-authors.

Chapter 4. Responses of the western equatorial Atlantic to millennial-scale climatic events since the Last Interglacial.

Igor M. Venancio, Stefan Mulitza, Aline Govin, Thiago P. Santos, Douglas Lessa, Ana Luiza S. Albuquerque, Cristiano M. Chiessi, Ralf Tiedemann, Maximilian Vahlenkamp, Torsten Bickert, Michael Schulz

In preparation for *Earth and Planetary Science Letters*

This work presents reconstructions of terrigenous input to the ocean and water column stratification off northeastern Brazil since the Last Interglacial. Results provide evidence of the influence of Dansgaard-Oeschger cycles on the hydrological cycle and surface ocean circulation in the western equatorial Atlantic. Furthermore, it shows a comparison between the impacts of Heinrich stadials and Dansgaard-Oeschger stadials on the tropical climate.

Contribution: The study was designed by I. Venancio, A. Albuquerque and S. Mulitza. I. Venancio (core GL-1248), M. Vahlenkamp (core GeoB16202-2) and Nicole Huppertz (core GeoB16202-2) picked the planktonic foraminifers for stable isotopic analysis. I. Venancio and C. Chiessi performed the XRF analysis. A. Govin, S. Mulitza and I. Venancio generated the age model. I. Venancio interpreted the data and wrote the manuscript with contributions from the co-authors.

Appendix 1. Holocene oscillations of Southwest Atlantic shelf circulation based on planktonic foraminifera from a upwelling system (off Cabo Frio, Southeastern Brazil).

Douglas VO Lessa, Igor M Venancio, Thiago P dos Santos, André L Belem, Bruno J Turcq, Abdelfetah Sifeddine and Ana Luiza S Albuquerque.

Published in *The Holocene*

This study uses planktonic foraminifera assemblages and oxygen isotopes to reconstruct Holocene changes in the western South Atlantic. The data indicates five oceanographic phases during the Holocene, which are different in terms of dynamics of the Brazil Current and coastal upwelling intensity.

Contribution: The study was designed by D. Lessa and A. Albuquerque. D. Lessa generated the dataset. D. Lessa, I. Venancio and T. Santos interpreted the data. D. Lessa wrote the manuscript with contributions from the co-authors.

Appendix 2. Prolonged warming of the Brazil Current precedes deglaciations.

Thiago P. Santos, Douglas O. Lessa, Igor M. Venancio, Cristiano M. Chiessi, Stefan Mulitza, Henning Kuhnert, Aline Govin, Thiago Machado, Karen B. Costa, Felipe Toledo, Bruna B. Dias, Ana Luiza S. Albuquerque.

Published in *Earth and Planetary Science Letters*

This manuscript focus on the reconstruction surface and deep circulation changes in the Brazil Current domain. Results show a pattern of uninterruptedly warmings towards the last two terminations, which is explained as an effect of obliquity and AMOC changes. Also, the study highlights that during marine isotope stage 4, the Brazil Current was intensified, suggesting that the subtropics could have stored heat and salt during this period.

Contribution: The study was designed by T. Santos and A. Albuquerque. T. Santos generated the dataset. T. Santos, A. Govin, S. Mulitza and I. Venancio generated the age model. I. Venancio helped T. Santos in the interpretation of the Mg/Ca-SST record. T. Santos wrote the manuscript with contributions from the co-authors.

1.8. References

Al-Sabouni, N., Kucera, M., Schmidt, D.N., 2007. Vertical niche separation control of diversity and size disparity in planktonic foraminifera. Mar. Micropaleontol. 63, 75–90. doi:10.1016/j.marmicro.2006.11.002

Albuquerque, A.L.S., Belém, A.L., Zuluaga, F.J.B., Cordeiro, L.G.M., Mendoza, U., Knoppers, B. a., Gurgel, M.H.C., Meyers, P. a., Capilla, R., 2014. Particle fluxes and bulk geochemical characterization of the Cabo Frio Upwelling System in Southeastern Brazil: Sediment trap experiments between spring 2010 and summer 2012. An. Acad. Bras. Cienc. 86, 601–619. doi:10.1590/0001-37652014107212

Atkinson, L., 2010. Western Boundary Currents Overview. In: Liu, K.-K. et al. Carbon and Nutrient Fluxes in Continental Margins. Berlim, Springer, pp. 121-169.

Barker, S., Elderfield, H., 2002. Foraminiferal Calcification Response to Glacial-Interglacial Changes in Atmospheric CO2. Science 297, 833–836. doi:10.1126/science.1072815

Bé, A. W. H. and Tolderlund, D. S., 1971.Distribution and ecology of the living planktonic foraminifera in the surface waters of the Atlantic and Indian Oceans, 105–149.

Bemis, B.E., Spero, H.J., Bijma, J., Lea, D.W., 1998. Reevaluation of the oxygen isotopic composition of planktonic foraminifera: Experimental results and revised paleotemperature equations. Paleoceanography 13, 150–160. doi:10.1029/98PA00070

Berger, W., 1970. Planktonic Foraminifera: Differential production and expatriation off Baja California. Limnol. Oceanogr. 15, 183–204. doi:10.4319/lo.1970.15.2.0183

Bijma, J., Erez, J., Hemleben, C., 1990. Lunar and semi-lunar reproductive cycles in some spinose planktonic foraminifers. J. Foraminifer. Res. 20, 117–127.

Bijma, J., Faber, W.W., Hemleben, C., 1990. Temperature and salinity limits for growth and survival of some planktonic foraminifers in laboratory cultures. J. Foraminifer. Res. doi:10.2113/gsjfr.20.2.95

Black, D.E., Peterson, L.C., Overpeck, J.T., Kaplan, A., Evans, M.N., Kashgarian, M., 1999. Eight Centuries of North Atlantic Ocean Atmosphere Variability. Science 286,

1709–1713.
doi:10.1126/science.286.5445.1709

Boltovskoy, E., Boltovskoy, D., Correa, N., Brandini, F., 1996. Planktic foraminifera from the southwestern Atlantic (30 °–60 °S): species-specific patterns in the upper 50 m. Mar. Micropaleontol. 28, 53–72. doi:10.1016/0377-8398(95)00076-3

Campos, E.J.D., Velhote, D., Area, T.S., 2000. Shelf break upwelling driven by Brazil Current cyclonic meanders. Geophys. Res. Lett. 27, 751–754.

Conan, S.M., Brummer, G.A., 2000. Fluxes of planktic foraminifera in response to monsoonal upwelling on the Somalia Basin margin. Deep Sea Res. Part II Top. Stud. Oceanogr. 47, 2207–2227.

Conan, S.M., Ivanova, E.M., Brummer, G.A., 2002. Quantifying carbonate dissolution and calibration of foraminiferal dissolution indices in the Somali Basin. Mar. Geol. 182, 325–349.

Cordeiro, L.G.M.S., Belem, A.L., Bouloubassi, I., Rangel, B., Sifeddine, A., Capilla, R., Albuquerque, A.L.S., 2014. Reconstruction of southwestern Atlantic sea surface temperatures during the last Century: Cabo Frio continental shelf (Brazil). Palaeogeogr. Palaeoclimatol. Palaeoecol. doi:10.1016/j.palaeo.2014.01.020

Davis, C. V., Russel, A.D., Gaylord, B.P., Jahncke, J., Hill, T.M., 2016. Seasonality in Planktic Foraminifera of the Central California Coastal Upwelling Region. Biogeosciences Discuss. 5139–5150. doi:10.5194/bg-2015-626

Diaz, R., Moreira, M., Mendoza, U., Machado, W., Böttcher, M.E., Santos, H., Belém, A., Capilla, R., Escher, P., Albuquerque, A.L., 2012. Early diagenesis of sulfur in a tropical upwelling system, Cabo Frio, southeastern Brazil. Geology 40, 879–882. doi:10.1130/G33111.1

Duplessy, J., Blanc, P., Bé, A., 1981. Oxygen-18 enrichmente of planktonic foraminifera due to gametogenic calcification below the euphotic zone. Science 213, 1247–1249.

Eguchi, N.O., Ujiié, H., Kawahata, H., Taira, A., 2003. Seasonal variations in planktonic foraminifera at three sediment traps in the Subarctic, Transition and Subtropical zones of the central North Pacific Ocean. Mar. Micropaleontol. 48, 149–163. doi:10.1016/S0377-8398(03)00020-3

Emiliani, C., 1955. Pleistocene temperatures. Journal of Geology, 63, 538–578.

Epstein, S., Buchsbaum, H. A., Lowenstam, H. A., Urey, H. C., 1953. Revised carbonate-water isotopic temperature scale. Geological Society of America Bulletin, 64, 1315–1326.

Farmer, E.C., Kaplan, A., de Menocal, P.B., Lynch-Stieglitz, J., 2007. Corroborating ecological depth preferences of planktonic foraminifera in the tropical Atlantic with the stable oxygen isotope ratios of core top specimens. Paleoceanography 22, n/a-n/a. doi:10.1029/2006PA001361

Field, D.B., 2004. Variability in vertical distributions of planktonic foraminifera in the California Current: Relationships to vertical ocean structure. Paleoceanography 19, PA2014. doi:10.1029/2003PA000970

Fonseca, C.A., Goni, G.J., Johns, W.E., Campos, E.J.D., 2004. Investigation of the North Brazil Current retroflection and North Equatorial Countercurrent variability. Geophys. Res. Lett. 31, 1–5. doi:10.1029/2004GL020054

Fraile, I., Mulitza, S., Schulz, M., 2009. Modeling planktonic foraminiferal seasonality: Implications for sea-surface temperature reconstructions. Mar. Micropaleontol. 72, 1–9. doi:10.1016/j.marmicro.2009.01.003

Fratantoni, D.M., Johns, W.E., Townsend, T.L., 1995. Rings of the North Brazil Current: Their structure and behavior inferred from observations and a numerical simulation. J. Geophys. Res. 100, 10633. doi:10.1029/95JC00925

Garzoli, S., Richardson, P.L., 1989. Low-Frequency Meandering of the Atlantic North Equatorial Countercurrent. J. Geophys. Res. 94, 2079–2090. doi:10.1029/JC094iC02p02079

Garzoli, S.L., 1993. Geostrophic velocity and transport variability in the Brazil-Malvinas Confluence. Deep. Res. Part I 40, 1379–1403. doi:10.1016/0967-0637(93)90118-M

Goni, G.J., Johns, E., 2001. A Census of North Brazil Current Rings Observed from TOPEX/POSEIDON Altimetry: 1992-1998. Geophys. Res. Lett. 28, 1–4.

Govin, A., Chiessi, C.M., Zabel, M., Sawakuchi, A.O., Heslop, D., Hörner, T., Zhang, Y., Mulitza, S., 2014. Terrigenous input off northern South America driven by changes in Amazonian climate and the North Brazil Current retroflection during the last 250 ka. Clim. Past 10, 843–862. doi:10.5194/cp-10-843-2014

Haug, G.H., Hughen, K. A, Sigman, D.M., Peterson, L.C., Röhl, U., 2001. Southward migration of the intertropical convergence zone through the Holocene. Science 293, 1304–8. doi:10.1126/science.1059725

Hemleben, C., Spindler, M., Anderson, O.R., 1989. Modern Planktonic Foraminifera. doi:10.1007/978-1-4612-3544-6

Hutson, W.H., 1980. The Agulhas current during the late Pleistocene: analysis of modern faunal analogs. Science 207, 64–66.

Imawaki, S., Bower, A.S., Beal, L., Qiu, B., 2013. Western Boundary Currents, In: International Geophysics. pp. 305–338. doi:10.1016/B978-0-12-391851-2.00013-1

Imbrie, J. and Kipp, N., 1971. A new micropaleontological method for quantitative paleoclimatology: Application to a late Pleistocene Caribbean core. In: K. K. Turekian (Ed.), The Late Cenozoic glacial ages pp. 71–181. New Haven, Connecticut: Yale University Press.

Johns, W.E., Lee, T.N., Beardsley, R., Candela, J., Limeburner, R., Castro, B.M., 1998. Annual Cycle and Variability of the North Brazil Current. J. Phys. Oceanogr. 28, 103–128.

Johnstone, H.J.H., Kiefer, T., Elderfield, H., Schulz, M., 2014. Calcite saturation, foraminiferal test mass, and Mg/Ca-based temperatures dissolution corrected using XDX - A 150 ka record from the western Indian Ocean. Geochemistry, Geophys. Geosystems 15, 781–797. doi:10.1002/2013GC004994

Jonkers, L., Reynolds, C.E., Richey, J., Hall, I.R., 2015. Lunar periodicity in the shell flux of planktonic foraminifera in the Gulf of Mexico. Biogeosciences 12, 3061–3070. doi:10.5194/bg-12-3061-2015

Kawahata, H., Nishimura, A., Gagan, M.K., 2002. Seasonal change in foraminiferal production in the western equatorial Pacific warm pool : evidence from sediment trap experiments. Deep Sea Res. Part I Oceanogr. Res. Pap. 49, 2783–2800.

King, A.L., Howard, W.R., 2003. Planktonic foraminiferal flux seasonality in Subantarctic sediment traps: A test for paleoclimate reconstructions. Paleoceanography 18, 1–17. doi:10.1029/2002PA000839

Kucera, M., 2007. Planktonic Foraminifera as Tracers of Past Oceanic Environments. Dev. Mar. Geol. 1, 213–262. doi:10.1016/S1572-5480(07)01011-1

Kucera, M., Darling, K.F., 2002. Cryptic species of planktonic foraminifera: their effect on palaeoceanographic reconstructions. Philos. Trans. A. Math. Phys. Eng. Sci. 360, 695–718. doi:10.1098/rsta.2001.0962

Lin, H.-L., 2014. The seasonal succession of modern planktonic foraminifera: Sediment traps observations from southwest Taiwan waters. Cont. Shelf Res. 84, 13–22. doi:10.1016/j.csr.2014.04.020

Lombard, F., Labeyrie, L., Michel, E., Spero, H.J., Lea, D.W., 2009. Modelling the temperature dependent growth rates of planktic foraminifera. Mar. Micropaleontol. 70, 1–7. doi:10.1016/j.marmicro.2008.09.004

Lončarić, N., Brummer, G.-J. a., Kroon, D., 2005. Lunar cycles and seasonal variations in deposition fluxes of planktic foraminiferal shell carbonate to the deep South Atlantic (central Walvis Ridge). Deep Sea Res. Part I Oceanogr. Res. Pap. 52, 1178–1188. doi:10.1016/j.dsr.2005.02.003

Malmgren, B. A., and Nordlund, U., 1996. Application of artificial neural networks to chemostratigraphy, Paleoceanography 11, 505 – 512.

Marshall, B.J., Thunell, R.C., Henehan, M.J., Astor, Y., Wejnert, K.E., 2013. Planktonic foraminiferal area density as a proxy for carbonate ion concentration: A calibration study using the Cariaco Basin ocean time series. Paleoceanography 28, 363–376. doi:10.1002/palo.20034

Mix, A., 1987. The oxygen-isotope record of glaciation. The Geology of North America, K-3, edited by: Ruddiman, W. F. and Wright, H. E., Geol. Soc. Am., Boulder CO, 111–135.

Morey, A.E., Mix, A.C., Pisias, N.G., 2005. Planktonic foraminiferal assemblages preserved in surface sediments correspond to multiple environment variables. Quat. Sci. Rev. 24, 925–950. doi:10.1016/j.quascirev.2003.09.011

Mulitza, S., Dürkoop, A., Hale, W., Wefer, G., Niebler, H.S., 1997. Planktonic foraminifera as recorders of past surface-water stratification. Geology 25, 335–338. doi:10.1130/0091-7613(1997)025<0335:PFAROP>2.3.CO;2

Mulitza, S., Prange, M., Stuut, J.B., Zabel, M., Von Dobeneck, T., Itambi, A.C., Nizou, J., Schulz, M., Wefer, G., 2008. Sahel megadroughts triggered by glacial slowdowns of Atlantic meridional overturning. Paleoceanography 23, 1–11. doi:10.1029/2008PA001637

Naidu, P.D., Malmgren, B.A., 1996. A high-resolution record of late Quaternary upwelling along the Oman Margin, Arabian Sea based on planktonic foraminifera. Paleoceanography 11, 129–140.

Ortiz, J.D., Mix, A.C., Collier, R.W., 1995. Environmental of living symbiotic and and asymbiotic foraminifera of the California Current. Paleoceanography 10, 987–1009.

Pearson, P.N., 2012. Oxygen Isotopes in Foraminifera : Overview and Historical Review. Paleontol. Soc. Pap. 18, 1–38.

Peeters, F.J.C., Acheson, R., Brummer, G.-J. De Ruijter, W.P.M., Schneider, R.R., Ganssen, G.M., Ufkes, E., Kroon, D., 2004. Vigorous exchange between the Indian and Atlantic oceans at the end of the past five glacial periods. Nature 430, 661–5. doi:10.1038/nature02785

Peterson, R.G., Stramma, L., 1991. Upper-level circulation in the South Atlantic Ocean. Prog. Oceanogr. 26, 1–73. doi:10.1016/0079-6611(91)90006-8

Rahmstorf, S., 2002. Ocean circulation and climate during the past 120,000 years. Nature 419, 207–14. doi:10.1038/nature01090

Ravelo, A.C., Fairbanks, R.G., 1992. Oxygen isotopic composition of multiple species of planktonic foraminifera: recorders of the modern photic zone temperature gradient. Paleoceanography 7, 815–831. doi:10.1029/92PA02092

Ravelo, A.C., Hillaire-Marcel, C., 2007. The Use of Oxygen and Carbon Isotopes of Foraminifera in Paleoceanography. Dev. Mar. Geol. 1, 735–764. doi:10.1016/S1572-5480(07)01023-8

Rebotim, A., Voelker, A.H.L., Jonkers, L., Waniek, J.J., Meggers, H., Schiebel, R., Fraile, I., Schulz, M., Kucera, M., 2017. Factors controlling the depth habitat of planktonic foraminifera in the subtropical eastern North Atlantic. Biogeosciences 14, 827–859. doi:10.5194/bg-2016-348

Rigual-Hernández, A.S., Sierro, F.J., Bárcena, M. a., Flores, J. a., Heussner, S., 2012. Seasonal and interannual changes of planktic foraminiferal fluxes in the Gulf of Lions (NW Mediterranean) and their implications for paleoceanographic studies: Two 12-year sediment trap records. Deep. Res. Part I Oceanogr. Res. Pap. 66, 26–40. doi:10.1016/j.dsr.2012.03.011

Röhl, U., Abrams, L.J., 2000. High-resolution, downhole, and nondestructive core measurements from site 999 and 1001 in the Caribbean sea: application to the Late Paleocene thermal maximum. Procedings Ocean Drill. Program, Sci. Results 165, 191–203. doi:10.2973/odp.proc.sr.165.009.2000

Sautter, L.R., Thunell, R.C., 1989. Seasonal Succession of Planktonic-Foraminifera - Results From a 4-Year Time-Series Sediment Trap Experiment in the Northeast Pacific. J. Foraminifer. Res. 19, 253–267. doi:10.2113/gsjfr.19.4.253

Schiebel, R., Hemleben, C., 2005. Modern planktic foraminifera. Palaontogische Zeitschrift 79, 135–148. doi:10.1007/BF03021758

Schmidt, M.W., Spero, H.J., Lea, D.W., 2004. Links between salinity variation in the Caribbean and North Atlantic thermohaline circulation. Nature 428, 160–3. doi:10.1038/nature02346

Schott, F.A., Stramma, L., Fischer, J., 1995. The warm water inflow into the western tropical Atlantic boundary regime, spring 1994 waters of the equatorial circulation. J. Geophys. Res. 100, 24745–24760. doi:10.1029/95JC02803

Schott, F., Fischer, J., Reppin, J., Send, U., 1993. On mean and seasonal currents and transports at the Western Boundary of the Equatorial Atlantic. J. Geophys. Res. 98, 14353–14368. doi:10.1029/93JC01287

Shackleton, N. J., 1967. Oxygen isotope analyses and Pleistocene temperatures reassessed. Nature, 215, 15–17.

Silveira, I.C.A., Schmidt, A., Campos, E.J.D., Godoi, S.S. De, Ikeda, Y., 2000. A Corrente do Brasil ao Largo da Costa Leste Brasileira. Rev. Bras. Oceanogr. 48, 171–183.

Spero, H. J., 1992. Do planktic foraminifera accurately record shifts in the carbon isotopic composition of seawater sigma-CO2. Marine Micropaleontology, 19, 275–285.

Spero, H.J., Bijma, J., Lea, D.W., Bemis, B.E., 1997. Effect of seawater carbonate concentration on foraminiferal carbon and oxygen isotopes. Nature 497–500.

Spindler, M., Hemleben, C., Bayer, U., Bé, A., Anderson, O.R., 1979. Lunar Periodicity of Reproduction in the Planktonic Foraminifer Hastigerina pelagica. Mar. Ecol. Prog. Ser. 1, 61–64. doi:10.3354/meps001061

Stramma, L., Fischer, J., Reppin, J., 1995. The North Brazil Undercurrent. Deep Sea Res. Part I Oceanogr. Res. Pap. 42, 773–795. doi:10.1016/0967-0637(95)00014-W

Takahashi, K., Bé, A., 1984. Planktonic foraminifera: factors controlling sinking speeds. Deep Sea Res. Part A. Oceanogr. Res. Pap. 31, 1477–1500.

Tjallingii, R., Röhl, U., Kölling, M., Bickert, T., 2007. Influence of the water content on X-ray fluorescence corescanning measurements in soft marine sediments. Geochemistry, Geophys. Geosystems 8, 1–12. doi:10.1029/2006GC001393

Urey, H. C., 1947. The thermodynamic properties of isotopic substances. Liversidge lecture of 1946. Journal of the Chemical Society, 562–581.

Wejnert, K.E., Thunell, R.C., Astor, Y., 2013. Comparison of species-specific oxygen isotope paleotemperature equations: Sensitivity analysis using planktonic foraminifera from the Cariaco Basin, Venezuela. Mar. Micropaleontol. 101, 76–88. doi:10.1016/j.marmicro.2013.03.001

Wilson, K.E., Maslin, M.A., Burns, S.J., 2011. Evidence for a prolonged retroflection of the North Brazil Current during glacial stages. Palaeogeogr. Palaeoclimatol. Palaeoecol. 301, 86–96. doi:10.1016/j.palaeo.2011.01.003

Žarić, S., Donner, B., Fischer, G., Mulitza, S., Wefer, G., 2005. Sensitivity of planktic foraminifera to sea surface temperature and export production as derived from sediment trap data. Mar. Micropaleontol. 55, 75–105. doi:10.1016/j.marmicro.2005.01.002

Zeebe, R.E., 1999. An explanation of the effect of seawater carbonate concentration on foraminiferal oxygen isotopes. Geochim. Cosmochim. Acta 63, 2001–2007. doi:10.1016/S0016-7037(99)00091-5

Zhang, Y., Chiessi, C.M., Mulitza, S., Zabel, M., Trindade, R.I.F., Hollanda, M.H.B.M., Dantas, E.L., Govin, A., Tiedemann, R., Wefer, G., 2015. Origin of increased terrigenous supply to the NE South American

continental margin during Heinrich Stadial 1 and the Younger Dryas. Earth Planet. Sci. Lett. 432, 493–500. doi:10.1016/j.epsl.2015.09.054

Chapter 2. Planktonic foraminifera shell fluxes from a weekly resolved sediment trap record in the southwestern Atlantic: Evidence for synchronized reproduction

Igor M. Venancio[1, 2*], Daniel Franco[3], Andre L. Belem[4], Stefan Mulitza[1], Michael Siccha[1], Ana Luiza S. Albuquerque[2], Michael Schulz[1], Michal Kucera[1]

. [1] MARUM—Center for Marine Environmental Sciences and Faculty of Geosciences, University of Bremen, D-28359 Bremen, Germany

[2] Departamento de Geoquímica, Universidade Federal Fluminense, Outeiro de São João Batista, s/nº., Niterói, Rio de Janeiro, CEP: 24020-141, Brazil.

[3] Coordenação de Geofísica, Observatório Nacional, R. Gal. José Cristino, 77, 20921-400 Rio de Janeiro, RJ, Brazil.

[4] Departamento de Engenharia Agrícola e Meio Ambiente, Universidade Federal Fluminense, Niterói, Rio de Janeiro, 24210-240, Brazil.

Published in *Marine Micropaleontology*

2.1. Abstract

The reproductive behavior of planktonic foraminifera is an important variable for the interpretation of paleoproxies based on their shells and for the understanding of the role of these organisms in oceanic carbonate flux. Observations from plankton tows have initially provided evidence for the existence of reproductive cycles synchronized with lunar phases in several species. However, subsequent observations from sediment traps yielded inconclusive results. Here we report shell flux data of four key species of planktonic foraminifera (*Trilobatus sacculifer, Globigerinoides ruber, Orbulina universa* and *Neogloboquadrina dutertrei*) from multiple deployments of a high-resolution (3-7 days) sediment trap in the southwestern Atlantic. Despite the potential bias relat-

ed to lateral advection at the shallow deployment depths of the traps, the unusually high sampling resolution makes it possible to better constrain the short-term (lunar) dynamics of shell flux than most previous studies. Using periodic regression on the high-resolution series, we detected for all species evidence for a single flux maximum during one lunar cycle, occurring approximately 4-6 days after the full moon. In this series, 44-52 % of the shell flux in the deep (100 m) trap occurred during the last quarter. Different flux behavior between the shallow (50 m) and the deep (100 m) traps co-located on the same mooring revealed evidence for migration to deeper levels prior to reproduction in *T. sacculifer*. Although a monthly peak in shell flux was observed in the 3-day resolution deployment, its signature disappeared when all deployments were analyzed together. This analysis still reveals an elevated flux during the last quarter of the lunar cycle, but it seems that the period of the reproductive cycle is not fixed in time. Combined with aliasing at the sampling resolution of 5-7 days, this variable timing overwhelms the strictly periodic component of the shell flux series. We conclude that planktonic foraminifera shell flux and thus the carbonate export to the seafloor is affected by periodicity in the lunar band, but that reproduction does not seem to occur at exactly the same day of the lunar cycle in each month.

2.2. Introduction

Synchronized reproduction seems to be a common feature in many marine organisms. For instance, reproductive cycles in reef corals (Zakai et al., 2006) and crustaceans (Skov et al., 2005) were pointed out to be synchronized with the moon phases. These lunar-driven reproductive cycles can be interpreted as an evolutionary adaptation to enhance the probability of gamete union in gamete-broadcasting species (Spindler et al., 1979). Based on observations from the plankton, such a reproductive strategy has also been suggested for several species of planktonic foraminifera (Spindler et al., 1979; Hemleben et al., 1989; Bijma et al., 1990a). If the periodicity in planktonic foraminiferal reproduction is strong, it would affect the temporal pattern of carbonate flux to the seafloor. Since planktonic foraminifera are major contributors to the oceanic carbonate flux (Schiebel, 2002), investigations of the role of their reproductive cycles are needed to better constrain the role of foraminifera shell fluxes in oceanic carbon cycling and particle ballasting.

Laboratory experiments with *Hastigerina pelagica* showed that this species follows an endogenous lunar reproductive cycle (Spindler et al., 1979). Subsequent studies using plankton tows in the Red Sea demonstrated that lunar reproductive synchronization might also be present in other foraminifera species such as *Trilobatus sacculifer*, with a full synodic lunar cycle, and *Globigerinoides ruber* and *Globigerinella siphonifera*, which were associated with a semi-lunar cyclicity (Bijma et al., 1990a; Bijma et al., 1994; Erez et al., 1991). The study of Bijma et al. (1994) demonstrated that *T. sacculifer* fluxes are characterized by pulses instead of a constant particle rain and pointed to the relevance of this reproductive behavior for predictions of the carbonate flux. These observations support the theory of a synchronous reproduction in planktonic foraminifera, which would be an advantage for these organisms that reproduce by gamete broadcasting.

In contrast to plankton tows, which only provide snapshots of population dynamics in time and space, sediment trap data should in theory be more suitable to assess foraminifera reproductive cycles through temporal variations in their shell fluxes (Kawahata et al., 2002; Zaric et al., 2005; Rigual-Hernandez et al., 2012). Provided they are sampling at sufficient temporal resolution, sediment traps have the potential to provide time series of foraminiferal fluxes, from which periodic cycles in the lunar band could be detected (Khripounoff et al., 1998; Lončarić et al., 2005; Kuroyanagi et al., 2008). Unfortunately, the resolution of sediment trap series is usually too low for the detection of lunar cycles. Most sediment trap studies use variable temporal resolution de-

pending on the season (King and Howard, 2001; Bárcena et al., 2004) and have long periods with a biweekly sampling, which hampers the detection of cycles in the lunar band.

So far, there are only a few sediment trap series published that could provide meaningful insights into short timescales. A 12 to 15-day resolution study Kawahata et al. (2002) inferred the existence of a lunar reproduction cycle for *T. sacculifer* in the North of New Guinea. However, their resolution was too low and the cycle could only be evidenced during a short period of the entire time series. Lončarić et al. (2005) analyzed shell flux data for 28 planktonic foraminifera species in the South Atlantic (8 days sampling configuration, comprising 7-month sampling collection). These authors were able to infer a ~29.5 days synodic lunar cycle, but only for *H. pelagica*, whereas all other species did not seem to follow this pattern. A recent study of Lin (2014) off southwest Taiwan, with an outstanding resolution of 3 days, detected a probable influence of lunar reproduction on *T. sacculifer* and *G. ruber* fluxes. However, despite the combined analysis of flux data and shell sizes, the relationship between lunar phase and reproduction was not always present throughout the 3-months sampling interval. Finally, Jonkers et al. (2015) analyzed the flux variability of 11 species in a long sediment trap series from the Gulf of Mexico with a resolution of 9 days. These authors could detect lunar periodicity in all investigated species, but the lunar rhythm was not present in all size fractions.

Summarizing, it seems that foraminiferal fluxes are episodic on the time scale of weeks and the flux pattern is consistent with reproduction synchronized around the lunar band, but the lack of a clear signal in many studies (Kawahata et al., 2002; Lončarić et al., 2005) is puzzling. It is also unclear why the lunar cycle is not observed in all species investigated (Lončarić et al., 2005; Jonkers et al., 2015) and to what degree the postulated relationship with a specific lunar phase is universally applicable. Sediment trap studies alternatively indicate reproduction before full moon (Lin, 2014), shortly after (Lončarić et al., 2005), or at full moon (Kawahata et al., 2002). Recently, Jonkers et al. (2015) found highest fluxes around full moon for a group of species (*Globorotalia menardii*, *Orbulina universa*, *Trilobatus sacculifer*, *Pulleniatina obliquiloculata*, *Neogloboquadrina dutertrei*, *Globigerinella calida* and *Globigerinita glutinata*), and around the new moon for *G. siphonifera* and *G. calida* at the same location.

In this study, we aim to investigate short-term dynamics in the vertical flux variability of planktonic foraminifera using sediment trap samples from a mooring at the Southeastern Brazilian continental shelf. This region harbors typical subtropical as-

semblages of planktonic foraminifera (Lessa et al., 2014) with many species for which lunar synchronization of reproduction has been postulated (Bijma et al., 1990a). In order to assess the possible periodicities in the shell fluxes records, we evaluated the vertical mean flux in a shallow and deep traps co-located on the same mooring and analyzed a 16-month foraminiferal mean flux datasets of four different species (*G. ruber, T. sacculifer, N. dutertrei* and *O. universa*). Our time series is composed of an initial period with 36 days sampled at 3-day intervals and a longer subsequent period sampled with lower resolution (5-7 days). The duration of the full experiment covered approximately ten lunar cycles.

2.3. Materials and methods

2.3.1. Sediment trap sampling

The mooring line that was available for the study of reproductive synchronization was deployed within the Brazilian Project *Ressurgência*. The sediment traps at depths of 50 and 100 m, described as L = 50 or L = 100, are located on the Brazilian southeastern continental shelf at 23°36' S 041°34' W (Figure 1), at a depth of 145 m. The used sediment traps PARFLUX (model Mark 8-13) have an aperture area of 0.25 m^2 and 13 sequential bottles with 500 ml capacity. Each sample bottle was decontaminated and filled with pre-filtered MilliQ water with buffered (pH=8) formaldehyde (4%) after adjusting the salinity with marine salt (RedSea©) to 70 PSU to prevent mixing and bacterial decomposition of collected particles (Goswami, 2004). In addition to the traps, the mooring line contained temperature loggers (ONSET tidbits V2) between 30 m and 120 m, spaced at 5 m intervals and two current meters (400 kHz Nortek Aquadopp Profilers) configured for up and down looking acoustic current profiling. The physical parameters (temperature and velocities) were measured at 30-minute intervals. Current-meter data are provided as supplementary material (Appendices B and C). Albuquerque et al. (2014) recently published a general description of particle fluxes and bulk composition.

All samples and data used in this study were retrieved during four deployments between November 2010 and March 2012, resulting in time frames of 39 and 91 consecutive days. Sampling resolution was not identical for all deployments. The first experiment, from November 11th to December 19th 2010, had a 3 days sampling rate. The second experiment, from March 15th to June 14th 2011, had a 7 days sampling rate. The third experiment, from July 20th to September 26th 2011, had a 5 days sampling rate and the last experiment covered the time frame between December

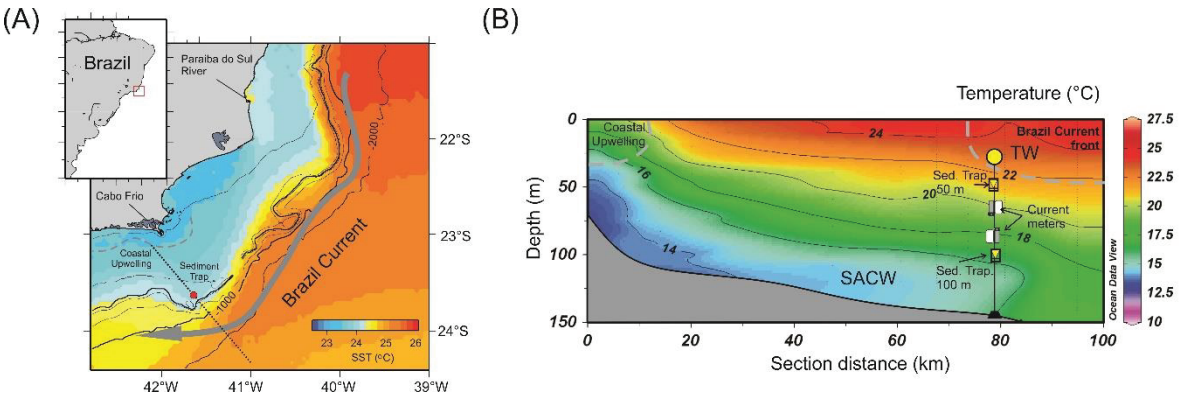

Figure 1: (A) Study area and oceanographic features. The mooring site is marked with a red circle. (B) Cross-shelf section showing the thermal gradient with isotherms, the main water masses SACW (South Atlantic Central Water) and TW (Tropical Water), and the position of the sediment traps and the current meters. Temperature data was extracted from the World Ocean Data Center and cross-shelf plot was generated with Ocean Data View (Schlitzer, 2014).

2nd 2011 and March 2nd 2012, with a 7 days sampling rate. Gaps in the time series were caused by operational constraints related to the maintenance of the instrument, mostly due to bad weather conditions. The complete dataset is provided as supplementary material (Appendix A).

2.3.2. Preparation of sediment trap samples

The sediment trap samples were wet-sieved through 1 mm and 500 µm meshes before being splitted into four aliquots. A quarter of each sample was used for foraminiferal analysis, as was the material trapped into the meshes of 1 mm and 500 µm. After the wet-sieving process, the > 125 µm fraction was used for species identification and counting. This size fraction was chosen because it covers the size range of recent assemblages and also contains all foraminifera > 150 µm, which are usually used for paleoceanographic studies (Al-Sabouni et al., 2007; Zaric et al., 2005). The samples were analyzed wet allowing the quantification of fragile taxa, which could disintegrate during drying. Wet picking was performed using a transparent gridded tray for zooplankton analysis. Benthic foraminifers were not found in the samples. The chosen species *Globigerinoides ruber, Trilobatus sacculifer, Orbulina universa and Neogloboquadrina dutertrei* were the most abundant ones, together representing more than 70 % of the assemblage in most samples. The counts of the two varieties of *Globigerinoides ruber* (white and pink) were added for the flux calculation and later analysis. No further distinction of *T. sacculifer* or a distinction between *G. ruber* and G. *elongatus* was made.

2.3.3. Evaluation of vertical mobility and possible lunar periodicities in the foraminifera record

The focus of this work was to determine whether lunar-induced cycles could be detected in the time series of vertical fluxes of planktonic foraminifera species. Therefore, it is important to understand how the fluxes evolve in comparison to the succession of lunations (average time for the synodic month, or the mean interval between two successive new moons) throughout the sampling period. To this end, we employed three different approaches to compare the flux data to the lunar periodicities for a given species: (i) with the day numbering sequence throughout the sampling periods; (ii) with the evolution of the lunar cycle expressed as the sequence of lunar brightness; and (iii) with the sequential, discrete lunar phases.

Census and flux calculation of the planktonic foraminifera species

Foraminiferal fluxes were calculated based on the duration of sampling for each bottle of the sediment trap (sampling rate) and the area of the sediment trap (0.25 m^2). The bulk sample was wet sieved over 1 mm and 500 μm meshes and all foraminifera were counted in these fractions. The residue was split using a rotary splitter into four aliquots and the foraminifera were counted in one aliquot and multiplied by four for the calculation of total abundances. The picked specimens were transferred to cardboard slides and identified under a stereomicroscope. Abundances and fluxes for the chosen species are provided as supplementary material (Appendix A). The fluxes were converted to a logarithmic scale for all further analysis, except for the raw flux plots in Figure 2 and 6. The log-transformation was performed because subsequent statistical analyses require normal distribution of the data.

Flux dataset – day numbering sequence

The second step was to present the fluxes from the two traps as a function of time. Day counting comprises all the time intervals related to the four moorings. The onset and the end of the time series were defined at the first (#1) and last (#486) days of the months when the first and last deployments occurred. For each sample, its corresponding day # was attributed to the middle day # of each sampling interval (from first to fourth experiment: 3-, 7-, 5- and 7-day days sampling intervals, respectively; see section 2.3). Days #12 and #477 correspond to the first and last collected samples. This approach allowed us to prepare flux data and day# datasets for each planktonic foraminiferal species, which were then employed for qualitative analysis of flux evolution throughout the sampling periods. The entire dataset is provided as supplementary material (Appendix A).

Flux dataset – lunar phase and brightness

Each day # of the overall sampling period was associated to its correspondent

percentage value of moon brightness at midnight (information extracted from Astronomical Applications Department website of the U.S. Naval Observatory (http://aa.usno.navy.mil/data/docs/MoonFraction.php). This strategy allowed us use the moon brightness datasets as a function of the day#. The percentage of lunar brightness can be associated with the moon phases as follows: New Moon (NM; 25-0 %); First Quarter (FQ; 25-75%); Full Moon (FM; 100-75 %); and Last Quarter (LQ; 75-25 %).

Variability of the vertical migration

In order to evaluate if lunar-induced periodicities could be related in some way to vertical migration during the reproductive cycle of each foraminiferal species, we calculated species-specific vertical flux proportionality between the traps at 50 m and 100 m depths using the following equation:

$$M_{sp;LPB} = \left\{ \frac{\left[\frac{\phi_{100\,m}}{\phi_{TOT}}\right]}{\left[\frac{\phi_{50\,m}}{\phi_{TOT}}\right]} \right\}_{sp;LPB}$$

where $M_{sp;LPB}$ is the vertical flux proportionality for a given species *sp* and brightness of lunar phase (LPB), while Φ_{100m}, Φ_{50m} and Φ_{TOT} are the absolute mean log-transformed fluxes of the 50m and 100m traps and the total flux, respectively. The total flux is the sum of the fluxes from both traps for a given species during a certain lunar phase. The equation employs the flux at the deeper trap as the numerator, since we expect a migration towards greater depths during gametogenesis (Erez et al., 1991). Values of $M_{sp;LPB}$ of 1.0 would imply that the flux of all dead shells originates from the water column shallower than 50 m. Higher values would indicate that a progressively larger part of the shelf flux derive from specimens that died below 50 m. Lower values could only occur in case of large lateral advection or in the case where the shallower trap collects live specimens.

2.3.4. Periodic regression

The possible link between fluxes and lunar cycles was tested by periodic regression analysis. In this analysis, the independent variable is an angular representation of time and this approach was demonstrated to be robust in order to detect lunar periodicity (deBruyn and Meeuwig, 2001). Furthermore, the analysis gives information about the timing of the maximum peak in the dataset and provides an equation, which can be used to estimate values for a given period. The methods and advantages in detecting lunar and seasonal cycles are summarized by deBruyn and Meeuwig (2001) and Jonkers and Kucera (2015), respectively. In this approach, we also used the log-transformed flux data with the lunar days. The zero values were replaced by half of the minimum flux value for each deployment dataset. The observations time scale was converted to lunar days (LD) and posteriorly transformed in radian units (LD/29 x 2π). In order to test

the cycles the following model was applied to observations:

$$F_{(t)} = A + B_{\sin(t)} + C_{\cos(t)}$$

where $F_{(t)}$ is the shell flux at a given time and A-C are the parameters that will be estimated in the analysis.

The significance of the periodic regression analysis was evaluated using ANOVA for multiple regression and the results are summarized in Table 1. Due to the small number of data points in each time series, spectral analysis was not used in the dataset. An approach with spectral analysis cannot be expected to produce robust results with our time series data.

2.4. Oceanographic setting

The mesoscale surface circulation of the western boundary of the South Atlantic is dominated by the warm and nutrient-poor Brazil Current (BC) (Figure 1), arising from the bifurcation of the South Equatorial Current (SSEC), typically located around 10°S, where two branches are generated with the North Brazil Current (NBC) flowing to the north and the Brazil Current (BC) flowing southward to the Brazil-Malvinas Convergence Zone (BMCZ) (Peterson and Stramma, 1991). As discussed by Walsh (1988), tropical areas of continental shelves that are linked to the western edge of oceanic systems are often related to less productive oceanic margins. However, mesoscale processes related to the dynamics of BC (encroachment, topographic acceleration, meandering and eddies) may induce the rise of cold and nutrient-rich South Atlantic Central Water (SACW) on the shelf, forming an upwelling system in the southeastern portion of the Brazilian shelf (Campos et al., 2000; Castelao and Barth, 2006; Silveira et al., 2008; Belem et al., 2013).

The continental shelf off southeastern Brazil, especially between 21°S and 25°S, is widely studied because of this upwelling system (Ikeda et al. 1974; Matsuura, 1996; Castro and Miranda, 1998; Rodrigues and Lorenzzetti, 2001; Castelao and Barth, 2006; Castelao, 2012; Cerda and Castro, 2014; Castro, 2014). The BC flows southward along the shelf break and slope of the Brazilian margin, as a component of the South Atlantic subtropical gyre, acquiring intensity and speed southward of the Abrolhos Bank (Silveira et al., 2000). As shown in Figure 1, this boundary current carries the Tropical Water (TW) at the upper layers of the water column, as well as the South Atlantic Central Water (SACW) at an intermediate depth southwards (Stramma and England, 1999). Therefore, the shallower trap (50 m) is more influenced by the TW and the deeper trap (100 m) by the SACW. The material collected by the deeper trap (100 m) is derived from both layers, while the shallower trap (50 m) material is mostly derived from the surface layer (TW), although SACW intrusions can be observed on the temperature

dataset for both traps. TW and SACW, besides the Coastal Water (CW) and the Subtropical Shelf Water (STSW), are the main water masses in the upper part of the water column of the southeastern Brazilian margin (Castro and Miranda, 1998; Castro, 2014; Venancio et al., 2014).

2.5. Results

2.5.1. Planktonic foraminifera fluxes

Among the foraminifera species analyzed in this study, *G. ruber* and *N. dutertrei* exhibited the highest flux variability throughout the sampling period (Figure 2). *G. ruber* showed fluxes ranging from 0 - 160 shells m^{-2} $day^{-1}$and 0 - 252 shells m^{-2} day^{-1}, whereas *N. dutertrei* fluxes ranged between 0 - 475 shells m^{-2} day^{-1} and 0 - 219 shells m^{-2} day^{-1} for the shallower and deeper trap, respectively. *Trilobatus sacculifer* exhibited a flux variation from 0 - 122 shells m^{-2} day^{-1} for the L = 50 m trap and 0 - 81 shells m^{-2} day^{-1} for the L = 100 m trap. The narrowest ranges were observed for *O. universa*, for which the fluxes varied between 0 - 59 shells m^{-2} day^{-1} in the shallower trap and between 0 - 63 shells m^{-2} day^{-1} in the deeper trap. In summary, *N. dutertrei* and *T. sacculifer* show a higher flux in the shallower than in the deeper trap (although for *N. dutertrei* this pattern may be caused by a single data point during the third deployment), whereas *G. ruber* was the only species that exhibited higher flux in the deeper trap. Fluxes at L = 50 m and L = 100 m appeared to be rather similar for *O. universa*.

Furthermore, we noted several striking patterns for the fluxes from the first to fourth deployments, especially from the *G. ruber*, *T. sacculifer* and *N. dutertrei*), which can be summarized by three observations: (i) the highest fluxes occurred at the first deployment (day # 12 – # 45; November – December 2010) for *G. ruber* and *O. universa*, and at the third deployment (day # 264 – # 319; July – September 2011). For *N. dutertrei* and *G. sacculifer*; (ii) an opposite trend can be observed for the fluxes of *G. ruber* (decreasing) in comparison to the *N. dutertrei* (increasing) from the first to the fourth deployment; and, interestingly (iii) for all species, the observed range variation for flux values at L=100m were higher than in its counterpart at L=50m at the first deployment whereas an opposite pattern was observed for third (day # 264 – # 319; July – September 2011) and fourth (day # 400 – # 477; December 2011 – February 2012) deployments.

2.5.2. Periodic regression

The results from the periodic regression demonstrate that there is a relationship between the lunar cycle and the foraminiferal fluxes for the first deployment (Table 1). However, the pattern does not

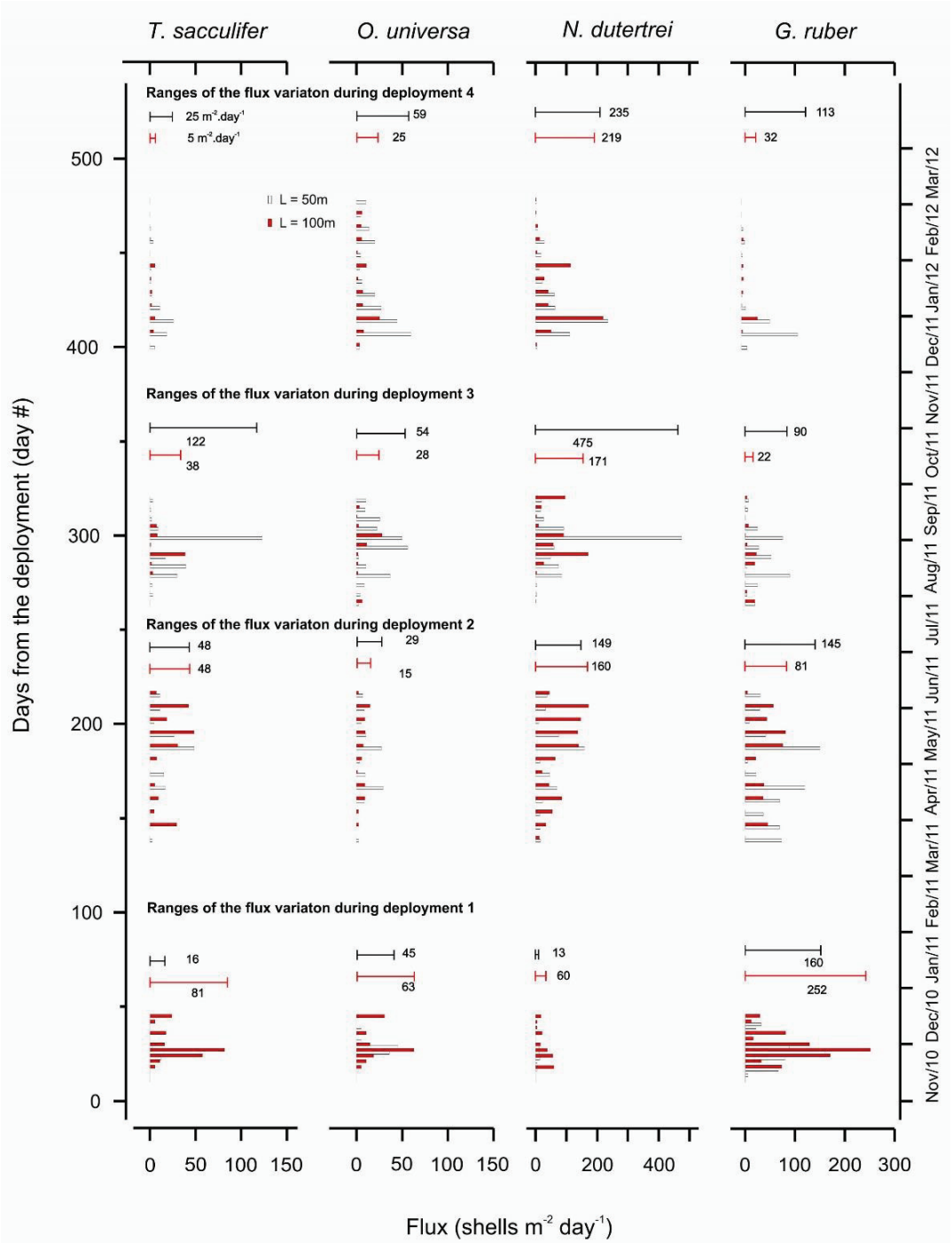

Figure 2: Planktonic foraminifera shell fluxes from the southwestern Atlantic for the entire time series. The time series is exhibited in sequential days (left axis), as described in the methods, and monthly (right axis). The white bars represent the fluxes for the upper trap (L = 50 m) and the red bars the fluxes for the deeper trap (L = 100 m). Ranges of the fluxes in both traps are represented by black (50 m) and red (100 m) lines.

hold when the entire time series is analyzed (Table 1). Data from the analysis is plotted only for the first deployment, which has the higher sampling resolution (3 days) and covers a full cycle, and for the entire time series (Figure 3). The data for the first de-

ployment systematically show highest fluxes for the first 3-7 lunar days and lowest around the 18-20 lunar days. For all species in both traps, except *O. universa* (L = 50m), the peaks are situated between 4 and 6 days after the full moon. The periodic regression against lunar day of the time series for the first deployment (Table 1) shows in most of the analyzed time series (per trap and species) that the periodic model with a synodic months period is statistically significant (p-value < 0.05) and explains about 50% of the variance in the data. The correlation values are surprisingly high, considering that our model assumes that the lunar reproductive cycle is the only factor modulating the shell flux of planktonic foraminifera. In contrast, periodic regression of shell flux series for the other three deployments and for the entire time series showed no clear pattern. This may indicate that the lunar signal is not constantly present with the same peak timing, or that its expression in the shell flux series may be masked by another environmental factor. An approach using spectral analysis would be able to disentangle even such a complex cyclic pattern in the lunar frequency band, but unfortunately such analyses is hampered by the presence of sampling gaps between the deployments.

2.5.3. Lunar phase vs. foraminifera flux datasets

In order to investigate whether flux variability corresponds to moon brightness and phases, we calculated mean fluxes for each moon phase (specifically, at its corresponding brightness interval). This approach allowed us to compare, for each trap, the mean log flux for each brightness interval and the corresponding moon phase – throughout the entire lunation (Figure 4).

Considering all deployments, from the NM to the first half of FQ, all species except *T. sacculifer* exhibited higher mean log fluxes at the L = 50 m trap compared to the L = 100 m trap. The mean log fluxes for *G. ruber, N. dutertrei, O. universa* and *T. sacculifer* show no significant change for the shallow trap during this period. From the first to the second half of the FQ, mean log fluxes for *G. ruber* at L = 50 m decreased, while for L = 100 m an increasing trend can be inferred for all species. An increase in the mean log flux values for both traps can be observed for all species except *O. universa* throughout the FM phase (first to second half). After the FM phase, distinctive flux patterns were observed for each species. For *G. ruber* and *N. dutertrei*, a decrease of mean log flux values for the shallow trap can be observed from the second half of the FM to the first half of LQ. Particularly, the L = 100 m mean log flux for *T. sacculifer* remained relative constant while at L = 50 m such values decreased from second half of FM to the first half of LQ. For all species, the mean log

(a) **Upper Trap / Deployment**

	1			2			3			4			all		
Species	*peak*	r^2	*p-value*	*peak*	r^2	*p-value*	*peak*	r^2	*p-value*	*peak*	r^2	*p-value*	*peak*	r^2	*p-value*
G. ruber	6.2	0.33	0.06	25.5	0.23	0.13	14.2	-0.10	0.63	3.8	-0.18	0.86	5.8	-0.02	0.55
T. sacculifer	5.7	0.56	0.01	27.5	0.01	0.38	24.7	-0.03	0.47	4.6	-0.18	0.86	2.3	0.01	0.29
N. dutertrei	4.6	0.50	0.02	24.5	0.17	0.18	26.0	-0.13	0.71	0.4	-0.21	0.97	2.2	-0.02	0.56
O. universa	9.4	0.49	0.02	25.2	0.15	0.19	22.9	0.01	0.38	4.2	-0.21	0.97	8.2	-0.04	0.83

(b) **Lower Trap / Deployment**

	1			2			3			4			all		
Species	*peak*	r^2	*p-value*	*peak*	r^2	*p-value*	*peak*	r^2	*p-value*	*peak*	r^2	*p-value*	*peak*	r^2	*p-value*
G. ruber	5.9	0.50	0.01	23.3	-0.17	0.84	9.8	0.25	0.11	11.3	-0.15	0.75	7.8	0.02	0.26
T. sacculifer	4.1	0.28	0.08	18.0	-0.10	0.62	4.3	-0.19	0.90	12.8	-0.10	0.64	6.0	-0.02	0.65
N. dutertrei	5.1	-0.05	0.52	18.2	-0.06	0.52	7.7	-0.05	0.51	12.4	-0.14	0.72	8.5	0.01	0.28
O. universa	4.2	0.39	0.04	18.9	-0.13	0.71	8.8	-0.04	0.49	10.4	-0.06	0.52	6.8	0.05	0.11

Table 1: Results from the periodic regression analysis and ANOVA for each species in both traps for the entire time series. The first panel (a) represents the upper trap and the panel below (b) represents the lower trap.

fluxes increase at both traps from the first to the second half of LQ. It is also noticeable that during the second half of the LQ, the four species exhibited maximal mean log fluxes for at least one trap, suggesting that the second half of the FQ may be related to the period of higher foraminifera shell deposition. For the upcoming NM, we observed a decrease in mean log fluxes for all species and both traps. This pattern suggests a connection between the lunar phase or moon brightness and mean foraminiferal fluxes patterns for the four chosen species throughout lunations, as will be discussed later.

2.5.4. Vertical migration

Vertical migration of the foraminifera species between both traps (Figure 5) was assessed for all deployments by the vertical flux proportionality, as outlined in section 2.3. Despite the assumption that the flux proportionality is directly linked to the vertical migration process, other potential biases, such as lateral advection, may influence the signal. These potential biases will be addressed in the discussion. Vertical migration is commonly associated with spinose species, since they are believed to shed their spines and sink to deeper waters to initiate gametogenesis. This process may

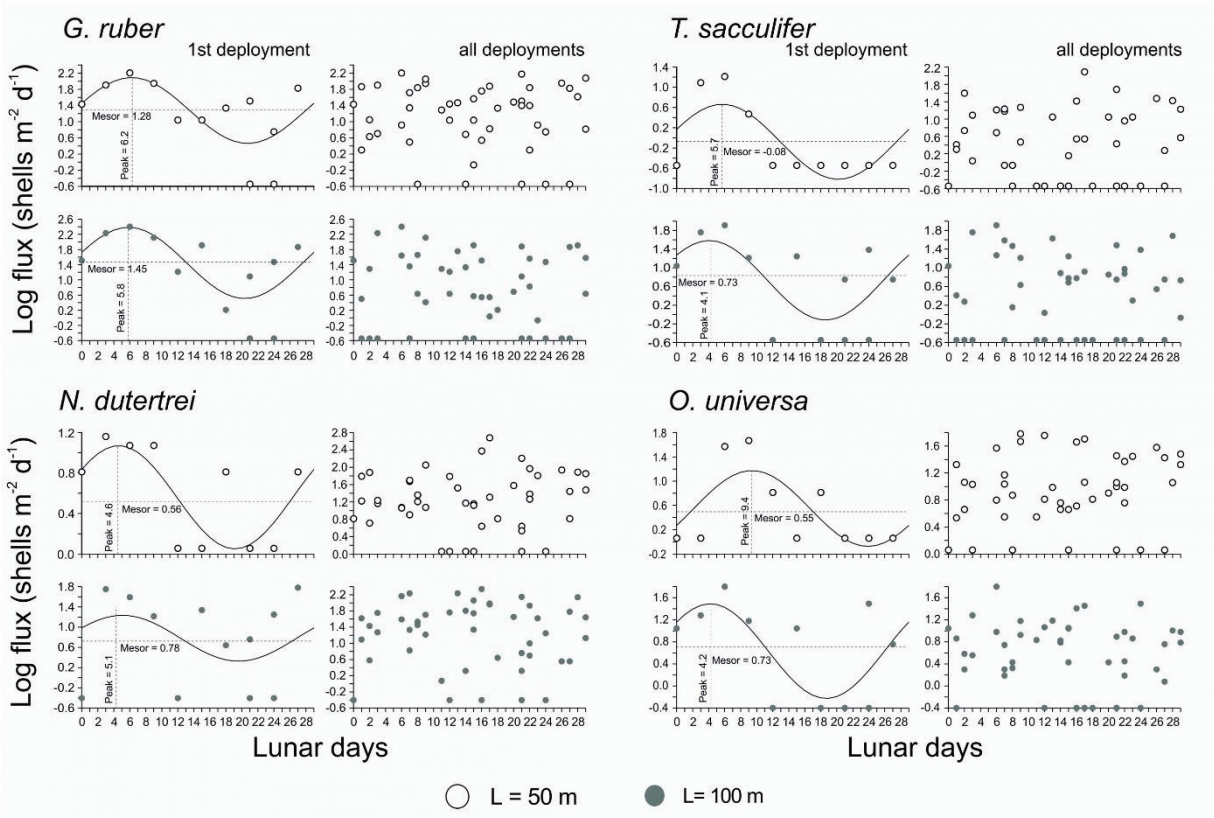

Figure 3: Log-transformed fluxes plotted against the lunar days. The periodic regression and its parameters are plotted for each species for the first deployment. The thick black line represents the best fit. The horizontal dashed line is the periodic mean (mesor) and the vertical dashed line is peak time. The entire time series is exhibited without the parameters. Data from the upper trap (L = 50 m) is represented by white circles and from the deeper trap (L = 100 m) by grey circles.

be triggered by changes in light intensity as they sink below the photic zone (Erez et al., 1991).

We observe values lower than 1.0 for the vertical migration during almost all lunar phases for *G. ruber* and *O. universa*, except on the first half of the LQ for *O. universa*. These values could indicate that lateral advection or collection of live non-sinking specimens in the shallower trap influence their fluxes. However, for *T. sacculifer*, especially during the LQ and NM, we observe values higher than 1.0, which indicate that a large part of the flux during these phases is composed by specimens that died below 50 m. Values higher than 1.0 are also observed for *N. dutertrei*, although the variation is weaker. Despite these observations, all the species have their minimum ratio values during the NM phase that occur right after the LQ and at the first half of the FQ, and their maximum ratio values during the LQ, which indicate that all species have higher flux values in the deeper trap (100 m) during the last quarter.

2.6. Discussion

2.6.1. Lunar reproduction cycles

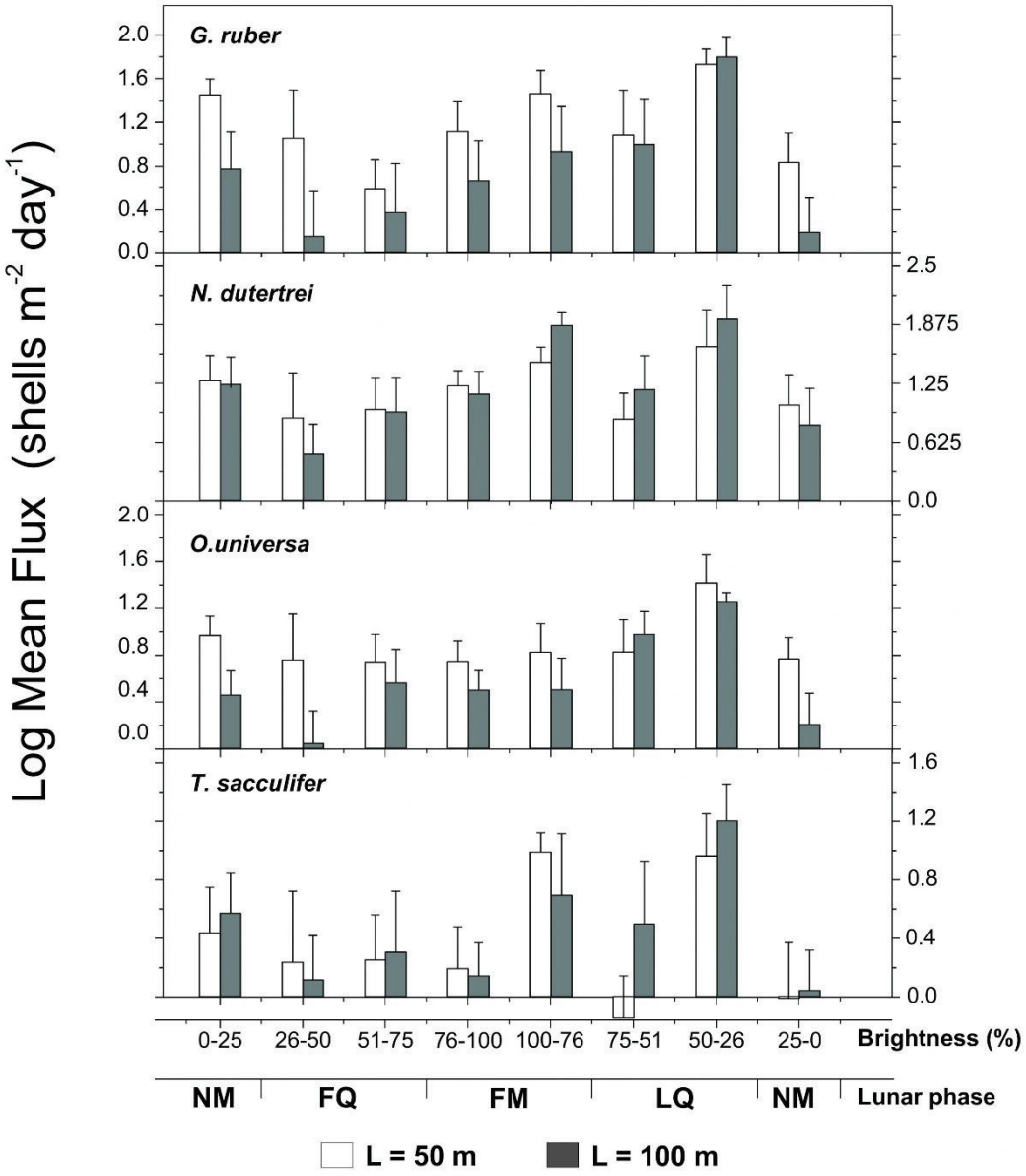

Figure 4: Mean log-transformed fluxes per lunar phase using all deployments. The intervals for each phase where defined using the lunar brightness values. The white bars represent the data from the upper trap (L = 50 m) and the grey bars from the deeper trap (L = 100 m). The bars represent the mean logarithmic flux for each phase and the lines above each bar represent the standard deviation.

Previously, lunar cyclicity in planktonic foraminiferal reproduction was studied from sediment traps moored at 100 m or deeper (Kawahata et al., 2002; Lončarić et al., 2005; Lin, 2014; Jonkers et al., 2015). In our study, the sediment traps were placed in a shallow water column on the continental shelf and not deep in the open ocean. Hence, lateral advection could potentially transport planktonic foraminifera and bias the flux rates recorded in the traps. The current-meter data (Appendix B) shows indeed mean current velocities higher than 12 cm/s (Barker et al., 1988) and an influence of

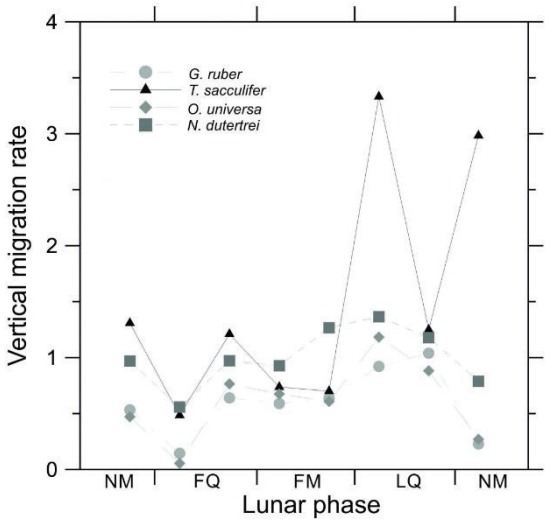

Figure 5: Estimate of the vertical migration for each species per lunar phase. The vertical flux proportionality is described in the methods (Section 2.3) and represents the difference of fluxes between the traps.

lateral advection on our planktonic foraminiferal fluxes seems possible. However, this putative influence is difficult to quantify, since we did not perform measurements of size or density of the foraminiferal shells. These parameters are crucial for the determination of particle velocities and consequently the potential alteration of fluxes caused by lateral transport (Barker et al. 1988). Assuming a large size fraction (>125 μm) and a density value higher than 1.6 g/cm^3, which would be reasonable since calcite density is close to 2.71 g/cm^3, the flux change could vary from -50% to +40%, which means that the trap efficiency could either decrease or increase (Barker et al. 1988). Furthermore, other studies pointed out that the traps may catch larger foraminifera with higher efficiency, since the hydrodynamics for solid particles is different from that for fine particles or aggregates (Gardner, 2000; Yu et al., 2001). Consequently, we can neither exclude nor quantify a potential bias through lateral advection. However, as pointed out by Zaric et al. (2005), even if the lateral component in particle fluxes cannot be excluded, lateral displacement is likely not a significant factor affecting sediment trap time series, when the size and weight of foraminiferal shells are considered. We also note that in our case, the vertical profile of current velocity and current direction appears to have remained relatively stable between deployments (Appendix B) and should have thus affected all sampling periods equally.

The shallow water depth of our trap location might also lead to generally lower abundance of planktonic foraminifers, compared to the open ocean locations, due to ecological exclusion (Schmuker, 2000). However, if lunar cycles exist, they should still be present in our time series, because foraminifera occur abundantly on the studied outer shelf. The mean fluxes observed in the studied period (Figure 2) correspond well to those reported for the same subtropical province (Bé, 1977) by Lončarić et al. (2005), indicating that the flux recorded by the trap corresponded to a normal population that was not significantly affected by ecological exclusion from the shallow shelf.

Because of the shallow position of our sediment traps, it cannot be excluded that a certain part of the flux represents living specimens that were caught by the traps during passive or active vertical migration in the upper water layer. We consider the shallow position of the trap unlikely to have biased the results because the mixed layer in the region is typically shallower than 50 m (Cerda and Castro, 2014) and the flux of trapped specimens should have been proportionate to the population density (Figure 3). Irrespective of the presence or absence of a lunar reproductive cycle, the trapping of live specimens would thus only elevate the baseline flux value, but not induce any artificial cycles.

Due to the shallow position of the traps, resuspension of sediments from the sea floor could be another potential bias. However, our analysis of the current meter data (Appendix C) demonstrated that resuspension is restricted to 5 meters above the seafloor and very probably did not reach the traps. The study of Albuquerque et al. (2014) also pointed out that resuspension was either not significant or even non-detectable in these experiments.

Assuming that the flux variability represents a largely undisturbed vertical flux of a representative population of planktonic foraminifera, we can search for the signature of lunar synchronization. The periodic regression for the first (3 day resolution) deployment shows that in both traps and for all species, except *O. universa* (L = 50m), there is a significant periodic component with a peak approximately 4 to 6 days after the full moon (Figure 3). However, the periodic regression for the other deployments, and the entire time series showed no regular peak time. Our results for the first deployment could be in agreement with reproduction triggered by the full moon, but we stress that the period of reproductive cycle may be not stable. In the case of reproduction triggered by the full moon, the reproductive process would begin at or shortly after the full moon, be completed within about a day (compare reproductive cycle duration for *H. pelagica*, Spindler et al., 1979) with dead shells arriving in the trap almost immediately afterwards. Such a synchronization would also be consistent with the large drop in shell fluxes in the period immediately following the high-flux interval. This drop in shell flux may represent a period where most of the population consists of small juveniles not captured by the trap and where the adult population responsible for the observed shell flux has been largely depleted by the reproductive event. This interpretation requires that not all specimens of the analyzed species participated in the synchronized reproduction, but a smaller part of the adult population remained alive and contributed to the shell flux outside the main reproductive window (Bijma et al., 1990a). Depending on species and trap depth, the shell flux as-

sociated with the reproductive window after the full moon would account for 31-52 % of the total flux of that species when all deployments are considered together, except for 21 % of *T. sacculifer* flux for the shallow trap (Figure 4).

The relationship between the putative reproductive event and the lunations as observed in our data is consistent with that deduced for *H. pelagica* by Spindler et al. (1979) and for *G. ruber* in the Gulf of Mexico by Jonkers et al. (2015). The observation of *T. sacculifer* decreasing in abundance in plankton tows already during the full moon (Bijma et al., 1990a) may also be consistent with reproduction after the full moon. If we assume that, the pattern observed by Bijma et al. (1990a) represents a vertical migration (see also Erez et al., 1991) prior to reproduction, as also indicated by the higher flux of this species in the deeper trap observed in our data (Figure 5). However, since the mean current speeds are higher than 10 cm/s in our region, the interpretation of the vertical flux proportionality may be biased.

Jonkers et al. (2015) showed that *O. universa* and *T. sacculifer* shell fluxes in the Gulf of Mexico peaked at the full moon and Kawahata et al. (2002) also observed peaks in flux at full moon for *T. sacculifer*. Because in both cases the traps were deployed deeper (> 400m) than in our study (50 and 100m) these observations can only be interpreted as a primary offset comparative to our results, with reproduction being triggered prior to full moon. These findings indicate that the flux peaks may not consistently correspond to a specific lunar phase. It is possible that the exact phasing depends on location or reflects the influence of other environmental factors that modulate the factor triggering reproduction. Another possibility is that intensified sedimentation of planktonic foraminifera species due to the formation of aggregates (Turner, 2002) is affecting the flux pattern, which would also lead to synchronous fluxes. However, foraminiferal tests are quite large compared to other particles and do not need to be scavenged in order to sink (De La Rocha and Passow, 2007). In fact, La Rocha and Passow (2007) observed a very low correlation (r^2 = 0.25) between POC and foraminiferal fluxes at an Atlantic site. In addition, aggregates only seem to have major influence on the transport of juvenile planktonic foraminifera (Bé et al., 1985), which were not analyzed here. Based on the previous arguments, we think that aggregate formation plays a minor role in the flux variations and is not very a likely cause of synchronous flux patterns. We note that both in our study and in that by Jonkers et al. (2015) almost all analyzed species had synchronous peak fluxes. This may indicate that the reproduction is triggered collectively, but the exact period (lunar phase) when all species present peak fluxes may vary.

The temporal stability of the flux peaks in the studied species has been investigated by joint analysis of flux data covering the entire deployment period of one year. Whereas the periodic regression fails to identify any cyclicity in the merged data (Figure 3), the mean fluxes for each lunar phase (Figure 4) indicate a common pattern of higher fluxes at the end of the last quarter. Instability of the period between two reproductive events would lead to precisely such a weakening of the periodic signal. This effect is further enhanced by the coarser resolution of the remaining part of the flux series, such that the periodic signal is no longer detectable. Similar phenomena can provide an explanation for the results by Lončarić et al. (2005), who found pronounced lunar cyclicity in the spectral analysis only for *H. pelagica*. We speculate that the strict endogenous timing of reproduction of *H. pelagica* (Spindler et al., 1979) leads to a strong signal in the flux data despite the low resolution (8 days) of the traps. In contrast, the synchronization of reproduction in the remaining species may follow an external trigger, leading to variable period and signal attenuation in the flux data.

Our results thus seem to support the hypothesis that reproductive synchronization occurs in planktonic foraminifera. This reproductive mode seems to be widespread among planktonic foraminifera (Jonkers et al., 2015), but it is still not clear whether it is present universally, whether it occurs in all marine provinces and whether and how it is related to lunar cyclicity. Similar to the findings of Jonkers et al. (2015) we detected a lunar cycle in the flux series of *N. dutertrei* (Figure 3). Interestingly, this species shows higher fluxes in the deeper trap for most of the trap series, suggesting that a significant portion of the population constantly lives below 50 m, which is consistent with a deeper habitat indicated for this species by geochemical studies (e.g., Wejnert et al., 2013). Clearly, the short-term dynamics of planktonic foraminiferal populations, including their reproductive behavior, still deserves further investigations, and studies applying stratified high-resolution sediment trap designs have an excellent potential to support such investigations. Although lunar reproductive cycles appear to play an important role for the modulation of the foraminiferal fluxes, there is not yet a consensus regarding the timing of the flux, the involved species, and if the cycle is endogenous or triggered by an exogenous force.

2.6.2. Other factors controlling the fluxes of planktonic foraminifera

In order to understand the short-term (lunar) variability in planktonic foraminifera shell fluxes, other environmental factors influencing their magnitude and also the detectability of the lunar periodicity have to be taken in account. Sediment trap studies have shown that planktonic foraminiferal

fluxes can be influenced by seasonality, physical circulation patterns, productivity and the species reproductive cycles (Sautter and Thunell, 1991; Kincaid et al., 2000; King and Howard, 2001; Kawahata et al., 2002; Zaric et al., 2005; Rigual-Hernandez et al., 2012).

Among these factors, sea-surface temperature is one of the most important parameters controlling the distribution and abundance of planktonic foraminifera (Bé and Tolderlund, 1971). Thermal preferences are different between planktonic foraminiferal species, which could explain interspecific flux differences (Bijma et al., 1990b; Zaric et al., 2005). Food supply can be also an important factor modulating foraminiferal fluxes (Watkins et al., 1996). Species without symbionts, like *G. bulloides*, are dependent on the productivity of the environment, while species with symbionts benefit from the photosynthetic activity and are more independent in respect to changes in food supply (Sautter and Thunell, 1991; Watkins et al., 1996). For symbiont-bearing species like *G. ruber* the light intensity and consequently the depth of the photic zone is also a relevant element. Other possible influences are vertical advection, i.e. up- or downwelling and the intensity of lateral displacement.

To place the probable influence of lunar cyclicity on the foraminiferal fluxes into a longer-term context, we plotted the flux of *G. ruber* for the shallower and deeper traps throughout the one-year deployment period along other parameters (temperature, depth of the euphotic zone, chlorophyll and wind stress curl) in order to assess other factors controlling the flux (Figure 6). The variability of productivity, inferred from the chlorophyll concentration and consequently the depth of the euphotic zone can cause changes in the foraminiferal fluxes (Watkins et al., 1996). However, in our data, the variability of the chlorophyll concentration or the depth of the euphotic zone does not show any direct relationship to the fluxes. There does not seem to be any phase lag relationship either, linking episodes of higher food availability earlier to higher flux later (Figure 6).

Alternatively, for symbiont-hosting species, the intensity of light might be an important factor influencing their symbiont activity. To test whether times with higher light intensity are indeed associated with higher fluxes, we compared the fluxes with moon brightness and cloud coverage (Figure 6). Although we do not observe any direct effect of cloud coverage on flux timing or magnitude, there may be a relationship between cloud coverage and moon phase on

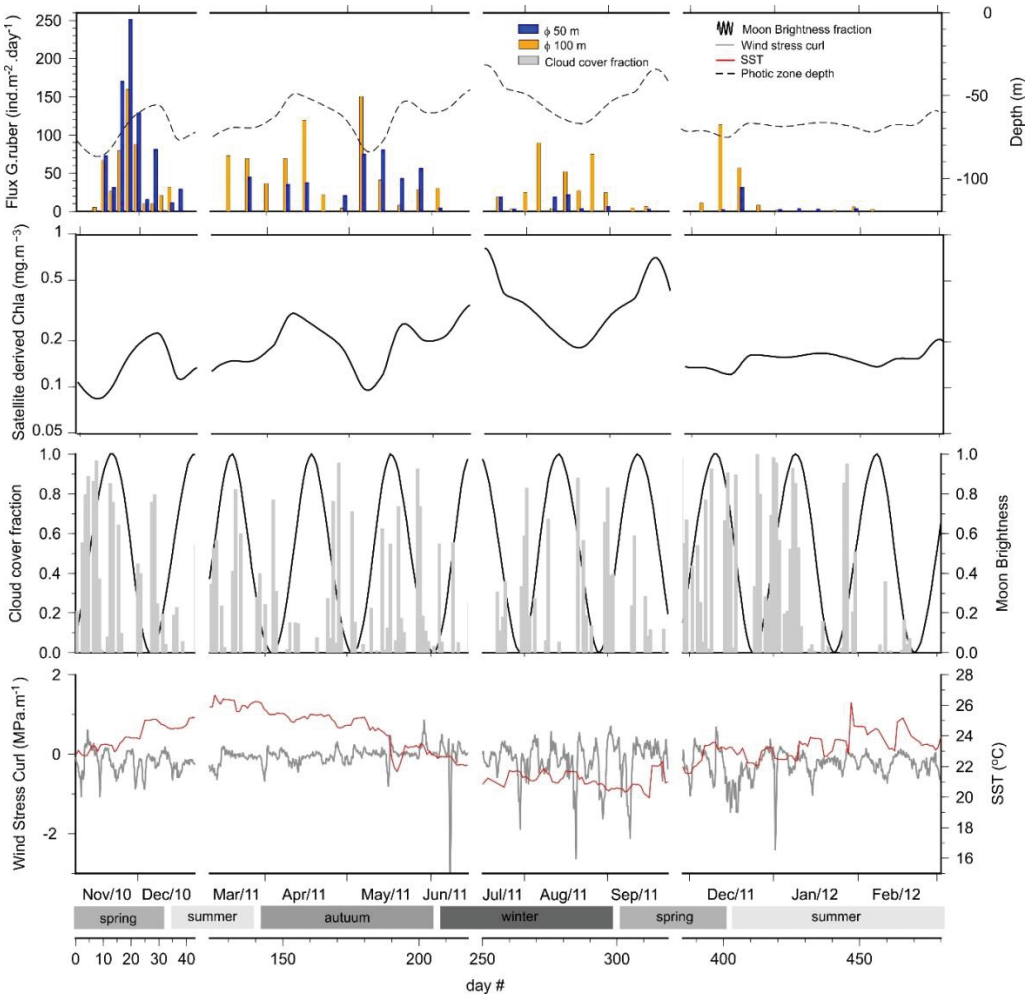

Figure 6: Fluxes of *G. ruber* for the entire time series exhibited with multiple parameters. Colored bars represent the *G. ruber* fluxes for 50 m (blue) and 100 m (yellow). The dashed line represents the depth of the photic zone estimated from MODIS/AQUA Chlorophyll 8-day data. The solid black line in the panel below represents the Chlorophyll-a derived from MODIS/AQUA. The moon brightness (thick black line) is plotted with the cloud cover (grey bars) indicating periods with high/low light intensity. Cloud cover was extracted from the NASA catalog dataset (OMTO3e). The SST (red line) is plotted with the wind stress curl (grey line) showing the main physical oceanographic parameters that influence the study area. Temperature was extracted from NOAA OceanWatch program (ID: satellite.BA.ssta.5day) and wind stress curl data is derived from NOAA CoastWatch (ID: erdQAdivmodmday).

the triggering of reproduction. For example, during the high-resolution sampling period in November 2010, the sky was cloudy during full moon and maximum fluxes appeared 5-7 days after the full moon. A similar situation occurred in December, April and August 2011, whereas peak flux occurred at full moon, when the sky was cloudless. These observations would support an exogenous forcing of the lunar cycles in species other than *H. pelagica*, as suggested by Jonkers et al. (2015).

A closer investigation of *G. ruber* fluxes in other deployments of our time se-

ries is further hampered by the significant decrease of *G. ruber* fluxes from spring 2010 to winter 2011 (Figure 6). This steady decrease in the fluxes of *G. ruber* is probably linked to seasonal variability (Sautter and Thunell, 1991, Jonkers and Kucera, 2015). A decrease in *G. ruber* fluxes occurs in periods with lower temperature and higher variability of the wind stress curl. This wind stress curl variability is related to the intrusions of the SACW in the upper layers at our site (Castelao and Barth, 2006). Since *G. ruber* is a species related to warm and oligotrophic waters, these conditions are unfavorable for the population (Bé and Tolderlund, 1971). At the same time, these conditions are favorable for *N. dutertrei* (Figure 2), which is associated with lower temperatures, variations in the thermocline depth and increased productivity (Sautter and Thunell, 1991). Thus, we can conclude that the seasonal variability is an important modulator of planktonic foraminiferal fluxes on longer than monthly time scales in this area. Jonkers et al. (2015) in the Gulf of Mexico also noticed the influence of seasonal trend in the shell fluxes and its influence on the detection of lunar cycles.

2.7. Conclusions

We found evidence for synchronized fluxes of four species of planktonic foraminifera (*G. ruber*, *T. sacculifer*, *N. dutertrei* and *O. universa*) at the continental margin off Brazil in the southwestern Atlantic Ocean. For the first deployment, the shell fluxes increase after the full moon, with the highest flux rates during the last quarter. Periodic regression indicates that the maximum flux occurs approximately 4-6 days after full moon. These findings appear consistent with the concept of reproduction in planktonic foraminifera being episodic and synchronized by lunar periodicity. However, periodic regression for the other deployments and for the entire dataset suggests that the period of the reproductive cycle cannot be strictly synchronous with the phases of the moon during each month. Although the reproductive cycle is not the only factor that determines the flux of planktonic foraminifera in the water column, this study demonstrates its relevance in modulating fluxes of *G. ruber*, *T. sacculifer*, *N. dutertrei* and *O. universa*. These are clearly episodic with peaks accounting for up to one half of total flux. Whilst the average spacing of the peaks seems to point to lunar periodicity, the reproduction in these species is unlikely to be controlled by an endogenous clock. Instead, we suggest that lunar reproductive cycles may be triggered by an exogenous factor and the variable expression of this factor between months leads to uneven peak spacing. Further high-resolution studies are needed to better constrain the lunar modulation of foraminiferal carbonate export to the sea floor.

2.8. Acknowledgments

The Geochemistry Network from PETROBRAS/National Petroleum Agency (ANP) of Brazil (Grant 0050.004388.08.9) financially supported this study. A.L.S. Albuquerque is senior scholar from CNPq (National Council for the Development of Science and Technology, Brazil, Grant 306385/2013-9). The CNPq also financially supported Igor Venancio with a scholarship from the CsF ("Ciencia sem Fronteiras") project (Grant 248819/2013-5). We are also especially grateful to the two reviewers for their valuable comments, which strengthened the manuscript.

2.9. References

Albuquerque, A.L.S., Belem, A.L., Zuluaga, F.J.B., Cordeiro, L.G.M., Mendoza, U., Knoppers B.A., Gurgel, M.H.C., Meyers, P.A., Capilla, R., 2014. Particle Fluxes and Bulk Geochemical Characterization of the Cabo Frio Upwelling System in Southeastern Brazil: Sediment Trap Experiments between Spring 2010 and Summer 2012. An. Acad. Bras. Cienc. 86, 601-619.

Al-Sabouni, N., Kucera, M., Schmidt, D.N., 2007. Vertical niche separation control of diversity and size disparity in planktonic foraminifera. Mar. Micropaleontol. 63, 75-90.

Baker, E.T., Milburn, H.B., Tennant, D.A., 1988. Field assessment of sediment trap efficiency under varying flow conditions. J. Mar. Res. 46, 573-592.

Bé, A.W.H., Tolderlund, D.S., 1971. Distribution and ecology of living planktonic foraminifera in surface waters of the Atlantic and Indian Oceans. In: Funnell, B.M., Riedel, W.R. (Eds.), The Micropaleontology of the Oceans. Cambridge University Press, New York, pp. 105–139.

Bé, A.W.H., 1977. An ecological, zoogeographic and taxonomic review of recent planktonic foraminifera. In: Ramsay, A.T.S. (Ed.), Oceanic Micropalaeontology. Academic Press, London, pp. 1–100.

Bé, A.W.H., Bishop, J.K.B., Sverdlove, M.S., Gardner, W.D., 1985. Standing stock, vertical distribution and flux of planktonic foraminifera in the Panama basin. Mar. Micropaleontol. 9, 307-333.

Belem, A., Castelao, R., Albuquerque, A.L., 2013. Controls of subsurface temperature variability in a western boundary upwelling system. Geophys. Res. Lett. 40, 1362-1366.

Bijma, J., Erez, J., Hemleben, C., 1990. Lunar and semi-lunar reproductive cycles in some spinose planktonic foraminifers. J. Foraminifer. Res. 20, 117–127.

Bjima, J., Faber Jr, W.W., Hemleben, C., 1990. Temperature and salinity limits for growth and survival of some planktonic foraminifers in laboratory cultures. J. Foraminifer. Res. 20, 95-116.

Bijma, J., Hemleben, C., Wellnitz, K., 1994. Lunar-influenced carbonate flux of the planktic foraminifer *Globigerinoides sacculifer* (Brady) from the central Red Sea. Deep-Sea Res. I 41, 511–530.

Campos, E.J.D., Velhote, D., Silveira, I.C.A., 2000. Shelf break upwelling driven by Brazil Current cyclonic meanders. Geophys. Res. Lett. 27, 751–754.

Castelao, R.M., Barth, J.A., 2006 Upwelling around Cabo Frio, Brazil: The importance of wind stress curl. Geophys. Res. Lett. 33, L03602.

Castelao, R.M., 2012. Sea surface temperature and wind stress curl variability near a cape. J. Phys. Oceanogr. 42, 2073-2087.

Castro, B.M., 2014. Summer/winter stratification variability in the central part of the South Brazil Bight. Cont. Shelf Res. 89, 15-23.

Castro, B.M., Miranda, L.B., 1998. Physical oceanography of the western Atlantic continental shelf located between 4N and 34S, in

The Sea, vol. 11, edited by A. R. Robinson, and K. H. Brink, pp. 209–251, John Wiley, Hoboken, N. J.

Cerda, C., Castro, B.M., 2014. Hydrographic climatology of South Brazil Bight shelf waters between Sao Sebastiao (24°S) and Cabo Sao Tome (22°S). Cont. Shelf Res. 89, 5-14.

deBruyn, A.M.H., and Meeuwig, J.J., 2001. Detecting lunar cycles in marine ecology: periodic regression versus categorical ANOVA. Mar. Ecol. Prog. Ser. 214, 307-310.

De La Rocha, C.L. and Passow, U., 2007. Factors influencing the sinking of POC and the efficiency of the biological carbon pump. Deep-Sea Res. II 54, 639-658.

Erez, J., Almogi-Labin, A., Avraham, S., 1991. On the life history of planktonic foraminifera: lunar reproduction cycle in Globigerinoides sacculifer (Brady). Paleoceanography 6, 295–306.

Gardner, W.D., 2000. Sediment trap sampling in surface waters. In: Hanson, R.B., Ducklow, H.W., Field, J.G. (Eds.), The Changing Ocean Carbon Cycle: A Midterm Synthesis of the Joint Ocean Global Flux Study. Cambridge Univ. Press, Cambridge, UK, pp. 240 – 281.

Goswami, S.C., 2004. Zooplankton Methodology, Collection & Identification a field manual, 1st ed., Goa: National Institute of Oceanography, 26 p.

Hemleben, C., Spindler, M., Anderson, O.R., 1989. Modern Planktonic Foraminifera. Springer, New York (363p).

Ikeda, Y., Miranda, L.B., Miniussi, I.C., 1974. Observations on stages of upwelling in the region of Cabo Frio (Brazil) as conducted by continuous surface temperature and salinity measurements. Bol. Inst. Oceanogr. 23, 33–46.

Jonkers, L., Reynolds, C.E., Richey, J., Hall, I.R., 2015. Lunar periodicity in the shell flux of some planktonic foraminifera in the Gulf of Mexico. Biogeosciences Discuss. 11, 17187-17205.

Jonkers, L., Kucera, M., 2015. Global analysis of seasonality in the shell flux of extant planktonic Foraminifera. Biogeosciences Discuss. 12, 2207-2226.

Kawahata, H., Nishimura, A., Gagan, M.K., 2002. Seasonal change in foraminiferal production in the western equatorial Pacific warm pool: evidence from sediment trap experiments. Deep-Sea Res. II 49, 2783–2800.

Khripounoff, A., Vangriesheim, A., Crassous, P., 1998. Vertical and temporal variations of particle fluxes in the deep tropical atlantic. Deep Sea Res. Part I: Oceanographic Research Papers 45, 193-216.

Kincaid, E., Thunell, R.C., Le, J., Lange, C.B., Weinheimer, A.L., Reid, F.M.H., 2000. Planktonic foraminiferal fluxes in the Santa Barbara Basin: response to seasonal and interannual hydrographic changes. Deep Sea Res. Part II: Topical Studies in Oceanography 47, 1157–1176.

King, A.L., Howard, W.R., 2001. Seasonality of foraminiferal flux in sediment traps at Chatham Rise, SW Pacific: implications for paleotemperature estimates. Deep-Sea Res. Part I 48, 1687– 1708.

Kuroyanagi, A., Kawahata, H., Nishi, H., Honda, M.C., 2008. Seasonal to interannual changes in planktonic foraminiferal assemblages in the northwestern North Pacific: Sediment trap results encompassing a warm period related to El Niño. Palaeogeogr. Palaeoclimatol. Palaeoecol. 262, 107-127.

Lessa, D.V.O., Portilho-Ramos, R., Barbosa, C.F., Silva, A.R., Belem, A., Turcq, B., Albuquerque, A.L.S., 2014. Planktonic foraminifera in the sediment of a western boundary upwelling system off Cabo Frio, Brazil. Mar. Micropaleontol. 106, 55-68.

Lin, H.L., 2014. The seasonal succession of modern planktonic foraminifera: Sediment traps observations from southwest Taiwan waters. Cont. Shelf Res. 84, 13-22.

Lončarić, N., Brummer, G.A., Kroon, D., 2005. Lunar cycles and seasonal variations in deposition fluxes of planktic foraminiferal

shell carbonate to the deep South Atlantic (central Walvis Ridge). Deep Sea Res. Part I 52, 1178-1188.

Matsuura, Y., 1996. A probable cause of recruitment failure of Brazilian Sardine (Sardinella aurita) population during the 1974/75 spawning season. South African J. Mar. Sci. 17, 29-35.

Peterson, R.G., Stramma, L., 1991. Upper-level circulation in the South Atlantic Ocean. Prog. in Oceanogr. 26, 1-73.

Rigual-Hernández, A.S., Sierro, F.J., Bárcena, M.A., Flores, J.A., Heussner, S., 2012. Seasonal and interannual changes of planktic foraminiferal fluxes in the Gulf of Lions (NW Mediterranean) and their implications for paleoceanographic studies: Two 12-year sediment trap records. Deep-Sea Res. 66, 26–40.

Rodrigues, R.R., Lorenzzetti, J.A., 2001. A numerical study of theeffects of bottom topography and coastline geometry on the Southeast Brazilian coastal upwelling. Cont. Shelf Res. 21, 371–394.

Sautter, L.R., Thunell, R.C., 1991. Planktonic foraminiferal response to upwelling and seasonal hydrographic conditions: sediment trap results from San Pedro Basin, Southern California Bight. J. Foraminifer. Res. 21, 347-363.

Schiebel, R., 2002. Planktic foraminiferal sedimentation and the marine calcite budget. Glob. Biogeochem. Cycles 16, 1065.

Schlitzer, R., 2014. Ocean Data View, http://odv.awi.de.

Schmuker, B., 2000. The influence of shelf vicinity on the distribution of planktic foraminifera south of Puerto Rico. Mar. Geol. 166, 125-143.

Silveira, I.C.A., Lima, J.A.M., Schimdt, A.C.K., Ceccopierib, W., Sartori, A., Francisco, C.P.F., Fontes, R.F.C., 2008. Is the meander growth in the Brazil Current system off Southeast Brazil due to baroclinic instability? Dynamics of Atmospheres and Oceans 45, 187-207.

Silveira, I.C.A., Schmidt, A.C.K., Campos, E.J.D., Godoi, S.S., Ikeda, Y., 2000. The Brazil Current off the Eastern Brazilian Coast. Rev. Bras. Oceanogr. 48, 171–183.

Skov, M.W., Hartnoll, R.G., Ruwa, R.K., Shunula, J.P., Vannini, M., Cannici, S., 2005 Marching to a different drummer: crabs synchronize reproduction to a 14-month lunar-tidal cycle. Ecology 86, 1164-1171.

Spindler, M., Hemleben, C., Bayer, U., Bé, A.W.H., Anderson, O.R., 1979. Lunar periodicity of reproduction in the planktonic foraminifer Hastigerina pelagica. Mar. Ecol. Prog. Series 1, 61–64.

Stramma, L., England, M., 1999. On the water masses and mean circulation of the South Atlantic Ocean. J. Geophys. Res. 104, 20863-20883.

Turner, J.T., 2002. Zooplankton fecal pellets, marine snow and sinking phytoplankton blooms. Aquat. Microb. Ecol. 27, 57-102.

Venancio, I.M., Belem, A.L., Santos, T.H.R., Zucchi, M.R., Azevedo, A.E.G., Capilla, R., Albuquerque, A.L.S., 2014. Influence of continental shelf processes in the water mass balance and productivity from stable isotope data on the Southeastern Brazilian coast. J. Mar Syst. 139, 241-247.

Walsh, J.J., 1988. On the Nature of Continental Shelves.Academic Press, New York (520p).

Watkins, J.M., Mix, A.C., Wilson, J., 1996. Living planktic foraminifera: tracers of circulation and productivity regimes in the central equatorial Pacific. Deep Sea Res. Part II 43, 1257-1282.

Wejnert, K.E., Thunell, R.C., Astor, Y., 2013. Comparison of species-specific oxygen isotope paleotemperature equations: Sensitivity analysis using planktonic foraminifera from the Cariaco Basin, Venezuela. Mar. Micropaleontol. 101, 76-88.

Yu, E.F., Francois, R., Bacon, M.P., Honjo, S., Fleer, A.P., Manganini, S.J., Rutgers van der Loeff, M.M., Ittekot, V., 2001. Trapping efficiency of bottom tethered sediment traps estimated from the intercepted fluxes of

230Th and 231Pa, Deep Sea Res., Part I, 48, 865-889.

Zakai, D., Dubinsky, Z., Avishai, A., Caaras, T., Chadwick, N.E., 2006. Lunar periodicity of planula release in the reef-building coral *Stylophora pistillata*. Mar. Ecol. Prog. Series 311, 93-102.

Zaric, S., Donner, B., Fischer, G., Mulitza, S., Wefer, G., 2005. Sensitivity of planktic foraminifera to sea surface temperature and export production as derived from sediment trap data. Mar. Micropaleontol. 55, 75–105.

2.10. Supplementary material

Appendix A: Table with complete dataset: deployments, traps, cup number, sequential day (day #), dates (opening and closing), sample integration (SI), moon brightness (MB), moon phase (MP), abundances (AA) and fluxes.

Deploy	Trap	Cup	Day (#)	Date (open)	Date (close)	SI	MB	MP	AA G. ruber	Flux G. ruber	AA N. dutertrei	Flux N. dutertrei	AA G. sacculifer	Flux T. sacculifer	AA O. universa	Flux O. universa
1	50	1	12	11.11.10	13.11.10	3	0.36	FQ	0	0,0	0	0,0	0	0,0	0	0,0
1	50	2	15	14.11.10	16.11.10	3	0.64	FQ	4	5,3	0	0,0	0	0,0	0	0,0
1	50	3	18	17.11.10	19.11.10	3	0.88	FM	50	66,7	4	5,3	0	0,0	0	0,0
1	50	4	21	20.11.10	22.11.10	3	1.00	FM	20	26,7	4	5,3	0	0,0	0	0,0
1	50	5	24	23.11.10	25.11.10	3	0.93	FM	60	80,0	10	13,3	9	12,0	0	0,0
1	50	6	27	26.11.10	28.11.10	3	0.69	LQ	120	160,0	8	10,7	12	16,0	27	36,0
1	50	7	30	29.11.10	01.12.10	3	0.35	LQ	66	88,0	8	10,7	2	2,7	34	45,3
1	50	8	33	02.12.10	04.12.10	3	0.08	NM	8	10,7	0	0,0	0	0,0	4	5,3
1	50	9	36	05.12.10	07.12.10	3	0.00	NM	8	10,7	0	0,0	0	0,0	0	0,0
1	50	10	39	08.12.10	10.12.10	3	0.12	NM	16	21,3	4	5,3	0	0,0	4	5,3
1	50	11	42	11.12.10	13.12.10	3	0.37	FQ	24	32,0	0	0,0	0	0,0	0	0,0
1	50	12	45	14.12.10	16.12.10	3	0.65	FQ	0	0,0	0	0,0	0	0,0	0	0,0
1	100	1	12	11.11.10	13.11.10	3	0.36	FQ	0	0,0	0	0,0	0	0,0	0	0,0
1	100	2	15	14.11.10	16.11.10	3	0.64	FQ	0	0,0	0	0,0	0	0,0	0	0,0
1	100	3	18	17.11.10	19.11.10	3	0.88	FM	55	73,3	45	60,0	4	5,3	4	5,3
1	100	4	21	20.11.10	22.11.10	3	1.00	FM	24	32,0	0	0,0	8	10,7	8	10,7
1	100	5	24	23.11.10	25.11.10	3	0.93	FM	128	170,7	42	56,0	43	57,3	14	18,7
1	100	6	27	26.11.10	28.11.10	3	0.69	LQ	189	252,0	29	38,6	61	81,3	47	62,7
1	100	7	30	29.11.10	01.12.10	3	0.35	LQ	97	129,3	12	16,0	12	16,0	11	14,7
1	100	8	33	02.12.10	04.12.10	3	0.08	NM	12	16,0	0	0,0	0	0,0	0	0,0
1	100	9	36	05.12.10	07.12.10	3	0.00	NM	61	81,3	16	21,3	13	17,3	8	10,7
1	100	10	39	08.12.10	10.12.10	3	0.12	NM	1	1,3	3	4,0	0	0,0	0	0,0
1	100	11	42	11.12.10	13.12.10	3	0.37	FQ	9	12,0	4	5,3	4	5,3	0	0,0
1	100	12	45	14.12.10	16.12.10	3	0.65	FQ	22	29,3	13	17,3	18	24,0	23	30,7
2	50	1	138	15.03.11	21.03.11	7	0.96	FM	128	73,1	27	15,4	4	2,3	4	2,3
2	50	2	145	22.03.11	28.03.11	7	0.64	LQ	121	69,1	26	14,8	0	0,0	0	0,0
2	50	3	152	29.03.11	04.04.11	7	0.05	NM	64	36,6	23	13,1	0	0,0	0	0,0
2	50	4	159	05.04.11	11.04.11	7	0.18	NM	121	69,1	40	22,8	0	0,0	15	8,6
2	50	5	166	12.04.11	18.04.11	7	0.87	FM	209	119,4	122	69,7	29	16,6	51	29,1
2	50	6	173	19.04.11	25.04.11	7	0.79	FM	38	21,7	80	45,7	26	14,9	17	9,7
2	50	7	180	26.04.11	02.05.11	7	0.15	NM	8	4,6	24	13,7	0	0,0	6	3,4
2	50	8	187	03.05.11	09.05.11	7	0.08	NM	263	150,3	278	158,8	84	48,0	48	27,4
2	50	9	194	10.05.11	16.05.11	7	0.75	FQ	72	41,1	132	75,4	46	26,3	18	10,3
2	50	10	201	17.05.11	23.05.11	7	0.91	FM	14	8,0	18	10,3	8	4,6	9	5,1
2	50	11	208	24.05.11	30.05.11	7	0.28	LQ	51	29,1	56	32,0	19	10,9	15	8,6

2	50	12	215	31.05.11	06.06.11	7	0.02	NM	53	30,3	64	36,6	19	10,9	12	6,9
2	100	1	138	15.03.11	21.03.11	7	0.96	FM	0	0,0	21	12,0	0	0,0	0	0,0
2	100	2	145	22.03.11	28.03.11	7	0.64	LQ	79	45,1	59	33,7	51	29,1	4	2,3
2	100	3	152	29.03.11	04.04.11	7	0.05	NM	0	0,0	96	54,8	8	4,6	4	2,3
2	100	4	159	05.04.11	11.04.11	7	0.18	NM	63	36,0	149	85,1	16	9,1	16	9,1
2	100	5	166	12.04.11	18.04.11	7	0.87	FM	66	37,7	76	43,4	9	5,1	16	9,1
2	100	6	173	19.04.11	25.04.11	7	0.79	FM	0	0,0	37	21,1	0	0,0	2	1,1
2	100	7	180	26.04.11	02.05.11	7	0.15	NM	37	21,1	111	63,4	13	7,4	10	5,7
2	100	8	187	03.05.11	09.05.11	7	0.08	NM	132	75,4	245	140,0	53	30,3	13	7,4
2	100	9	194	10.05.11	16.05.11	7	0.75	FQ	142	81,1	240	137,1	84	48,0	17	9,7
2	100	10	201	17.05.11	23.05.11	7	0.91	FM	76	43,4	256	146,3	32	18,3	16	9,1
2	100	11	208	24.05.11	30.05.11	7	0.28	LQ	99	56,6	301	172,0	74	42,3	26	14,9
2	100	12	215	31.05.11	06.06.11	7	0.02	NM	8	4,6	78	44,6	12	6,9	4	2,3
3	50	1	264	20.07.11	24.07.11	5	0.60	LQ	22	19,2	0	0,0	0	0	3	2,4
3	50	2	269	25.07.11	29.07.11	5	0.15	NM	4	3,2	4	3,2	4	3,2	5	4
3	50	3	274	30.07.11	03.08.11	5	0.03	NM	31	24,8	4	3,2	3	2,4	11	8,8
3	50	4	279	04.08.11	08.08.11	5	0.47	FQ	118	89,6	112	84,8	39	29,6	47	36,8
3	50	5	284	09.08.11	13.08.11	5	0.93	FM	5	4	89	74,4	47	39,2	13	10,4
3	50	6	289	14.08.11	18.08.11	5	0.94	FM	68	52	63	48,8	22	16,8	3	2,4
3	50	7	294	19.08.11	23.08.11	5	0.57	LQ	33	27,2	73	60,0	0	0	69	56
3	50	8	299	24.08.11	28.08.11	5	0.12	NM	97	75,2	611	475,2	157	122,4	62	49,6
3	50	9	304	29.08.11	02.09.11	5	0.06	NM	33	24,8	122	91,2	12	8,8	28	22,4
3	50	10	309	03.09.11	07.09.11	5	0.55	FQ	0	0	33	26,4	2	1,6	32	25,6
3	50	11	314	08.09.11	12.09.11	5	0.95	FM	6	4,8	21	16,0	1	0,8	12	9,6
3	50	12	319	13.09.11	17.09.11	5	0.93	FM	9	6,4	26	19,2	4	3,2	13	10,4
3	100	1	264	20.07.11	24.07.11	5	0.60	LQ	24	19,2	1	0,8	0	0	8	6,4
3	100	2	269	25.07.11	29.07.11	5	0.15	NM	4	3,2	0	0,0	0	0	0	0
3	100	3	274	30.07.11	03.08.11	5	0.03	NM	0	0	0	0,0	0	0	0	0
3	100	4	279	04.08.11	08.08.11	5	0.47	FQ	0	0	5	3,2	5	3,2	2	1,6
3	100	5	284	09.08.11	13.08.11	5	0.93	FM	23	19,2	31	26,4	2	1,6	2	1,6
3	100	6	289	14.08.11	18.08.11	5	0.94	FM	29	22,4	222	171,2	50	38,4	2	1,6
3	100	7	294	19.08.11	23.08.11	5	0.57	LQ	4	4	67	57,6	1	0,8	12	11,2
3	100	8	299	24.08.11	28.08.11	5	0.12	NM	1	0,8	114	91,2	10	8	35	28
3	100	9	304	29.08.11	02.09.11	5	0.06	NM	8	6,4	12	9,6	9	7,2	3	2,4
3	100	10	309	03.09.11	07.09.11	5	0.55	FQ	0	0	4	3,2	0	0	1	0,8
3	100	11	314	08.09.11	12.09.11	5	0.95	FM	0	0	23	18,4	0	0	4	3,2
3	100	12	319	13.09.11	17.09.11	5	0.93	FM	5	3,2	159	96,0	0	0	0	0
4	50	1	400	02.12.11	08.12.11	7	0.75	FQ	19	10,9	7	4,0	9	5,1	6	3,4
4	50	2	407	09.12.11	15.12.11	7	0.98	FM	196	113,1	192	110,9	32	18,3	103	59,4
4	50	3	414	16.12.11	22.12.11	7	0.37	LQ	92	57,1	379	234,9	43	25,7	78	44,6
4	50	4	421	23.12.11	29.12.11	7	0.03	NM	14	8,0	110	62,8	19	10,9	47	26,9
4	50	5	428	30.12.11	05.01.12	7	0.59	FQ	3	1,7	106	60,6	3	1,7	35	20,0
4	50	6	435	06.01.12	12.01.12	7	1.00	FM	0	0,0	38	21,7	1	0,6	11	6,3
4	50	7	442	13.01.12	19.01.12	7	0.53	LQ	1	0,6	21	12,0	2	1,1	6	3,4
4	50	8	449	20.01.12	26.01.12	7	0.00	NM	3	1,7	31	17,1	0	0,0	8	4,6
4	50	9	456	27.01.12	02.02.12	7	0.41	FQ	11	6,3	50	28,6	6	3,4	35	20,0
4	50	10	463	03.02.12	09.02.12	7	0.96	FM	5	2,9	12	6,8	1	0,6	24	13,7
4	50	11	470	10.02.12	16.02.12	7	0.67	LQ	0	0,0	0	0,0	0	0,0	8	4,6
4	50	12	477	17.02.12	24.02.12	7	0.04	NM	0	0,0	4	2,3	0	0,0	18	10,3

4	100	1	400	02.12.11	08.12.11	7	0.75	FQ	0	0,0	6	3,4	0	0,0	6	3,4
4	100	2	407	09.12.11	15.12.11	7	0.98	FM	4	2,3	88	50,3	7	4,0	14	8,0
4	100	3	414	16.12.11	22.12.11	7	0.37	LQ	63	32,0	384	219,4	10	5,7	44	25,1
4	100	4	421	23.12.11	29.12.11	7	0.03	NM	1	0,6	72	41,1	3	1,7	12	6,9
4	100	5	428	30.12.11	05.01.12	7	0.59	FQ	5	2,9	72	41,1	4	2,3	12	6,9
4	100	6	435	06.01.12	12.01.12	7	1.00	FM	7	4,0	49	28,0	2	1,1	3	1,7
4	100	7	442	13.01.12	19.01.12	7	0.53	LQ	6	3,4	200	114,3	10	5,7	19	10,9
4	100	8	449	20.01.12	26.01.12	7	0.00	NM	0	0,0	8	4,6	0	0,0	2	1,1
4	100	9	456	27.01.12	02.02.12	7	0.41	FQ	7	4,0	23	13,1	1	0,6	10	5,7
4	100	10	463	03.02.12	09.02.12	7	0.96	FM	0	0,0	11	6,3	0	0,0	9	5,1
4	100	11	470	10.02.12	16.02.12	7	0.67	LQ	0	0,0	3	1,7	0	0,0	11	6,3
4	100	12	477	17.02.12	24.02.12	7	0.04	NM	0	0,0	3	1,7	0	0,0	0	0,0

Appendix B: Acoustic Doppler current profiler data (Aquadopp 400 KHz) and relative contribution of cross and along-shelf (m/s) components of the water velocity to both sediment traps for all deployments (colored dots). A threshold of 10 cm/s is represented by a vertical black dashed line.

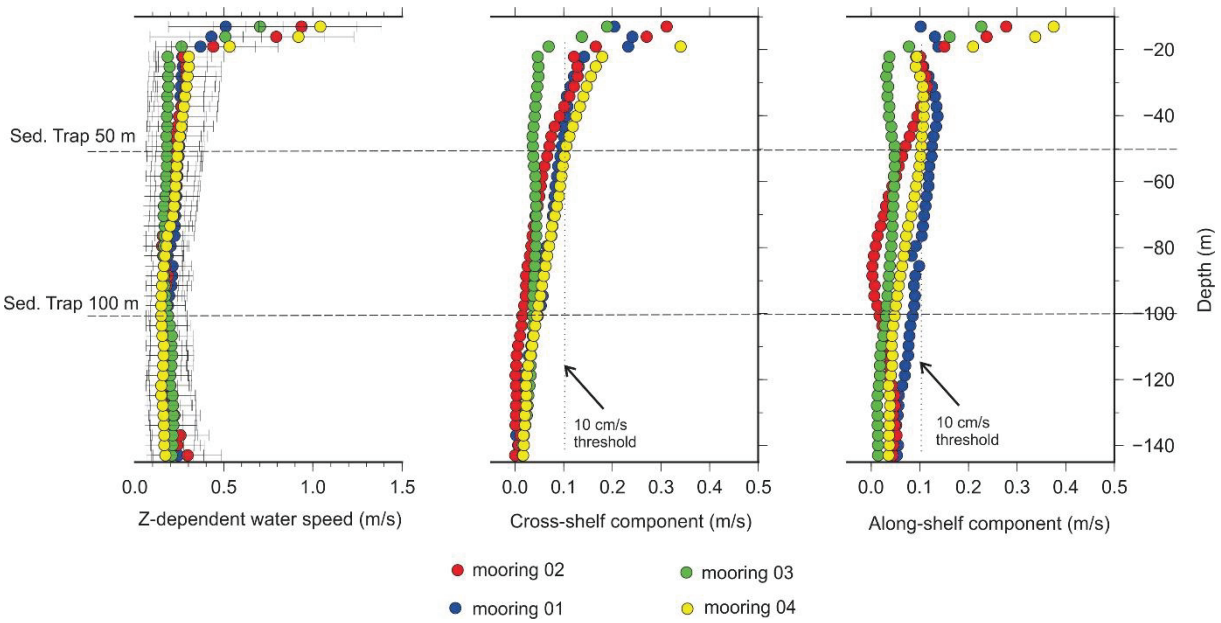

Appendix C: Acoustic Doppler current profiler data (Aquadopp 400 KHz) transformed in time dependent Z-corrected backscatter amplitudes. Color scale represents the amplitudes in decibel (dB). Red colors represent noise caused by resuspension (bottom) or disturbance of wind waves (surface).

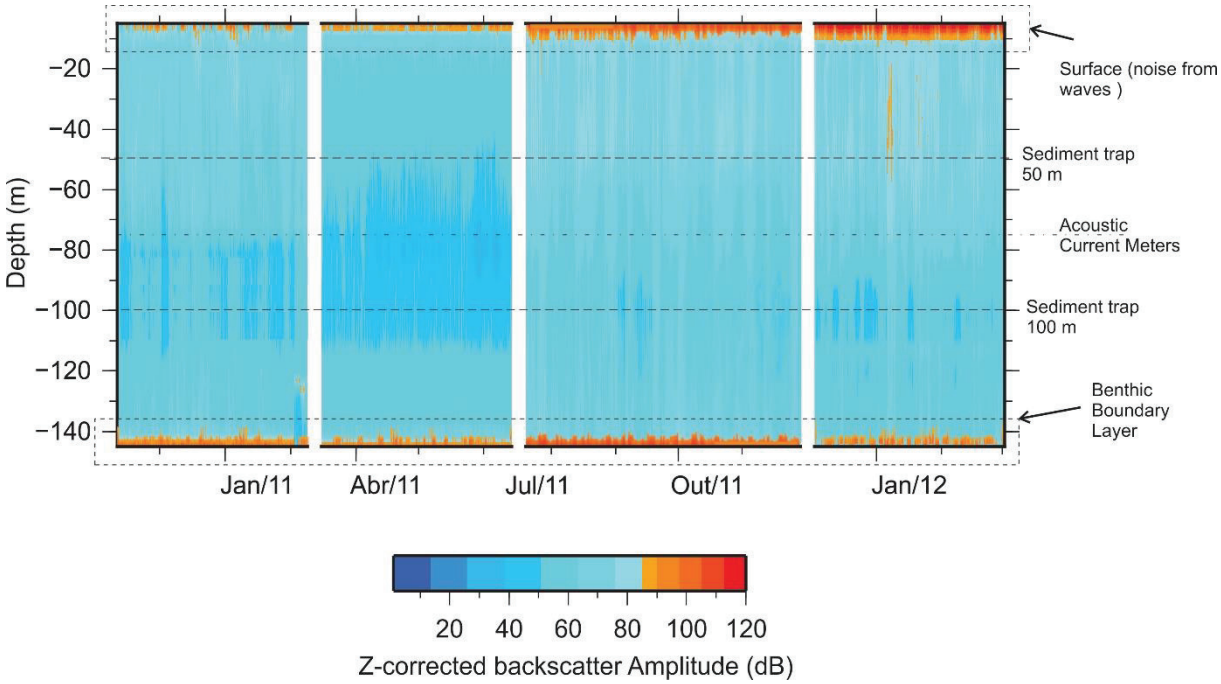

Chapter 3. Calcification depths of planktonic foraminifera from the southwestern Atlantic derived from oxygen isotope analyses of sediment trap material

I.M. Venancio[1,2], A. L. Belem[3], T. P. Santos[2], D.O. Lessa[2], A. L. S. Albuquerque[2], S. Mulitza[1], M. Schulz[1], M. Kucera[1]

[1]Departamento de Geoquímica, Universidade Federal Fluminense, Niterói, Brazil.

[2]MARUM-Center for Marine Environmental Sciences, University of Bremen, Bremen, Germany.

3Departamento de Engenharia Agrícola e Meio Ambiente, Universidade Federal Fluminense, Niterói, Rio de Janeiro, 24210-240, Brazil.

Under review in *Marine Micropaleontology*

3.1. Abstract

We present a multi-year record of shell fluxes and $\delta^{18}O$ of six planktonic foraminifera species (*Globigerinoides ruber* pink, *Globigerinoides ruber* white, *Trilobatus sacculifer*, *Orbulina universa*, *Neogloboquadrina dutertrei*, *Globorotalia menardii*) from sediment traps located in the southwestern Atlantic. Among the six species, only the fluxes of *G. ruber* white and *N. dutertrei* exhibit a significant seasonal component, with *G. ruber* white showing a single flux peak in austral summer, and *N. dutertrei* exhibiting two flux peaks in spring and autumn. To estimate calcification depths of the studied species, we then compare their measured $\delta^{18}O$ to vertical $\delta^{18}O$ profiles predicted for each collection time from in-situ temperature profiles and climatological salinity profiles. For the majority of the cases, the measured $\delta^{18}O$ could be accounted for by in-situ calcification, assuming species-specific temperature- $\delta^{18}O$ calibrations. The resulting estimates of the calcification depth imply that each species exhibits a characteristic typical mean calcification depth. The estimated calcification depths for *N. dutertrei* (mode 60-70 m) and *G. menardii* (mode 70-80 m) appear to track the depth of the thermocline in the region, whereas the calcification depths of the remaining four species correspond to conditions in the mixed layer. Among the apparent mixed-layer calcifiers, *G. ruber* pink and white appeared to calcify consistently shallower (mode 30-40 m) while

T. sacculifer calcified deeper (mode 50-60 m). Because of the low flux seasonality, the observed oxygen isotope offsets among the species are similar to the flux-weighted mean annual $\delta^{18}O$ offsets, indicating that isotopic offsets among the species in sediment samples are mainly due to different calcification depths. Since the habitat offsets among the species are consistent across seasons, $\delta^{18}O$ in sedimentary shells can be used to track conditions in different parts of the water column and the difference in the oxygen-isotope composition between surface species (best represented by *G. ruber* pink) and thermocline species (best represented by *N. dutertrei*) can be used as a proxy for stratification in the southwestern Atlantic.

3.2. Introduction

Our ability to reconstruct past oceanographic conditions depends on the understanding of how ocean properties are recorded by proxies. One of the most widely used proxies in paleoceanography is the oxygen-isotopic composition ($\delta^{18}O$) of planktonic foraminifera in marine sediments, which is used to estimate changes in $\delta^{18}O$ of seawater and temperature (Duplessy et al., 1991; Bemis et al., 2002). Since planktonic foraminifera species inhabit different habitat depths, which may vary temporally and spatially, and change during the life of each individual (Rebotim et al., 2017), assessments of their vertical habitats and especially the calcification depth is crucial for paleoceanography. Without knowledge of calcification depths, environmental conditions reconstructed from the chemical composition of foraminiferal shells cannot be assigned to the part of the water column, where the signals were generated. Since living depths (Rebotim et al., 2017) and by inference also calcification depths of planktonic foraminifera vary in response to environmental conditions, regional assessments, especially in areas that lacks this type of information, are needed to provide the basis for interpretations of the proxy signals in the fossil record. If species could be identified that consistently calcify in different parts of the water column, multi-species proxy data could be sued to evaluate past changes in the stratification of the upper water column (Williams and Healy-Williams, 1980; Mulitza et al., 1997).

A powerful means of constraining the origin of isotopic signatures in planktonic foraminifera is by analysis of shells from sediment-trap time-series, which are an effective method to constrain the effect of flux seasonality (Jonkers et al., 2010; Žarić et al., 2005). Studies using sediment traps have shown changes in planktonic foraminifera assemblages and shell fluxes (Thunell and Sautter, 1992; King and Howard, 2005; Jonkers et al., 2010) as well as changing calcification depths (Wejnert et al., 2013) throughout the seasonal cycle. These observations imply that planktonic foraminifera may adapt their habitat in order to stay within a preferred temperature range (Jonkers and Kucera, 2015). Thus, their calcification habitat can only be constrained by sampling at sufficient seasonal resolution with simultaneous recording of vertical temperature gradients above the sediment trap. In this respect, a deeply moored sediment trap collects foraminifera from a potentially large catchment area, which may include spatially variable vertical water column structure. Therefore, estimates of calcification depth from a shallow moored trap are likely to better constrain calcification habitat.

In this study, we use a sediment trap record from the southeastern continental shelf off Brazil to derive shell fluxes and

$\delta^{18}O$ of the planktonic foraminifera species *Globigerinoides ruber* white, *Globigerinoides ruber* pink, *Trilobatus sacculifer, Orbulina universa, Globorotalia menardii,* and *Neogloboquadrina dutertrei*. The mooring was operated over four years with traps moored between 50 - 100 m depth, minimizing the potential catchment area. Instead of relying on data from unevenly spaced and scattered CTD profiles (Jonkers et al., 2010) or on information from climatological oceanographic data (Gibson et al., 2016), simultaneous in situ recording of the vertical temperature profile was available throughout the sampling period, allowing direct comparison of shell chemistry with local hydrography. By sampling over all four seasons (replicating three seasons), we can effectively investigate the seasonal variation of calcification depths. Combining calcification depths with flux data allows us to evaluate the implications of the sediment trap observations for paleoceanographic records.

3.3. Materials and methods

3.3.1. Sediment trap sampling

The mooring line that was available for the study was deployed by the Brazilian Project *Ressurgência*. The mooring is located over the Brazilian southeastern continental shelf at 23°36' S, 41°34' W (Figure 1) at a water depth of 145 m. Sediment traps were positioned at depths of 50 and 100 m (first to fourth deployment) and 75 m (single trap, sixth and seventh deployments). The used sediment traps PARFLUX (model Mark 8-13) have an aperture of 0.25 m² and 12 or 13 sequential bottles with 500 ml capacity. Each sample bottle was filled with pre-filtered MilliQ water with buffered (pH=8) formaldehyde (4%) after adjusting the salinity with marine salt (RedSea©) to 70 PSU to prevent mixing and bacterial decomposition of collected particles (Goswami, 2004). In addition to the traps, the mooring line contained temperature loggers (ONSET tidbits V2) between 30 m and 120 m, spaced at 5 m intervals and two current meters (400 kHz Nortek Aquadopp Profilers) configured to up and down looking acoustic current profiling. The physical parameters (temperature and velocities) were measured at 30-minute intervals. In general, our mean current velocities are higher than 12 cm/s with a strong along-shelf component towards the south, but with the current velocity and direction remaining relatively stable between the deployments. Regarding the recorded temperature (supporting information Figure S3), the 100-m trap is more influenced by water masses with temperatures below 18°C, while the shallow traps (50 and 75-m) are in contact with waters that have temperature higher than 18°C, but subsurface intrusions can bring cold waters to these shallower traps as well. A detailed description of the temperature, current-meter data (trap efficiency) and bulk composition was previously published (Albuquerque et al., 2014; Belem et al., 2013; Venancio et al., 2016a).

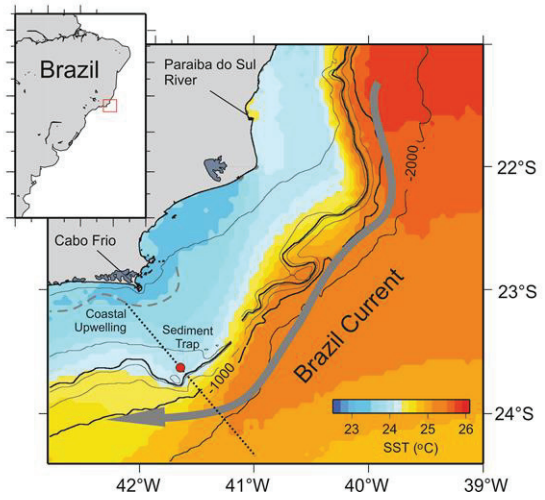

Figure 1. Study area and oceanographic features. The mooring site is marked with a red circle. The distribution of 10-year mean sea surface temperature is represented by the color scale. Data was extracted from the AVHRR dataset (AVHRR Pathfinder v.5).

The samples and data used in this study were retrieved during six deployments between November 2010 and March 2014 (Table 1). Sampling resolution varied among the deployments. The first experiment (F1) was from November 11th to December 19th 2010 (3-day sampling rate). The second experiment (F2) was from March 15th to June 14th 2011 (7-day sampling rate). The third experiment (F3), from July 20th to September 26th 2011 (5-day sampling rate) and the forth experiment (F4) covered the time frame between December 2nd 2011 and March 2nd 2012 (7-day sampling rate). Samples for the fifth experiment were not used due to technical problems in the equipment. The sixth experiment (F6) was from June 9th to September 8th 2013 (7-day sampling rate) and the seventh experiment (F7) covered the time frame between September 15th of 2013 and March 16th of 2014. Gaps in the time series were caused by operational constraints in recovering the experiments.

3.3.2. Sample treatment

The sediment trap samples were wet-sieved through 1 mm and 500 μm meshes before being split into four aliquots. A Folsom's plankton sample divider was used for splitting the samples. The volume of the resulting aliquots was determined to adjust the split factor used to calculate the concentration of foraminifera in the total sample. For deployments 1-4, a split factor close to 4 was used to calculate the foraminiferal fluxes, while for deployment 6-7 split factors were more variable ranging from 5.6 to 7.7. After wet-sieving, the > 125 μm fraction was used for species identification and counting. This size fraction was chosen because it covers the size range of most recent species and also contains all foraminifera > 150 μm, which are usually used for paleoceanographic studies (Al-Sabouni et al., 2007; Žarić et al., 2005). The samples were analyzed wet allowing the counting of fragile shells which could disintegrate during drying. Wet-picking was performed using a transparent gridded tray for zooplankton analysis. The species *G. ruber* (pink and white), *T. sacculifer* (without sac-chamber), *O. universa, G. menardii* and *N. dutertrei* were the most abundant, representing more than 70-80 % of the

assemblage in most samples, and were therefore analyzed further in this study. The remaining part of the assemblage is composed by *Globigerinella siphonifera*, *Globigerinoides conglobatus*, *Globigerina bulloides*, *Globigerinita glutinata*, *Globoturborotalita rubescens* and *Globigerinella calida*, with minor contributions by *Turborotalita quinqueloba*, *Globoturborotalita tenella* and *Globorotalia truncatulinoides*. The taxonomy of *Trilobatus sacculifer* follows the proposal by Spezzaferri et al. (2015). Whereas the two colour varieties of *G. ruber* (white and pink) were separated, no distinction was made between *G. ruber* and *G. elongatus* (Aurahs et al., 2011). Planktonic foraminifera fluxes from the first to the forth deployment were previously published by Venancio et al. (2016a). Flux data for the remaining deployments will be made available at Pangaea (www.pangaea.de).

Table 1. Mooring configurations for each of the deployments.

Deployments	Trap depths (m)	N° of cups analyzed	Time interval		Sample integration (days)
			Start	End	
F1	50;100	12	11 Nov 2010	19 Dec 2010	3
F2	50;100	12	15 Mar 2011	14 Jun 2011	7
F3	50;100	12	20 Jul 2011	26 Sep 2011	5
F4	50;100	12	02 Dec 2011	02 Mar 2012	7
F6	75	13	09 Jun 2013	08 Sep 2013	7
F7	75	13	15 Sep 2013	16 Mar 2014	14

For the oxygen isotopic analysis, 5-10 specimens of each of the chosen species were selected. Because in many of the sampling intervals, the flux of the studied species was low, the analyses could not be carried out specifically for a narrow size fraction. Instead, the size of the measured specimens was recorded by measuring the length of the major axis of the shells and varied for *G. ruber* pink (280-720 μm), *G. ruber* white (280-720 μm), *T. sacculifer* (400-800 μm), *N. dutertrei* (320-760 μm), *O. universa* (520-960 μm) and *G. menardii* (520-960 μm). Stable oxygen isotopes were analyzed with a Finnigan MAT 252 mass spectrometer coupled to an automated carbonate preparation device at MARUM, University of Bremen. The isotopic results were calibrated relative to the Vienna Pee Dee Belemnite (VPDB) by using the NBS 19 standard. The long-term analytical standard deviation was less than 0.07 ‰. All data, including sizes of the measured specimens will be made available at Pangaea (www.pangaea.de).

3.3.3. *Evaluation of seasonal cycles*

Shell fluxes of each species, sea surface temperatures (SST) from the Advanced

Very High Resolution Radiometer (AVHRR) dataset, temperatures recorded by the mooring and the estimations of calcification depths (see section 2.4) were tested for the presence of seasonal cycles using a periodic regression analysis. For the analysis of the shell flux data we used the deployments 2 (100 m trap), 6 and 7 that cover all seasons and also have sampling time integrations ranging from 7 to 14 days, which avoids the interference of short-term flux variations. The models generated using these three deployments (2, 6 and 7) were then applied to the entire dataset. The mooring temperatures were binned in 10-meter sections starting at 30 m, first level of measurements available, and ending at 100 m, which is the depth of the deepest sediment trap. Both AVHRR-SST and mooring temperatures were analyzed as daily averages covering the entire time series. For the calcification depths the entire dataset was analyzed.

In the periodic regression analysis the independent variable is an angular representation of time and this approach was demonstrated to be robust for detection of lunar periodicity (deBruyn and Meeuwig, 2001) and seasonality (Bell et al., 2001; Jonkers and Kucera, 2015). Furthermore, the analysis gives information about the timing of the maximum in the dataset and provides an equation which can be used to estimate values for a given period. The methods and advantages in detecting lunar and seasonal cycles are summarized by deBruyn and Meeuwig (2001) and Jonkers and Kucera (2015), respectively. Regarding the shell fluxes, we followed Jonkers and Kucera (2015) and performed a log transformation of the flux data prior to the analysis. To facilitate the log transformation, zero flux values were replaced by half of the second lowest flux value for each deployment, also following Jonkers and Kucera (2015). The observation time was converted to days of the year (DOY) and transformed in radian units (DOY/365 x 2π). In order to test the cycles the following models were applied to observations:

$$F_{(t)} = A + B_{\sin(t)} + C_{\cos(t)}$$

$$F_{(t)} = A + D_{\sin(2t)} + E_{\cos(2t)}$$

where $F_{(t)}$ is the shell flux or temperature at a given time and A-E are the parameters that will be estimated in the analysis. The statistical significance of the terms of the periodic regression analysis was evaluated using ANOVA for multiple regression.

3.3.4. *Calcification depths and flux-weighted $\delta^{18}O$*

In order to estimate the calcification depths for each species, we applied species-specific paleotemperature equations and inverted these to predict the $\delta^{18}O$ of the calcite ($\delta^{18}O_{predicted}$) from the in-situ temperature profiles, $\delta^{18}O$ of seawater ($\delta^{18}O_{sw}$) was calculated using monthly salinity values from the World Ocean Atlas 2013 (WOA13) and the $\delta^{18}O_{sw}$-salinity relationship derived from

the dataset of Pierre et al. (1991). This $\delta^{18}O_{sw}$-salinity was previously used for salinity reconstructions in the Brazilian margin by Toledo et al. (2007) . The $\delta^{18}O_{sw}$ values were converted from VSMOW to VPDB by subtracting 0.27‰ (Hut, 1987) from the values derived from equations (1), (2) and (5). In the case of the equations (3) and (4) we subtracted 0.20‰ (Bemis et al., 1998). Since we used monthly salinity values for our $\delta^{18}O_{sw}$ estimations, sub-monthly and interannual variabilities were not considered. The assumption of this approach is that the collected planktonic foraminifera calcified during the sampling period in the studied area. The species-specific paleotemperature equations are as follows:

(1) $T\ (°C) = 14.2 - 4.44 \times (\delta c - \delta sw)$; (Mulitza et al., 2003)

(2) $T\ (°C) = 14.91 - 4.35 \times (\delta c - \delta sw)$; (Mulitza et al., 2003)

(3) $T\ (°C) = 15.4 - 4.81 \times (\delta c - \delta sw)$; (Bouvier-Soumagnac and Duplessy, 1985)

(4) $T\ (°C) = 14.6 - 5.03 \times (\delta c - \delta sw)$; (Bouvier-Soumagnac and Duplessy, 1985)

(5) $T\ (°C) = 16.5 - 4.8 \times (\delta c - \delta sw)$; (Bemis et al., 1998)

Equation (1) was used for *G. ruber* (pink and white), (2) for *T. sacculifer*, (3) for *O. universa*, (4) for *G. menardii* and (5) for *N. dutertrei*. In all cases, except *N. dutertrei*, we used equations derived from plankton tow studies. For *N. dutertrei* we use the equation derived from a culture study using *O. universa* at low-light conditions (Bemis et al., 1998). The species-specific equation for *N. dutertrei* from Bouvier-Soumagnac and Duplessy (1985) is known to produce estimates that are too cold (Wejnert et al., 2013). It indeed generated unrealistic values for the region and was therefore not used. Alternative equations based on plankton tow calibrations exist for some of the species, but these differ only marginally (e.g., Wejnert et al., 2013).

Profiles of $\delta^{18}O_{predicted}$ with their respective measured $\delta^{18}O$ for *G. ruber* white are shown as examples of our calcification depth approach (supporting information Figure S4). We used the maximum and minimum temperatures from each depth interval to generate the $\delta^{18}O_{predicted}$ profiles for a given period (supporting information Figure S4). Since the studied foraminifera may have calcified different portions of their shell at different times and depths, the resulting isotopic composition is reflecting the average conditions in the total calcification habitat. It is difficult to constrain the effect of calcification across habitats precisely, which is why we opted for a conservative approach and estimated the possible range of calcification depths by determining the deepest and shallowest possible calcification depth given the temperature variation during the sam-

pling interval, when the analyzed foraminifera lived.

Considering the analytical error of $\delta^{18}O$ measurements and the statistical uncertainties of the $\delta^{18}O_{sw}$-salinity and paleotemperature equations, we can estimate the magnitude of uncertainty for a calcification depth value due to these processes. For example, taking the $\delta^{18}O$ value of *G. ruber* white for a sample (6th bottle of 50-m in the 1st deployment) and representing the calcification temperature range by a mean profile throughout he sampling interval, we estimate an error on the calcification depth estimate due to analytical error and calibration uncertainty of 16.7 m. Using an approach based only on the temperature profile variation yield an uncertainty of 16.4 m. For deeper layers, the uncertainty due to variation within the sampling interval will be larger than the uncertainty due to calibration, because temperature variation is higher reflecting the changes in thermocline depth, whereas calibration uncertainty remains the same. Thus, by showing the range of possible calcification depths based on minimum and maximum temperatures during a given sampling period, we are making a conservative approach that is equivalent to error estimates. Calcification depths for the entire time series were further evaluated for seasonal component using periodic regression analysis (section 3.3.3).

Next, to assess the effect of seasonal fluxes on the mean $\delta^{18}O$ signal exported to the sediments, we determined the flux-weighted annual $\delta^{18}O$ values for each of the chosen species. The fundamentals of this approach were discussed by Mulitza et al. (1998), using the model proposed by Mix (1987). The flux-weighted annual $\delta^{18}O$ values were calculated using the following equation:

$$Fw = \sum_{i=1}^{n} (flux_i \times \delta c_i) \Big/ total\ flux$$

where *Fw* is the flux-weighted $\delta^{18}O$ value, $flux_i$ and δc_i are the shell flux and the $\delta^{18}O$ of calcite in a specific sample, respectively.

3.4. Oceanographic setting

The mesoscale surface circulation of the western boundary of the South Atlantic is dominated by the warm and nutrient-poor Brazil Current (Peterson and Stramma, 1991). As discussed by Walsh (1988), continental shelves located in the tropics and linked to the western edge of oceanic systems are often related to less productive oceanic margins. However, mesoscale processes related to the dynamics of Brazil Current (BC) (encroachment, topographic acceleration, meandering and eddies) may induce the upwelling of cold and nutrient-rich South Atlantic Central Water (SACW) on the shelf, forming an upwelling system in the southeastern portion of the Brazilian shelf (Belem et al., 2013; Campos et al., 2000;

Castelao and Barth, 2006; Silveira et al., 2008). This upwelling system (Cabo Frio Upwelling system-CFUS) is one of the most productive areas of the southeastern Brazilian shelf. Despite the control of the nutrient-poor western boundary BC, it interacts with the instabilities of the southward trajectory of the BC carrying oligotrophic Tropical Waters (Belem et al. 2013) andwith the wind-driven coastal Ekman transport (Castelao and Barth 2006), and allows a mid-shelf eddy-induced cold-water intrusion of South Atlantic Central Water (SACW) to the photic zone (Brandini 1990, Campos et al. 2000, Calado et al. 2010). Following Albuquerque et al (2013), the complex interactions of such system leads to a heterogeneous pattern of primary productivity (Franchito et al. 1998, Lopes et al. 2006), recycling and transport of particulate material on the shelf.

The continental shelf circulation off southeastern Brazil (Figure 1), especially between 21°S and 25°S, has been widely studied due to this upwelling system (Ikeda et al., 1974; Rodrigues and Lorenzzetti, 2001; Castelao and Barth, 2006; Castelao, 2012; Castro, 2014; Cerda and Castro, 2014). The BC flows southward along the shelf break and slope of the Brazilian margin, as a component of the South Atlantic subtropical gyre, acquiring intensity and speed southward of the Abrolhos Bank (Silveira et al., 2000). This boundary current carries Tropical Water (TW) at the upper layers of the water column, as well as the South Atlantic Central Water (SACW) at an intermediate depth southwards (Figure 1; Stramma and England, 1999). The BC exhibits an annual cycle in SST in our study area, where SST values range from 26°C in March, to 22°C during August and September. Regional hydrographic data also point to similar seasonal temperature variation at our study site (Cerda and Castro, 2014; Chiessi et al., 2014). As pointed out by Chiessi et al. (2014), variations in surface salinity are less pronounced than temperature during the annual cycle. Therefore the shallower trap (50 m) is more influenced by the TW and the deeper trap (100 m) by the SACW. The material collected by the deeper trap (100 m) is derived from both layers, while the shallower trap (50 m) material is mostly derived from the surface layer (TW), although SACW intrusions can be identified on the temperature dataset for both traps. TW and SACW, besides the Coastal Water (CW) and the Subtropical Shelf Water (STSW), are the main water masses at the upper part of the water column of the southeastern Brazilian margin (Castro, 2014; Venancio et al., 2014). Our recorded mean temperature profile (supporting information Figure S3) also shows that a shoaling of the thermocline (18°C isotherm) is more frequent during spring and autumn, with a strong deepening during the winter. As pointed out by Belem et al. (2013), the subsurface temperature variability in this area is influenced by several

mechanisms, with the proximity of the BC to the shelf break being the most dominant factor modulating the temperatures at the top 80 m.

3.5. Results

3.5.1 Planktonic foraminifera shell fluxes

Shell fluxes for each of the investigated planktonic foraminifera species for the entire time series are shown in Figure 2. Shell fluxes ranged from 0 to 489 shells m^{-2} d^{-1} and the values differed among the species. Fluxes of *G. ruber* pink ranged from 0 to 149 shells m^{-2} d^{-1}, while *G. ruber* white ranged from 0 to 193 shells m^{-2} d^{-1}. In the case of *T. sacculifer* and *O. universa* the values ranged from 0 to 49 shells m^{-2} d^{-1} and from 0 to 63 shells m^{-2} d^{-1}, respectively. Finally, the fluxes from *N. dutertrei* and *G. menardii* showed wider ranges with values from 0 to 489 shells m^{-2} d^{-1} and from 0 to 382, respectively.

Similar patterns of shell fluxes were observed during certain deployments. The first of these patterns occurred during the first deployment (November-December 2010), where *N. dutertrei* and *G. menardii* presented very low shell fluxes, while the other species presented flux peaks at the end of November. Shell fluxes from all species were generally higher at the deepest trap (100 m) during this first deployment, which is not necessarily a persistent pattern for the subsequent deployments. Other distinctive patterns occur during the fourth and seventh deployments. During the fourth deployment (December 2011-March 2012) all the species showed flux peaks in December 2011 and lower fluxes until March 2012. During the seventh deployment (September 2013-March 2014), *G. ruber* pink and *G. ruber* white showed comparable flux patterns with a decreasing trend from September to December of 2013 and subsequent increase towards a maximum flux at February of 2014. However, the observed trends for *G. ruber* pink and *G. ruber* white are not statistically significant. The fluxes of the other species, except *G. menardii*, have a statistically significant ($p<0.05$) decreasing trend, but with no maximum flux occurring during February of 2014. The highest fluxes

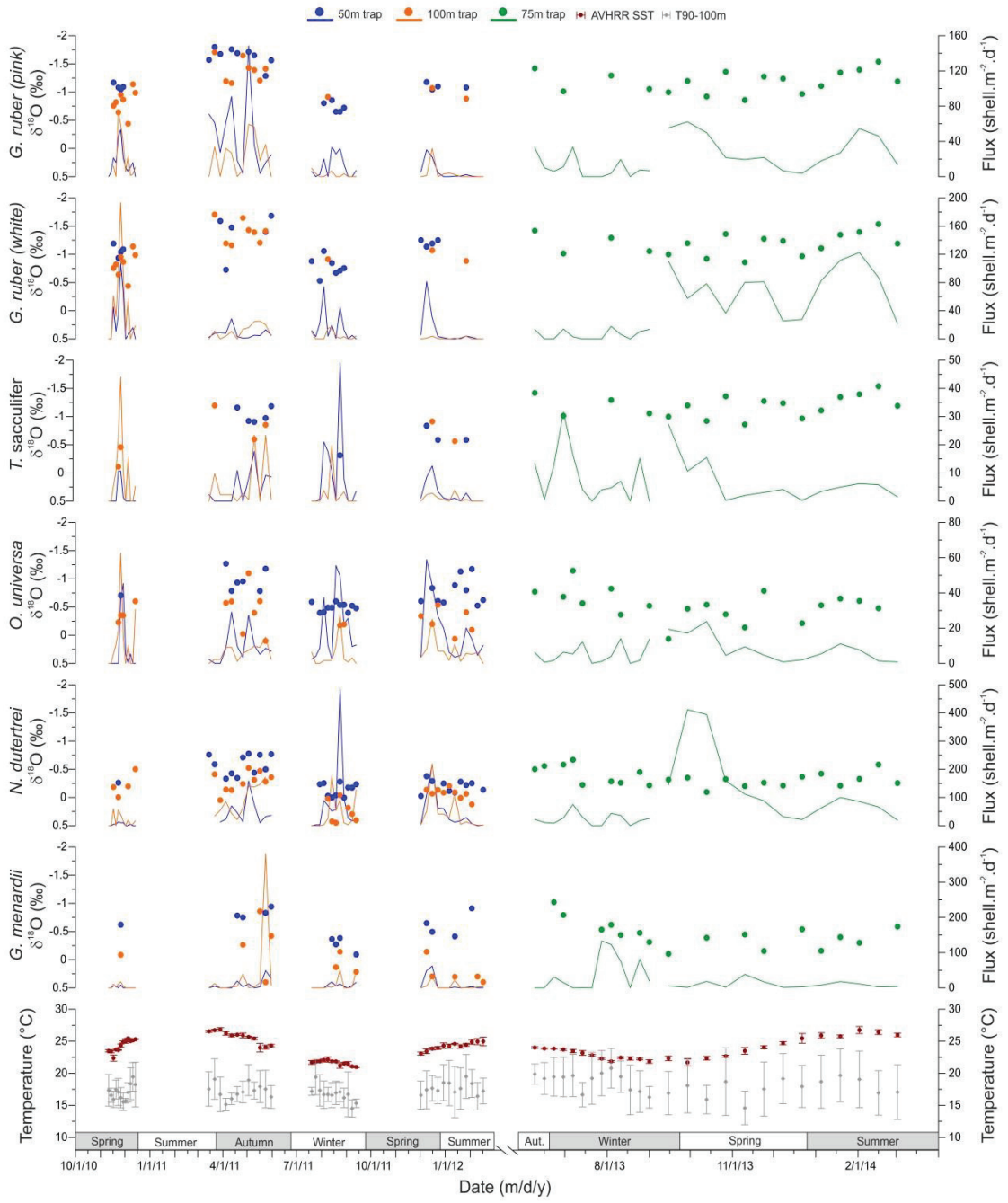

Figure 2. Shell fluxes, oxygen isotope ratios of the planktonic foraminifera species and temperature records. The shell fluxes are plotted as lines in blue (50m), orange (100m) and green (75m). Shell fluxes axes are variable between species. The oxygen isotopes are plotted as circles with the same color representation for each trap depth as the fluxes. The lowest panel displays the AVHRR-SST temperatures (red circles) and T90-100m temperature section (grey) recorded by the mooring. The temperatures were averaged according to time integrated by each sample and the standard deviations are represented by bars with the same color as the circles. Seasons are exhibited above the x-axis. Shell fluxes from the deployments 1-4 were previously published by Venancio et al. (2016a).

of *N. dutertrei* and *G. menardii*, 489 and 382 shells m^{-2} d^{-1} respectively, occurred during periods of lower SST values (22-23°C), while peak fluxes of *G. ruber* white and G. ruber pink coincide with higher SST values (>24°C).

3.5.2. Oxygen isotopes

The oxygen isotopic composition ($\delta^{18}O$) of the investigated planktonic foraminifera species showed distinct offsets (Figure 2). Values for *G. ruber* pink varied from -1.9 to -0.7 ‰ and from -1.7 to -0.4 ‰ for *G. ruber* white. In the case of *T. sacculifer* and *O. universa* the values ranged from -1.2 to -0.1 ‰ and from -1.3 to 0.1 ‰. The highest values were observed for *N. dutertrei* and *G. menardii*, from -0.8 to 0.4 ‰ and -1.0 to 0.4 ‰. Although the ranges of $\delta^{18}O$ values observed for each species were distinct, the amplitude is very similar with values around 1.2 to 1.4 ‰. It is also noticeable that $\delta^{18}O$ values between different sediment trap-depths showed comparable values, with the exception of *N. dutertrei* and G. *menardii* (Figure 2), where the $\delta^{18}O$ range from the shallower trap (50 m) was lower than in the simultaneously deployed lower trap (100 m).

3.5.3. Seasonality of shell flux and temperature

The periodic regression analysis indicates different patterns of intra-annual shell flux variability among the studied species (Table 2; supporting information Figure S1). Shell fluxes of *G. ruber* pink, *T. sacculifer*, *O. universa* and *G. menardii* appear to show no seasonal component in their flux variability ($p>0.05$), allowing us to assume that the fluxes fluctuated randomly around a mean value. For *N. dutertrei* and *G. ruber* white, the periodic regression identified a significant ($p<0.01$) seasonal component. The fluxes of *G. ruber* white presented higher values during austral summer, with the highest peak at the beginning of the summer, revealing a preference of that species for summer oceanographic conditions in the region. For *N. dutertrei*, the analysis indicates the presence of two cycles during the year in spring and autumn. The coefficients of determination for *G. ruber* white ($r^2 = 0.46$) and *N. dutertrei* ($r^2 = 0.39$) demonstrate that the periodic model explains a large part of the variance, and the significance remains even when excluding specific years or switching seasons between years (not shown), which confirms the substantial influence of seasonality on the shell fluxes of these species (Figure 3). Using polynomial regressions instead of a sinusoidal model, to account for alternative shapes of the flux distribution (supporting information Table S1 and Figure S5) also reveals no statistically significant results for *O. universa*, *T. sacculifer* and *G. menardii*, but confirms statistically significant results for *G. ruber* white and *N. dutertrei* with peak flux estimated during the same seasons. A

Table 2. Results from the periodic regression and ANOVA for the shell fluxes of each planktonic foraminifera species, estimated calcification depths and temperature records.

Data	N° of cycles	Model peak times (DOY)		Amplitude	r^2	p-value
Flux *G. ruber* (pink)	1	349	-	0.2	0.07	0.292
	2	119	302	0.2	0.14	0.293
Flux *G. ruber* (white)	1	342	-	0.7	0.46	**<0.001**
	2	132	315	0.2	0.02	0.635
Flux *T. sacculifer*	1	238	-	0.1	0.03	0.908
	2	4	187	0.1	0.02	0.749
Flux *O. universa*	1	272	-	0.2	0.08	0.214
	2	121	303	0.3	0.14	0.265
Flux *G. menardii*	1	261	-	0.2	0.06	0.745
	2	2	185	0.1	0.01	0.083
Flux *N. dutertrei*	1	334	-	0.2	0.10	0.147
	2	119	301	0.4	0.39	**<0.002**
AVHRR-SST	1	67	-	2.2	0.85	**<0.001**
	2	134	317	0.2	0.02	**<0.003**
T30-40	1	146	-	0.8	0.16	**<0.001**
	2	175	357	0.6	0.05	**<0.001**
T40-50	1	162	-	0.9	0.21	**<0.001**
	2	180	363	0.8	0.07	**<0.001**
T50-60	1	172	-	0.9	0.07	**<0.001**
	2	3	185	1.0	0.21	**<0.001**
T60-70	1	173	-	0.8	0.04	**<0.001**
	2	5	188	1.1	0.20	**<0.001**
T70-80	1	176	-	0.6	0.02	**<0.001**
	2	6	189	1.2	0.19	**<0.001**
T80-90	1	168	-	0.6	0.02	**<0.001**
	2	6	189	1.1	0.17	**<0.001**
T90-100	1	169	-	0.5	0.02	**<0.001**
	2	8	191	1.0	0.15	**<0.001**
Depth *G. ruber* (pink)	1	227	-	14.3	0.44	**<0.001**
	2	22	205	10.2	0.18	**0.007**
Depth *G. ruber* (white)	1	227	-	5.7	0.05	0.305
	2	22	204	10.5	0.28	**<0.01**
Depth *T. sacculifer*	1	256	-	11.5	0.32	0.064
	2	22	205	7.7	0.12	0.221
Depth *O. universa*	1	191	-	4.5	0.07	0.123
	2	10	193	7.8	0.09	0.182
Depth *G. menardii*	1	268	-	1.7	0.03	0.591
	2	25	208	12.6	0.30	**<0.01**
Depth *N. dutertrei*	1	223	-	2.2	0.04	0.164
	2	21	204	10.1	0.29	**<0.001**

general sinusoidal periodic model also indicates significant results for *G. ruber* pink fluxes with the presence of three peaks through the year (Figure S5). Since we see no mechanism causing this kind of flux vari-

ability, we conclude that the flux of this species is virtually constant throughout the year.

As expected, the periodic regression analysis (Table 2; supporting information Figure S2) showed a highly significant ($p<0.01$) seasonal component in the variation of the AVHRR-SST and the temperatures recorded by the mooring. However, the AVHRR-SST showed a higher coefficient of determination ($r^2 = 0.85$) than temperatures from different depths of the moorings (0.16 to 0.21), which indicates that a large portion of the subsurface temperature variability in the region is not seasonal or that the satellite temperature values are averaged over an area large enough to alias smaller-scale variability which is preserved in the mooring measurements. It is noteworthy that for AVHRR-SST and for T30-40m and T40-50m the analysis revealed the presence of one cycle, while for temperatures at depths below 50 m, we observed the presence of two cycles per year.

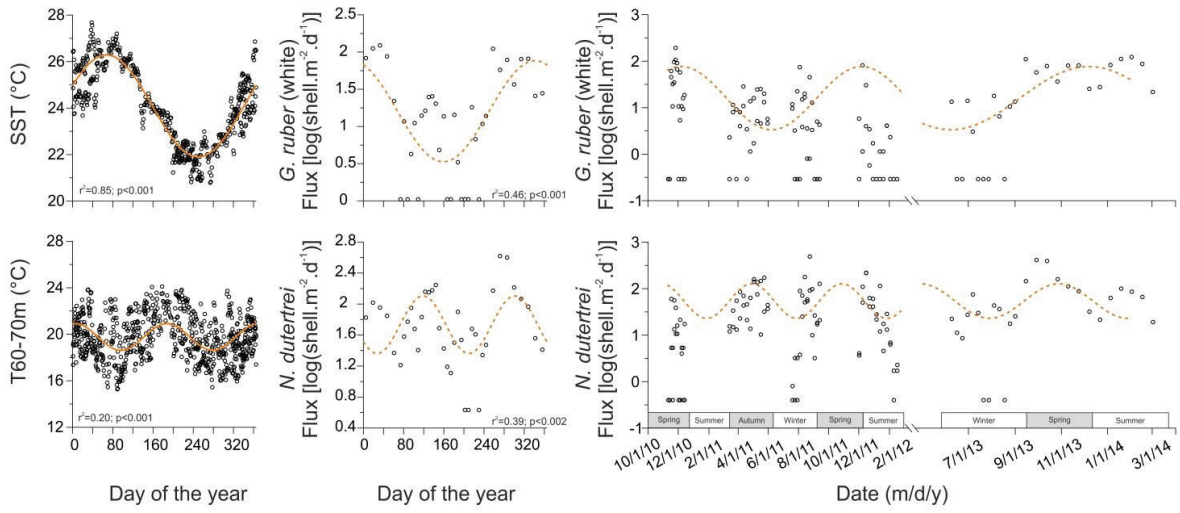

Figure 3. Periodic-regression results of two temperature sections (AVHRR-SST and T60-70m) and logarithmic shell fluxes of *G. ruber* (white) and *N. dutertrei*. Coefficients of determination values and p-values are given for each dataset. The lines in orange represent the models for the temperatures (solid lines) and for the shell fluxes (dashed lines). In the left panels the time is represented as days of the year and the shell fluxes are derived from the deployments 2, 6 and 7, while temperatures are daily records for the entire time series. In the right panels are the logarithmic shell fluxes of *G. ruber* (white) and *N. dutertrei* for the entire time series plotted with the model (orange dashed line) produced by the periodic regression. Seasons are exhibited above the x-axis of the right panel.

3.5.4. Calcification depths and flux-weighted $\delta^{18}O$

The estimated calcification depths revealed consistent differences among planktonic foraminifera species (Figure 4). *G. ruber* pink and *G. ruber* white (mode 30-40 m)

showed shallow calcification depths, followed by *T. sacculifer* and *O. universa* (mode 50-60 m) with more intermediate values, and *N. dutertrei* (mode 60-70 m) together with *G. menardii* (mode 70-80 m) showing the deepest calcification depths. The presence of vertical separation of calcification depths among the species is visible both in the distribution of the absolute values (Figure 4) as well as when considering the differences in estimated calcification depths of species from the same sediment trap samples (Figure 5). However, next to the strong interspecific signal, individual species showed a highly variable range of estimated calcification depths, which is also reflected in a large variability in offsets among the species. For individual species, there seems to be a pattern with the greatest calcification depths (>50m) more frequently observed in summer and winter. Indeed, periodic regression of the estimated calcification depths pooled for each species across all traps and sampling intervals (Table 2) indicates significant cyclic component in the variation of calcification depth in four out of the six analyzed species (Figure 4). The periodic regression explains about one third of the variance in the calcification depth data for those four species (*G. ruber pink* and white, *G. menardii* and *N. dutertrei*) and implies an objectively defined maximum calcification depth values in July (DOY 204-227) for these four species and also in January (DOY 21-25) for three of the species (*G. ruber* white, *G. menardii* and *N. dutretrei*) (Figure 4, Table 2). These are the times of the year (DOY 21-25 and 204-227) with deep (≈100m) mixed layer (Figure S3), which means the inferred calcification depth would be deeper without any change in habitat preference of those species. For *O. universa* and *T. sacculifer*, the variability in estimated calcification depths does not appear to have a periodic component.

When calculating the calcification depth, we noted that 4 % of the oxygen isotopic values exceed the range of possible predicted $\delta^{18}O$ ($\delta^{18}O_{predicted}$). This indicates that these foraminifera may have calcified in another (warmer) region, being subsequently transported to our site. This discrepancy is not observed for the deeper end of estimated calcification depths. Here, all of the observed $\delta^{18}O$ could have resulted from calcification above the sediment trap during the sampling interval. This is not to say that we can exclude that the calcification of some specimens occurred below 100 m and these specimens were still captured by the trap, because they ascended in the water column after the calcification due to water mass mixing or vertical migration. However, the data can be explained without requiring the existence of these mechanisms.

To obtain an estimate of the stable isotopic composition of sedimentary foraminifera that would be deposited below the sediment trap, we calculated flux

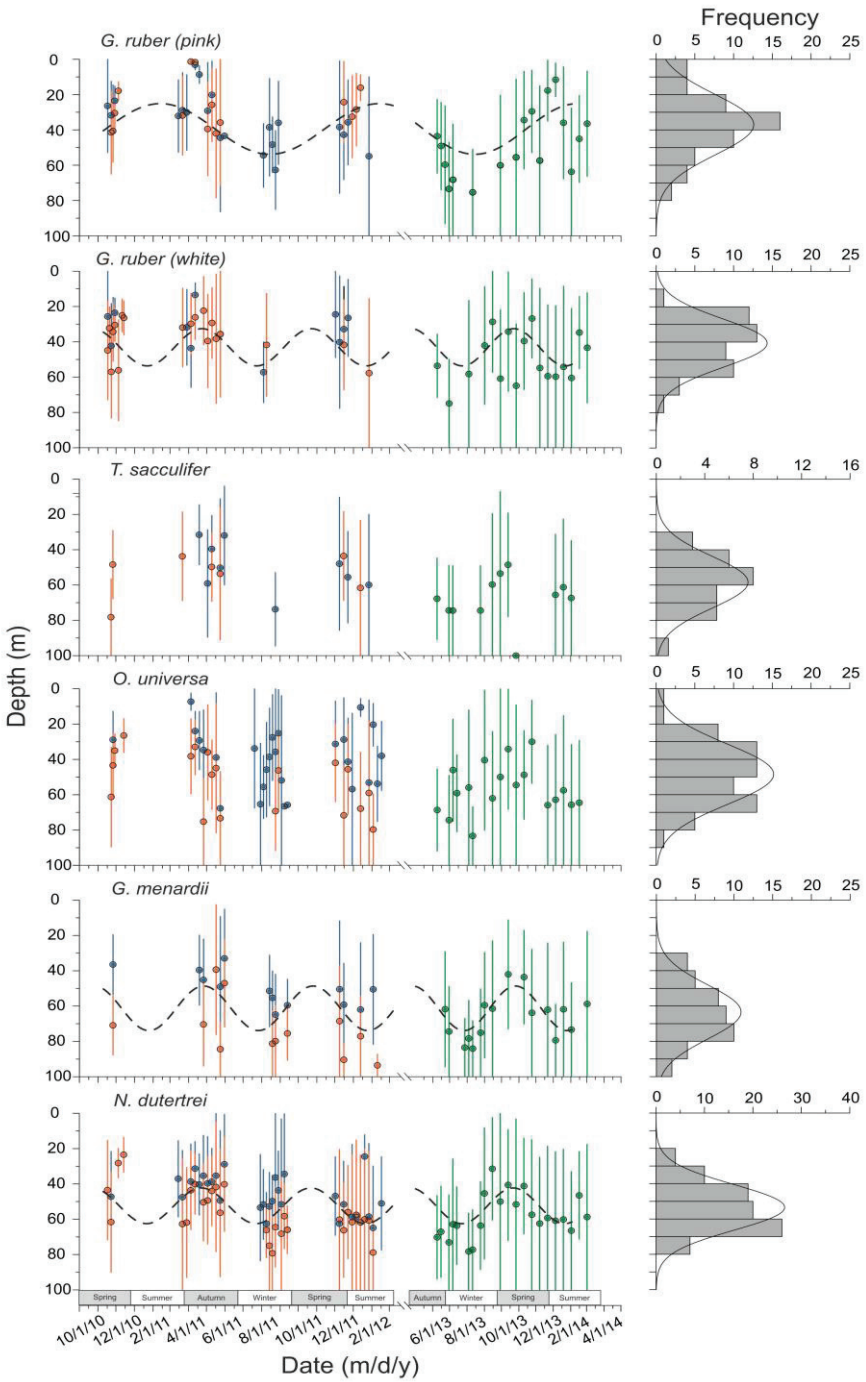

Figure 4. Calcification depths estimated for each planktonic foraminifera species for the entire time series. Maximum and minimum calcification depths are represented by the lines and the mean values are represented by circles. Colors represent the different trap depths 50m (blue), 100m (orange) and 75m (green). The right panels are histograms displaying the distribution of the mean values (grey bars) of calcification depths with the Gaussian distribution (black line). Seasonal component of the mean calcification depths was analyzed by periodic regression and the black dashed lines represent the models that were significant. Seasons are exhibited above the x-axis.

weighted annual mean $\delta^{18}O$ for the studied species. Because the seasonal component in shell fluxes was weak, the flux-weighted $\delta^{18}O$ values should mainly reflect specific calcification depths (Table 3). Indeed, the effect of flux weighting on the annual mean $\delta^{18}O$ was negligible (Table 3). The lowest value of flux-weighted mean annual $\delta^{18}O$ (-1.29 ‰) was shown by *G. ruber* pink, in line with the inferred shallower calcification depth for this species, while *N. dutertrei* showed the highest value (-0.26 ‰), in line with its deepest estimated calcification depth. Flux-weighted $\delta^{18}O$ values for *T. sacculifer* and *O. universa* were -0.67 and -0.56 ‰, in line with the similar calcification depth estimates for these species. This points to a comparable habitat for *T. sacculifer* and *O. universa* in the studied region.

Table 3. Species-specific estimations of $\delta^{18}O$ flux-weighted, annual mean $\delta^{18}O$, core tops $\delta^{18}O$, calcification depth, seasonal component in calcification depth and seasonal component in shell fluxes.

Species	$\delta^{18}O$ Flux-weighted (‰)	Annual mean $\delta^{18}O$ (‰)	Core tops $\delta^{18}O$ (‰)*	Calcification depth (m)	Seasonal depth (season; peak)	Model flux peak (season; peak)
G. ruber (pink)	-1.29	-1.27	-0.75 (±0.14)[a]; -1.16[c]	30-40	winter (DOY 227)	-
G. ruber (white)	-1.06	-1.08	-0.89[b];-0.99[c]	30-40	summer/winter (DOY 23; 205)	summer (DOY 342)
T. sacculifer	-0.67	-0.68	-0.54 (±0.14)[a]; -0.55[c]	50-60	-	-
O. universa	-0.56	-0.56	no data	≈50	-	-
G. menardii	-0.30	-0.37	0.06 (±0.18)[a]	70-80	summer/winter (DOY 25; 208)	-
N. dutertrei	-0.26	-0.25	0.13 (±0.16)[a]	60-70	summer/winter (DOY 21; 204)	fall/spring (DOY 119; 301)

*a: BCCF10-01 in Venancio et al. (2016b) – 100-yr mean values and standard deviations, recent age confirmed by age model based on 210Pb excess; b: CF10-01 in Lessa et al. (2016) – top centimeter with an age of 1030 yr confirmed by 14C dating; c: GeoB3207-2 in Chiessi et al. (2007) – uppermost centimeters with recent age confirmed by the presence of stained benthic foraminifera.

3.6. Discussion

Since the focus of this work is to provide information relevant for paleoceanographic studies using foraminifera-based proxies in the western South Atlantic, we begin by considering the main factors that can influence the interpretations of paleorecords in this region. We show the depth ranges in which each species calcify and how they may change seasonally (section 3.6.2), but we also present an evaluation of the magnitude and timing of the seasonal component in the foraminifera fluxes (section 3.6.1). Insights about both factors, seasonality of the shell fluxes and calcification depths, are necessary since a species may vary its

abundance in the water seasonally, independently from its habitat, resulting in a mixed signal in the sediment. A consideration of both the seasonal and vertical habitat of the studied species allowed us to predict the isotopic signal in surface sediments and show the potential of a multi-species approach for reconstructing past changes in the water column structure (section 3.6.3).

3.6.1. Seasonal fluxes

As pointed out by Jonkers and Kucera (2015), the seasonal component modulating shell fluxes in planktonic foraminifera is species-specific and varies spatially. For the six species analyzed in this study, the seasonal component in the flux data was significant only for *G. ruber* white and *N. dutertrei* (Table 2; supporting information Figure S1). This observation indicates that most of the warm-water species analyzed here (*G. ruber* pink, *T. sacculifer*, *O. universa*, *G. menardii*) show no seasonal bias in their flux and their sedimentation should reflect mean annual conditions. This is in line with the inferred decreasing amplitude of seasonal flux peak in warm-water species towards the tropics (Jonkers and Kucera, 2015). Even in the two species that showed a seasonal variation in their shell flux, the amplitude of the inferred seasonality is small and has little effect on the flux-weighted $\delta^{18}O$.

Because of the observed temperature dependency of flux seasonality in planktonic foraminifera (Jonkers and Kucera, 2015), a comparison with previous observations must be restricted to sediment traps from similar temperature settings. In this respect, a sediment trap record located at 11°S in western Atlantic (Žarić et al., 2005) also shows no significant seasonal component for any of the studied species, and nearby sediment trap record at 7°S (Žarić et al., 2005), shows seasonal components in the flux of *G. ruber* pink and *T. sacculifer*, but with a very low amplitude. These observations confirm that in the warm-water region of the western tropical Atlantic, shell fluxes of planktonic foraminifera show only weak seasonality.

For the species in which we observe a significant seasonal component (*G. ruber* white and *N. dutertrei*) one may ask which environmental conditions caused this preference towards a certain period or season (Figure 3). For *G. ruber* white, we observed higher fluxes during summer (Figure 3). This pattern cannot be solely attributed to the temperature preference of *G. ruber* white, because the species *G. ruber* pink and *T. sacculifer* show an equivalent degree of affinity towards warmer temperatures (Kucera, 2007), but none of them peaks in summer. An affinity to oligotrophic conditions cannot explain the summer peak of *G. ruber* white either, because other tropical surface-dwelling species appear to be even better adapted to such conditions (Siccha et al., 2009). Instead we hypothesize that the detection of the seasonal cycle in the flux of *G.*

ruber white reflects a combination of high SST and deep mixed layer during summer (Table 2; supporting information Figure S2). The fact that *G. ruber* pink does not show an increase in flux during these summer conditions is coherent, since previous studies suggested the dominance of *G. ruber* white over *G. ruber* pink when the mixed layer deepens (Ufkes et al., 1998; Sousa et al., 2014). In addition, the changes in habitat of *G. ruber* white are similar to the dynamics of the base of the mixed layer in the region (Figure 4; Table 2), unlike the other surface-dwelling species (*G. ruber* pink, *T. sacculifer* and *O. universa*), showing that this species is more sensitive to mixed layer changes and calcifying deeper during times when the mixed layer deepens.

The flux of *N. dutertrei* shows two peaks coinciding with periods of shoaling of the 18°C isotherm in our study area (Figure 3; supporting information Figure S3). Thus, it seems that *N. dutertrei* abundance increases when the thermocline is shallower, which is in agreement with previous findings, relating this species with thermocline dynamics (Fairbanks and Wiebe, 1980; Ravelo et al., 1990). Shoaling of the thermocline implies shoaling of the nutricline, which could stimulate population growth of the species either directly, by providing more nutrients to its symbionts or indirectly, by stimulating phytoplankton growth at depth. This hypothesis is supported by the consistently deepest estimated calcification depth for *N. dutertrei* (Figure 4, 5). The fact that the same pattern is not observed for *G. menardii* can be explained by lower abundances of this species, resulting in a more "noisy" flux pattern (Fig. 2, supporting information Figure S1).

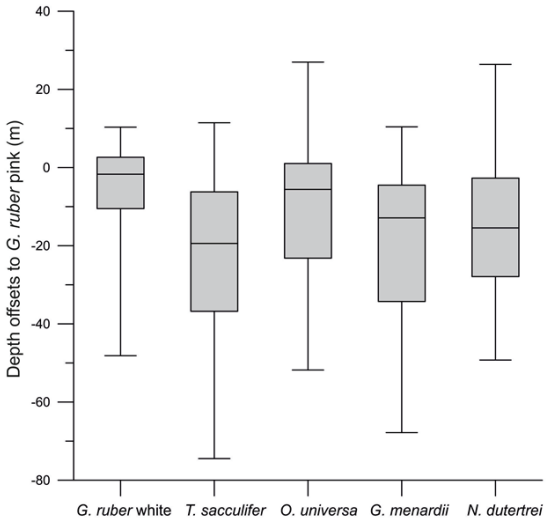

Figure 5. Box-and-whisker plots of the depth offsets of mean calcification depths of the investigated planktonic foraminifera species in relation to *G. ruber* pink calcification depths. The interspecific comparison was done only for calcification depths estimated in the same sample.

Considering the coefficients of determination of the periodic regression models, it is important to bear in mind that even for those species in which we observe a significant seasonal component, most of the flux variability cannot be explained in this way. As pointed out by Jonkers and Kucera (2015), this fact may be due to processes occurring at frequencies different from the annual cycle, such as lunar cycles, long-term trends or even non-periodic and random signals.

3.6.2. Calcification depths

The knowledge of the calcification depth of planktonic foraminifera species is indispensable in order to understand the signals derived from geochemical proxies recorded in their calcite. Because of discontinuous growth, calcification depth in planktonic foraminifera is not equivalent to habitat depth. Habitat depth is an ecological concept, describing the depth range where a population of a given species will be found. In contrast, calcification depth reflects the water depth at which most of the calcite of the shell has been precipitated and hence where the isotopic and trace-elemental signature of the shell is acquired. Habitat depth can be inferred directly from stratified plankton net samples. In contrast, calcification depth has to be inferred indirectly by comparing shell composition with vertical profiles of water properties and inferring at what depth the shell was most likely to be produced. This procedure incurs large uncertainties, and results from earlier studies are inconclusive as to the exact values of calcification depths and their regional (and temporal) stability (Cléroux et al., 2013; Farmer et al., 2007; Jonkers et al., 2010; Ravelo and Fairbanks, 1992; Sagawa et al., 2013; Simstich et al., 2003; Steph et al., 2009; Tedesco et al., 2007; Wejnert et al., 2013; Asahi et al., 2015).

Our study indicates species-specific typical calcification depths, which are variable in absolute values, but consistent in their order among the species. We observe that both varieties of *G. ruber* show shallowest calcification depths, with mode values around 30 to 40 m (Figure 4). Both species showed a seasonal component in the estimated calcification depth with deeper calcification during winter (G. *ruber* white also in summer), reflecting deepening of the mixed layer during this period, which necessarily leads to greater estimates of calcification depth. This observation implies that both species are consistently calcifying in the mixed layer, irrespective of its thickness. Shallow (mixed-layer) calcification depths for *G. ruber* white of 20 to 40 m were also estimated by Babila et al. (2014) using sediment traps from the Sargasso Sea. In sediment traps located in Cariaco Basin, calcification depths for *G. ruber* pink were also mostly in the same depth range, albeit with some deeper estimations up to 100 m during specific periods in the time series (Tedesco et al., 2007; Wejnert et al., 2013). Studies using surface sediments from the tropical Atlantic also pointed to a similar range of calcification depth for *G. ruber* (Farmer et al., 2007; Steph et al., 2009). Collectively, our findings and the literature data reviewed above suggest that despite temporal and regional variability in the oceanographic conditions in their habitat, the calcification of both varieties of *G. ruber* occurs within the mixed layer.

Estimated calcification depths for *O. universa* and *T. sacculifer* yielded slightly deeper values (50-60 m) than *G. ruber* (pink and white) (Figures 4 and 5). Thus, the calcification habitat of these species must extend below the mixed layer. This conclusion is supported by the observation that these species did not show a significant seasonal component in their calcification depths (Table 2), which indicates that their depth habitat is not strictly linked to the mixed layer. A study in the western tropical Indian Ocean also observed similar calcification depths between *O. universa* and *T. sacculifer*, characterizing both as deeper mixed layer species (Birch et al., 2013). Previous studies also pointed to deeper calcification of *O. universa* and *T. sacculifer* in comparison to *G. ruber* (Steph et al., 2009; Tedesco et al., 2007; Wejnert et al., 2013). In contrast, Farmer et al. (2007) found no differences in calcification depths among these three species, although they also noted a wider calcification depth range for *O. universa.*

For the deep-dwelling species (*N. dutertrei* and *G. menardii*), the estimated calcification depths are also consistently below those of *G. ruber* (Figure 5), ranging mostly below 50 m (Figure 4). Both species show a seasonal component in their calcification depths (Table 2), with greater calcification depths during summer and winter when the mixed layer deepens. This is consistent with tracking of a subsurface habitat throughout the year. Indeed, the estimated calcification depths for *N. dutertrei* have a mode in the interval between 60-70m. This value is in agreement with the reported thermocline depth or the 18°C isotherm for the region (Valentin, 2001; Albuquerque et al., 2014) and with our temperature records (supporting information Figure S3), which shows the presence of the 18°C isotherm between 60 and 80 m, mainly during spring and autumn. An upper thermocline calcification depth for this species is in agreement with previous studies (Farmer et al., 2007; Steph et al., 2009), including the estimates from Sagawa et al. (2013) who estimated a 25-35 m calcification depth for *N. dutertrei* in the western North Pacific in summer, where the seasonal mixed layer is shallow. In the Cariaco Basin (Tedesco et al., 2007; Wejnert et al., 2013), the calcification habitat of this species also corresponds to the uppermost thermocline and it appears to follow the seasonal upwelling pattern with deep calcification coinciding with the cessation of upwelling in fall. Although the number of observations on *G. menardii* is lower in our study due to lower abundance, it shows similar behavior as *N. dutertrei* in all respects, which is consistent with observations from Cariaco Basin (Tedesco et al., 2007; Wejnert et al., 2013).

Because of the observed high level of consistency between the measured $\delta^{18}O$ values in the investigated foraminifera species and predicted values for the water col-

umn above the sediment traps, we can exclude expatriation (Berger, 1970) as a significant process affecting the foraminiferal flux. Only 4% of $\delta^{18}O$ values were out of range of possible species-specific $\delta^{18}O_{predicted}$ curves. All of these values exceeded predictions towards the warmer end, but with different probabilities between the analyzed species. This was more frequent for *G. ruber* white, *G. ruber* pink and *O. universa*, which showed 9.3, 5.4 and 6.2 % of $\delta^{18}O$ values out of range, while this was observed in less than 3 % of the cases for the other species. These discrepancies may remain even when changing the paleotemperature equations (not shown). Thus, some of the analyzed foraminifera appear to have calcified under warmer conditions outside of the studied area and were then transported to the sediment traps. This is a reasonable assumption, since our mooring is located over the southeastern continental shelf, which can be influenced by intense lateral transport. Therefore, specimens with a distinct oxygen isotopic signature may have been passively transported to our region by lateral advection, but their flux appears to have been overwhelmed by local production.

Finally, we consider the bias that may arise from the fact that our $\delta^{18}O$ measurements could not be carried in a narrow size range. In this scenario, part of the intraspecific $\delta^{18}O$ signal may be due to the size variation of the analyzed specimens. Indeed, Ezard et al. (2015) using a statistical model approach suggest a size dependency in $\delta^{18}O$ for species analyzed in this study. However, the trend arises from values recorded mainly in small specimens and no clear $\delta^{18}O$ trend with size can be identified in their raw data compilation for the analyzed species within the size range used here for the isotopic measurements. Furthermore, Birch et al. (2013) in a study in the western Indian Ocean analyzed multi-species through different size ranges and although a significant size-dependent effect was observed for the $\delta^{13}C$, the authors concluded that no significant correlation was observed between the size of the test and the $\delta^{18}O$ composition of *G. ruber*, *T. sacculifer* and *O. universa*. These observations suggest that although an influence of the test size on the $\delta^{18}O$ may exist, it is unlikely to have accounted for a substantial part of the variance in the $\delta^{18}O$ signal of the analyzed species. The existence of a stronger dependency of $\delta^{13}C$ on size is also the reason why $\delta^{13}C$ variation is not being considered in this study.

3.6.3. Paleoceanographic implications

The southwestern Atlantic has been the focus of recent paleoceanographic studies, with most of these reconstructions using planktonic foraminifera assemblages or the geochemical composition of their shells in order to reconstruct past surface water conditions (Chiessi et al., 2014; Chiessi et al., 2015; Lessa et al., 2016). For instance, these

studies used the geochemical composition of the shells of *G. ruber* (white) (Chiessi et al., 2014; Lessa et al., 2016) without considering the possibility that this species might not be recording mean annual conditions or that the recorded signal might come from deeper layers. Our results for *G. ruber* (white) show that the fluxes of this species are slightly biased towards summer conditions and that their calcification depths are variable and linked to the dynamics of the mixed layer, although the mean signal is linked to the depths of 30-40 m. Thus, our findings can provide important constraints on the temporal and vertical distribution of the planktonic foraminifera species fluxes and the resulting $\delta^{18}O$ signatures in their shells, which may help improve paleoceanographic interpretations for the region Moreover, with this information it becomes easier to evaluate which species are more suitable for paleoceanographic reconstructions in the area. To this end, we first compared the $\delta^{18}O$ signature exported by the different species to the sediment (flux-weighted mean annual $\delta^{18}O$) with $\delta^{18}O$ values observed in recent sediments from the same area. We observe that for all species, the flux-weighted mean annual $\delta^{18}O$ preserve the same species offsets, but the values are lower than the $\delta^{18}O$ values measured in recent sediments (Table 3, Figure 6), except *O. universa* for which no data is available from recent sediments.

The higher sedimentary values could occur for several reasons. First, sediment samples represent multi-annual averages and their mean isotopic signal is therefore skewed towards years with higher flux. However, as the species fluxes showed little or no seasonality in our region (Figure 3; supporting information), this process is unlikely to account for the large offsets we observe (up to 0.4 ‰; Table 3). Alternatively, the difference could reflect recent warming in the region, which is not reflected in the sediment signature because of temporal averaging. This is not unreasonable, because the observed $\delta^{18}O$ offset corresponds to < 2°C. Finally, the offset may be due to the fact that planktonic foraminifera form a secondary layer of calcite at the end of their life cycle, which results in higher values of $\delta^{18}O$ (Bé, 1980; Erez and Honjo, 1981). Because of their shallow position at 50-100 m, our traps may have collected not only dead specimens (empty shells) but also live specimens that would have continued growing if they had not entered the trap. Therefore, there is a higher probability to found individuals which have acquired the heavier $\delta^{18}O$ signal associated with secondary calcite in the sediments than in our traps.

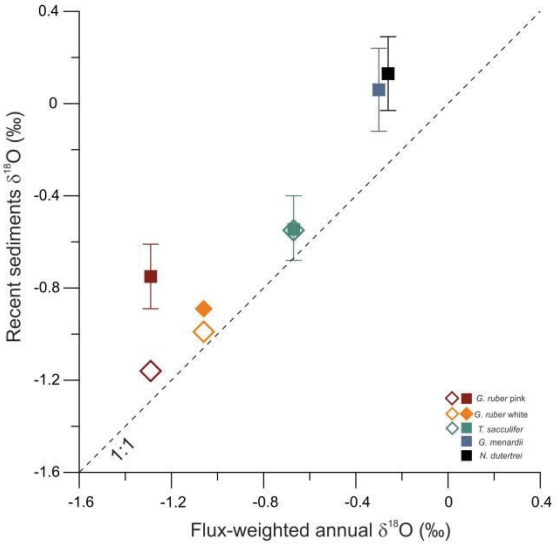

Figure 6. Offset between flux-weighted mean annual $\delta^{18}O$ and $\delta^{18}O$ values from recent sediments provided by several studies for each of the investigated planktonic foraminifera species, except *O. universa*. Open diamonds represent the offsets using the core top $\delta^{18}O$ values derived from GeoB3207-2 (Chiessi et al., 2007). Diamonds represent core top $\delta^{18}O$ values derived from CF10-01 (Lessa et al., 2016). Squares with standard deviations represent a 100-yr average of $\delta^{18}O$ values derived from the box-core BCCF10-01 (Venancio et al., 2016b).

Since the sediment and the trap have different mechanisms of particle delivery, the difference could also reflect lateral transport of shells along the sea floor. An intense along-shelf and cross-shelf transport could entrain foraminifera that were originally deposited shallower, closer to coast. Due to the presence of upwelling systems along the southeastern Brazilian coast, these shells could have acquired a heavier $\delta^{18}O$ signature due to lower surface (or subsurface) temperatures in these regions, being subsequently transported to the sediments below our mooring line. However, we observe that $\delta^{18}O$ differences between species are still in agreement in both set of samples (traps and sediments), which means that the vertical differences in calcification depths were kept in the fossil record. We also note that planktonic foraminifera are known to avoid shallow waters (Schmuker and Schiebel, 2002) and the flux of specimens that would calcify over shelf areas substantially shallower and thus far away from the traps was likely small. Thus, we conclude that the main pattern of interspecies isotopic offsets is preserved in sediment assemblages.

Since *G. ruber* pink exhibits the shallowest calcification depth with relatively constant annual fluxes, it would be the best species to characterize surface-ocean conditions in the southwestern Atlantic. Moreover, this species is very abundant in surface sediments in the area (Lessa et al., 2014). In contrast, *N. dutertrei* appears to calcify within the seasonal thermocline and it consistently tracks this habitat throughout the year (Figure 4). Its fluxes also appear to be influenced by the depth of the thermocline, but the amplitude of the signal is low and does not affect the flux-weighted annual mean (Table 3). Consequently, *N. dutertrei* $\delta^{18}O$ could be used to reconstruct the temperature of the seasonal thermocline. Although *G. menardii* could also be used to reconstruct the thermocline conditions, this species has low

abundances in the trap and sediment samples in the area, and is absent during glacial periods in the cores located in the Brazilian margin (Vicalvi, 1997; Portilho-Ramos et al., 2015), making it difficult to use the $\delta^{18}O$ of *G. menardii* for paleoceanographic reconstructions on glacial-interglacial timescales.

The difference between shell geochemistry of *G. ruber* pink and *N. dutertrei*, for example the $\Delta\delta^{18}O$ of these species, should thus be a proxy for stratification. The use of such proxy for paleoceanographic reconstructions was also proposed by sediment traps studies from the Cariaco Basin (Tedesco et al., 2007; Wejnert et al., 2013). In order to validate this approach in our region, we compared the $\Delta\delta^{18}O$ between *N. dutertrei* and *G. ruber* pink with temperature difference between depths where the specimens calcified (Figure 7). Although, *G. ruber* pink calcifies mostly around 30-40 m, we used the temperature difference from the surface (SST) to the thermocline (60-70 m), since *G. ruber* pink may calcify at shallower depths. For the thermocline layer we used the temperatures extracted from 60-70 m, which coincide with the mean calcification depth of *N. dutertrei*, and represent the same seasonal temperature pattern of the temperatures recorded below 50 meters (Table 2; supporting information).

The estimated calcification depths of *G. ruber* pink were mostly around 30-40 m, with the presence of a seasonal cycle in calcification depth, indicating calcification within the mixed layer, while estimated calcification depths for *N. dutertrei* were mostly around 60-70, also with a significant seasonal component, but with calcification corresponding to the uppermost thermocline (Figure 4). Since the annually averaged sedimentary signal cannot resolve such seasonal habitat migration it would instead record a flux-weighted mean offset in calcification depths between the species. We observed that the annual mean flux weighted $\Delta\delta^{18}O$ offset between the species is 1.03 ‰, which corresponds well to the annual mean difference in predicted $\delta^{18}O$ of 1.08 ‰ between 30-40 m and 60-70 m.

In summary, we show that planktonic foraminifera species in the studied area show consistent isotopic offsets reflecting mainly their preferred habitats and that this signal is preserved in the sediment and only minimally modified by secondary calcite formation or expatriation. Therefore, stratification is captured by interspecific oxygen isotopic signatures. The apparent ability to reconstruct stratification in the studied region could provide valuable information regarding the strength of the Brazil Current (Belem et al., 2013) and the state of the nearby upwelling systems (Cordeiro et al., 2014; Souto et al., 2011; Lessa et al., 2016). This exemplifies the potential of species-specific calcification depth estimations and highlights the importance of local assess-

ments using continuous high-resolution records with co-registered hydrography. The information here presented also provide the basis for future foraminifera-based proxy development, since it shows to what water depth (or depth range) the chemical composition of each planktonic foraminifera species should be attributed, thus indicating to what water depth must a target environmental parameter be calibrated when developing a proxy using one of the species here analyzed.

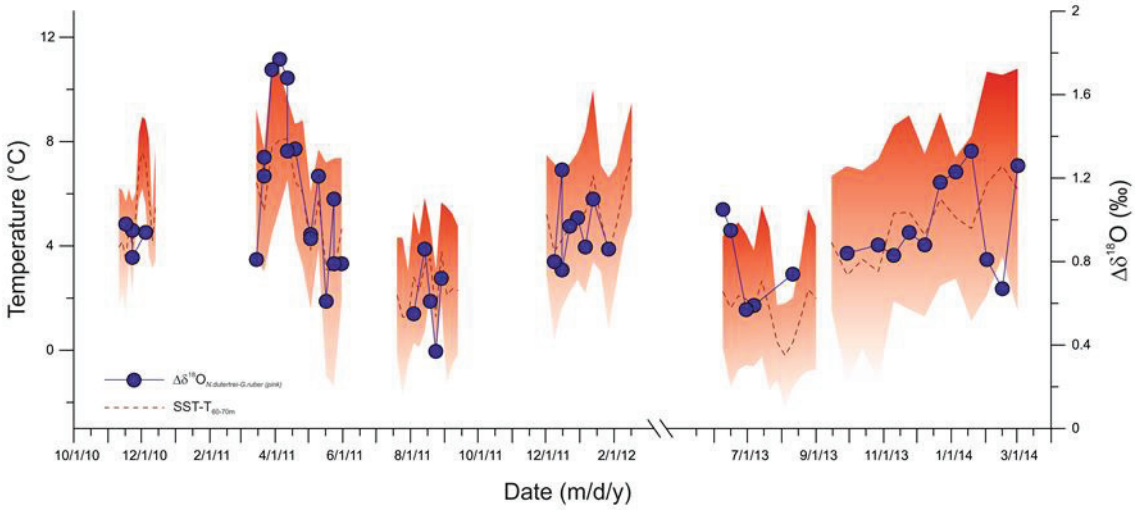

Figure 7. Temperature difference between AVHRR-SST and T60-70m plotted with the oxygen isotopic difference ($\Delta\delta^{18}O$) between *G. ruber* pink and *N. dutertrei*. Temperature difference is represented by the red dashed line, with the errors estimated by error propagation represented by the shades of red. The ($\Delta\delta^{18}O$) between *G. ruber* pink and *N. dutertrei* is represented by the blue line and circles.

3.7. Conclusions

Based on our mooring records we estimated the influence of the seasonal component in the shell fluxes of six planktonic foraminifera species and their calcification depth ranges in the southwestern Atlantic. Our main observations revealed the following:

(1) The majority of the warm-water species analyzed here (*G. ruber* pink, *T. sacculifer*, *O. universa*, *G. menardii*) exhibit no significant seasonal component in their shell fluxes and most likely reflect mean annual conditions. Only the fluxes of *G. ruber* white and *N. dutertrei* exhibit a significant seasonal component, with *G. ruber* white showing a single flux peak in austral summer, while *N. dutertrei* exhibits two flux peaks in spring and autumn, but the amplitude of the inferred flux seasonality was small.

(2) Estimated calcification depths indicate species-specific mean calcification depth, albeit overprinted by a considerable variability throughout the year. The estimated calcification depths for *N. dutertrei* (mode

60-70 m) and *G. menardii* (mode 70-80 m) appear to track the depth of the thermocline in the region, whereas the calcification depths of *G. ruber* pink and white correspond to conditions in the mixed layer. The calcification habitat of *O. universa* and *T. sacculifer* extends below the mixed layer and these species show no systematic seasonal variation in their calcification depth.

(3) Isotopic offsets among the species in sediment samples are mainly due to different calcification depths. The lower values in oxygen isotopic composition in sediment samples (up to 0.4 ‰) relative to the trap samples can be explained by the presence of specimens, which added a secondary layer of calcite at the end of their life cycle.

(4) Our calcification depth estimations and assessments of the influence of seasonality provide the basis for paleoceanographic interpretations in the study area and allow further studies to reconstruct water column parameters at specific depth ranges using multi-species approach. For example, as shown by our $\Delta\delta^{18}O$ between surface species (best represented by *G. ruber* pink) and thermocline species (best represented by *N. dutertrei*), it can be used for evaluating stratification in the southwestern Atlantic.

3.8. Acknowledgments

This study was financially supported by the Geochemistry Network from PETROBRAS/National Petroleum Agency (ANP) of Brazil (Grant 0050.004388.08.9). A.L.S. Albuquerque is senior scholar from CNPq (National Council for the Development of Science and Technology, Brazil, Grant 306385/2013-9). The CNPq also financially supported Igor Venancio with a scholarship from the CsF ("Ciencia sem Fronteiras") project (Grant 248819/2013-5). This work was also funded through the DFG Research Center/Cluster of Excellence "The Ocean in the Earth System".

3.9. References

Al-Sabouni, N., Kucera, M., Schmidt, D.N., 2007. Vertical niche separation control of diversity and size disparity in planktonic foraminifera. Mar. Micropaleontol. 63, 75–90. doi:10.1016/j.marmicro.2006.11.002

Albuquerque, A.L.S., Belém, A.L., Zuluaga, F.J.B., Cordeiro, L.G.M., Mendoza, U., Knoppers, B. a., Gurgel, M.H.C., Meyers, P. a., Capilla, R., 2014. Particle fluxes and bulk geochemical characterization of the Cabo Frio Upwelling System in Southeastern Brazil: Sediment trap experiments between spring 2010 and summer 2012. An. Acad. Bras. Cienc. 86, 601–619. doi:10.1590/0001-37652014107212

Aurahs, R., Treis, Y., Darling, K., Kucera, M., 2011. A revised taxonomic and phylogenetic concept for the planktonic foraminifer species *Globigerinoides ruber* based on molecular and morphometric evidence. Mar. Micropaleontol. 79, 1–14. doi:10.1016/j.marmicro.2010.12.001

Asahi, H., Okazaki, Y., Ikehara, M., Khim, B.K., Nam, S. Il, Takahashi, K., 2015. Seasonal variability of $\delta^{18}O$ and $\delta^{13}C$ of planktic foraminifera in the Bering Sea and central subarctic Pacific during 1990-2000. Paleoceanography 30, 1328–1346. doi:10.1002/2015PA002801

Babila, T.L., Rosenthal, Y., Conte, M.H., 2014. Evaluation of the biogeochemical controls on B/Ca of Globigerinoides ruber white from the Oceanic Flux Program, Bermuda. Earth Planet. Sci. Lett. 404, 67–76. doi:10.1016/j.epsl.2014.05.053

Bé, A. W. H.,1980. Gametogenic calcification in a spinose planktonic foraminifer, Globigerinoides sacculifer (Brady), Mar. Micropaleontol., 5(3), 283–310, doi:10.1016/0377-8398(80)90014-6.

Belem, A.L., Castelao, R.M., Albuquerque, A.L., 2013. Controls of subsurface temperature variability in a western boundary upwelling system. Geophys. Res. Lett. 40, 1362–1366. doi:10.1002/grl.50297

Bell, K.N.I., Cowley, P.D., Whitfield, A. K., 2001. Seasonality in Frequency of Marine Access to an Intermittently Open Estuary: Implications for Recruitment Strategies. Estuar. Coast. Shelf Sci. 52, 327–337. doi:10.1006/ecss.2000.0709

Bemis, B.E., Spero, H.J., Bijma, J., Lea, D.W., 1998. Reevaluation of the oxygen isotopic composition of planktonic foraminifera: Experimental results and revised paleotemperature equations. Paleoceanography 13, 150–160. doi:10.1029/98PA00070

Bemis, B.E., Spero, H.J., Thunell, R.C., 2002. Using species-specic paleotemperature equations with foraminifera : a case study in the Southern California Bight. Mar. Micropaleontol. 46, 405–430.

Berger, W., 1970. Planktonic Foraminifera: Differential production and expatriation off Baja California. Limnol. Oceanogr. 15, 183–204. doi:10.4319/lo.1970.15.2.0183

Birch, H., Coxall, H.K., Pearson, P.N., Kroon, D., O'Regan, M., 2013. Planktonic foraminifera stable isotopes and water column structure: Disentangling ecological signals. Mar. Micropaleontol. 101, 127–145. doi:10.1016/j.marmicro.2013.02.002

Bouvier-Soumagnac, Y., Duplessy, J. C., 1985. Carbon and oxygen isotopic composition of planktonic foraminifera from laboratory culture, plankton tows and recent sediment: Implications for the reconstruction of paleoclimatic conditions and of the global carbon cycle, J. Foraminiferal Res., 15(4), 302–320.

Brandini, F.P., 1990. Hydrography and characteristics of the phytoplankton in shelf and oceanic waters off southeastern Brazil during winter (July/August 1982) and summer (February/March 1984). Hydrobiologia 196, 111–148. doi:10.1007/BF00006105

Calado, L., da Silveira, I.C.A., Gangopadhyay, A., de Castro, B.M., 2010. Eddy-induced upwelling off Cape São Tomé (22°S, Brazil). Cont. Shelf Res. 30, 1181–1188. doi:10.1016/j.csr.2010.03.007

Campos, E.J.D., Velhote, D., Area, T.S., 2000. Shelf break upwelling driven by Brazil Current cyclonic meanders. Geophys. Res. Lett. 27, 751–754.

Castelao, R.M., 2012. Sea Surface Temperature and Wind Stress Curl Variability near a Cape. J. Phys. Oceanogr. 42, 2073–2087. doi:10.1175/JPO-D-11-0224.1

Castelao, R.M., Barth, J. a., 2006. Upwelling around Cabo Frio, Brazil: The importance of wind stress curl. Geophys. Res. Lett. 33, L03602. doi:10.1029/2005GL025182

Castro, B.M., 2014. Summer/winter stratification variability in the central part of the South Brazil Bight. Cont. Shelf Res. 89, 15–23. doi:10.1016/j.csr.2013.12.002

Cerda, C., Castro, B.M., 2014. Hydrographic climatology of South Brazil Bight shelf waters between Sao Sebastiao (24°S) and Cabo Sao Tome (22°S). Cont. Shelf Res. 89, 5–14. doi:10.1016/j.csr.2013.11.003

Chiessi, C.M., Mulitza, S., Groeneveld, J., Silva, J.B., Campos, M.C., Gurgel, M.H.C., 2014. Variability of the Brazil Current during the late Holocene. Palaeogeogr. Palaeoclimatol. Palaeoecol. 415, 28–36. doi:10.1016/j.palaeo.2013.12.005

Chiessi, C.M., Mulitza, S., Mollenhauer, G., Silva, J.B., Groeneveld, J., Prange, M., 2015. Thermal evolution of the western South Atlantic and the adjacent continent during

Termination 1. Clim. Past 11, 915–929. doi:10.5194/cp-11-915-2015

Cléroux, C., DeMenocal, P., Arbuszewski, J., Linsley, B., 2013. Reconstructing the upper water column thermal structure in the Atlantic Ocean. Paleoceanography 28, 503–516. doi:10.1002/palo.20050

Cordeiro, L.G.M.S., Belem, A.L., Bouloubassi, I., Rangel, B., Sifeddine, A., Capilla, R., Albuquerque, A.L.S., 2014. Reconstruction of southwestern Atlantic sea surface temperatures during the last Century: Cabo Frio continental shelf (Brazil). Palaeogeogr. Palaeoclimatol. Palaeoecol. doi:10.1016/j.palaeo.2014.01.020

deBruyn, a. M.H., Meeuwig, J.J., 2001. Detecting lunar cycles in marine ecology: Periodic regression versus categorical ANOVA. Mar. Ecol. Prog. Ser. 214, 307–310. doi:10.3354/meps214307

Duplessy, J., Labeyrie, L., Juillet-Leclerc, A., 1991. Surface salinity reconstruction of the North Atlantic Ocean during the last glacial maximum. Oceanol. Acta 311–324.

Erez, J., Honjo S., 1981. Comparison of isotopic composition of planktonic foraminifera in plankton tows, sediment traps, and sediments, Palaeogeogr. Palaeoclimatol. Palaeoecol., 33(1–3), 129–156.

Ezard, T.H.G., Edgar, K.M., Hull, P.M., 2015. Environmental and biological controls on size-specific δ13C and $\delta^{18}O$ in recent planktonic foraminifera. Paleoceanography 151–173. doi:10.1002/2014PA002735

Fairbanks, R.G., Wiebe, P., 1980. Foraminifera and chlorophyll maximum: vertical distribution, seasonal succession, and paleoceanographic significance. Science, 209, 1524–1525.

Farmer, E.C., Kaplan, A., de Menocal, P.B., Lynch-Stieglitz, J., 2007. Corroborating ecological depth preferences of planktonic foraminifera in the tropical Atlantic with the stable oxygen isotope ratios of core top specimens. Paleoceanography 22, n/a-n/a. doi:10.1029/2006PA001361

Franchito, S.H., Rao, V.B., Stech, J.L., Lorenzzetti, J.A., 1998. The effect of coastal upwelling on the sea-breeze circulation at Cabo Frio, Brazil : a numerical experiment. Ann. Geophys. 16, 866–881. doi:10.1007/s005850050656

Gibson, K.A., Thunell, R.C., Machain-Castillo, M.L., Fehrenbacher, J., Spero, H.J., Wejnert, K., Nava-Fernandez, X., Tappa, E.J., 2016. Evaluating controls on planktonic foraminiferal geochemistry in the Eastern Tropical North Pacific. Earth Planet. Sci. Lett. 452, 90–103. doi:10.1016/j.epsl.2016.07.039

Goswami, S., 2004. Zooplankton Methodology, Collection & identyification - A field manual. Natl. Inst. Oceanogr. 16.

Hammer, Ø., Harper, D.A.T. A. T., Ryan, P.D., 2001. PAST: Paleontological Statistics Software Package for Education and Data Analysis. Palaeontol. Electron. 4(1), 1–9. doi:10.1016/j.bcp.2008.05.025

Hut, G., 1987. Consultants' group meeting on stable isotope reference samples for geochemical and hydrological investigations. Rep. to Dir. Gen. 16–18. doi:18075746

Ikeda, Y., Miranda, L.B., Rock, N.J., 1974. Observations on stages of upwelling in the region of Cabo Frio (Brazil) as conducted by continuous surface temperature and salinity measurements. Bol. do Inst. Ocean. São Paulo 23, 33–46.

Jonkers, L., Brummer, G.J. a, Peeters, F.J.C., Van Aken, H.M., De Jong, M.F., 2010. Seasonal stratification, shell flux, and oxygen isotope dynamics of leftcoiling N. pachyderma and T. quinqueloba in the western subpolar North Atlantic. Paleoceanography 25, 1–13. doi:10.1029/2009PA001849

Jonkers, L., Kucera, M., 2015. Global analysis of seasonality in the shell flux of extant planktonic foraminifera. Biogeosciences 1327–1372. doi:10.5194/bgd-12-1327-2015

King, A.L., Howard, W.R., 2005. $\delta^{18}O$ seasonality of planktonic foraminifera from Southern Ocean sediment traps: Latitudinal gradients and implications for paleoclimate

reconstructions. Mar. Micropaleontol. 56, 1–24. doi:10.1016/j.marmicro.2005.02.008

Kucera, M. 2007. Planktonic foraminifera as tracers of past oceanic environments, in Proxies in Late Cenozoic Paleoceanography, vol. 1,edited by C. Hillaire-Marcel and A. de Vernal, chap. 6, pp. 213–262, Elsevier, Amsterdam., doi:10.1016/S1572-5480(07)01011-1.

Lessa, D.V. de O., Ramos, R.P., Barbosa, C.F., da Silva, A.R., Belem, A., Turcq, B., Albuquerque, A.L., 2014. Planktonic foraminifera in the sediment of a western boundary upwelling system off Cabo Frio, Brazil. Mar. Micropaleontol. 106, 55–68. doi:10.1016/j.marmicro.2013.12.003

Lessa, D. V., Venancio, I.M., dos Santos, T.P., Belem, A. L., Turcq, B.J., Sifeddine, a., Albuquerque, a. L.S., 2016. Holocene oscillations of Southwest Atlantic shelf circulation based on planktonic foraminifera from an upwelling system (off Cabo Frio, Southeastern Brazil). The Holocene. doi:10.1177/0959683616638433

Lopes, R.M., Katsuragawa, M., Dias, J.F., Monica, A., Muelbert, J.H., Gorri, C., Brandini, F.P., 2006. Zooplankton and ichthyoplankton distribution on the southern Brazilian shelf : an overview. Sci. Mar. 70, 189–202.

Mix, A., 1987. The oxygen-isotope record of glaciation. The Geology of North America, K-3, edited by: Ruddiman, W. F. and Wright, H. E., Geol. Soc. Am., Boulder CO, 111–135.

Mulitza, S., Boltovskoy, D., Donner, B., Meggers, H., 2003. Temperature:$\delta^{18}O$ relationships of planktonic foraminifera collected from surface waters. Palaeogeogr. Palaeoclimatol. Palaeoecol. 202, 143–152. doi:10.1016/S0031-0182(03)00633-3

Mulitza, S., Dürkoop, A., Hale, W., Wefer, G., Niebler, H.S., 1997. Planktonic foraminifera as recorders of past surface-water stratification. Geology 25, 335–338. doi:10.1130/0091-7613(1997)025<0335

Mulitza, S., Wolff, T., Pätzold, J., Hale, W., Wefer, G., 1998. Temperature sensitivity of planktic foraminifera and its influence on the oxygen isotope record. Mar. Micropaleontol. 33, 223–240.

Peterson, R.G., Stramma, L., 1991. Upper-level circulation in the South Atlantic Ocean. Prog. Oceanogr. 26, 1–73. doi:10.1016/0079-6611(91)90006-8

Pierre, C., Vergnaud-grazzini, C., Faughres, J., 1990. Oxygen and carbon stable isotope tracers of the water masses in the Central Brazil Basin. Deep Sea Res. Part A. Oceanogr. Res. Pap. 38, 597–606.

Portilho-Ramos, R. da C., Ferreira, F., Calado, L., Frontalini, F., de Toledo, M.B., 2015. Variability of the upwelling system in the southeastern Brazilian margin for the last 110,000 years. Glob. Planet. Change 135, 179–189. doi:10.1016/j.gloplacha.2015.11.003

Ravelo, A.C., Fairbanks, R.G., 1992. Oxygen isotopic composition of multiple species of planktonic foraminifera: recorders of the modern photic zone temperature gradient. Paleoceanography 7, 815–831. doi:10.1029/92PA02092

Ravelo, A.C., Fairbanks, R.G., Philander, S.G.H., 1990. Reconstructing tropical Atlantic hydrography using planktonic foraminifera and an ocean model. Paleoceanography 5, 409–431.

Rebotim, A., Voelker, A.H.L., Jonkers, L., Waniek, J.J., Meggers, H., Schiebel, R., Fraile, I., Schulz, M., Kucera, M., 2017. Factors controlling the depth habitat of planktonic foraminifera in the subtropical eastern North Atlantic. Biogeosciences 14, 827–859. doi:10.5194/bg-2016-348

Rodrigues, R.R., Lorenzzetti, J. a., 2001. A numerical study of the effects of bottom topography and coastline geometry on the Southeast Brazilian coastal upwelling. Cont. Shelf Res. 21, 371–394. doi:10.1016/S0278-4343(00)00094-7

Sagawa, T., Kuroyanagi, A., Irino, T., Kuwae, M., Kawahata, H., 2013. Seasonal varia-

tions in planktonic foraminiferal flux and oxygen isotopic composition in the western North Pacific: Implications for paleoceanographic reconstruction. Mar. Micropaleontol. 100, 11–20. doi:10.1016/j.marmicro.2013.03.013

Schmuker, B., Schiebel, R., 2002. Planktic foraminifers and hydrography of the eastern and northern Caribbean Sea. Mar. Micropaleontol. 46, 387–403. doi:10.1016/S0377-8398(02)00082-8

Siccha, M., Trommer, G., Schulz, H., Hemleben, C., Kucera, M., 2009. Factors controlling the distribution of planktonic foraminifera in the Red Sea and implications for the development of transfer functions. Mar. Micropaleontol. 72, 146–156. doi:10.1016/j.marmicro.2009.04.002

Silveira, I.C.A., Lima, J.A.M., Schmidt, A.C.K., Ceccopieri, W., Sartori, A., Franscisco, C.P.F., Fontes, R.F.C., 2008. Is the meander growth in the Brazil Current system off Southeast Brazil due to baroclinic instability? Dyn. Atmos. Ocean. 45, 187–207. doi:10.1016/j.dynatmoce.2008.01.002

Silveira, I.C.A., Schmidt, A., Campos, E.J.D., Godoi, S.S. De, Ikeda, Y., 2000. A Corrente do Brasil ao Largo da Costa Leste Brasileira. Rev. Bras. Oceanogr. 48, 171–183.

Simstich, J., Sarnthein, M., Erlenkeuser, H., 2003. Paired $\delta^{18}O$ signals of Neogloboquadrina pachyderma (s) and Turborotalita quinqueloba show thermal stratification structure in Nordic Seas. Mar. Micropaleontol. 48, 107–125. doi:10.1016/S0377-8398(02)00165-2

Sousa, S.H.M., de Godoi, S.S., Amaral, P.G.C., Vicente, T.M., Martins, M.V. a, Sorano, M.R.G.S., Gaeta, S. a., Passos, R.F., Mahiques, M.M., 2014. Distribution of living planktonic foraminifera in relation to oceanic processes on the southeastern continental Brazilian margin (23°S-25°S and 40°W-44°W). Cont. Shelf Res. 89, 76–87. doi:10.1016/j.csr.2013.11.027

Souto, D.D., de Oliveira Lessa, D.V., Albuquerque, A.L.S., Sifeddine, A., Turcq, B.J., Barbosa, C.F., 2011. Marine sediments from southeastern Brazilian continental shelf: A 1200-year record of upwelling productivity. Palaeogeogr. Palaeoclimatol. Palaeoecol. 299, 49–55. doi:10.1016/j.palaeo.2010.10.032

Spezzaferri, S., Kucera, M., Pearson, P.N., Wade, B.S., Rappo, S., Poole, C.R., Morard, R., Stalder, C., 2015. Fossil and genetic evidence for the polyphyletic nature of the Planktonic foraminifera "Globigerinoides", and description of the new genus Trilobatus. PLoS One 10, 1–20. doi:10.1371/journal.pone.0128108

Steph, S., Regenberg, M., Tiedemann, R., Mulitza, S., Nürnberg, D., 2009. Stable isotopes of planktonic foraminifera from tropical Atlantic/Caribbean core- tops: Implications for reconstructing upper ocean stratification. Mar. Micropaleontol. 71, 1–19. doi:10.1016/j.marmicro.2008.12.004

Stramma, L., England, M., 1999. On the water massed and mean circulation of the South Atlantic Ocean. J. Geophys. Res. 104, 20863–20883.

Tedesco, K., Thunell, R., Astor, Y., Muller-karger, F., 2007. The oxygen isotope composition of planktonic foraminifera from the Cariaco Basin, Venezuela : Seasonal and interannual variations. Mar. Micropaleontol. 62, 180–193. doi:10.1016/j.marmicro.2006.08.002

Thunell, R., Sautter, L.R., 1992. Planktonic foraminiferal faunal and stable isotopic indices of upwelling: a sediment trap study in the San Pedro Basin, Southern California Bight. Geol. Soc. London, Spec. Publ. 64, 77–91. doi:10.1144/GSL.SP.1992.064.01.05

Toledo, F.A.L., Costa, K.B., Pivel, M.A.G., 2007. Salinity changes in the western tropical South Atlantic during the last 30 kyr. Glob. Planet. Change 57, 383–395. doi:10.1016/j.gloplacha.2007.01.001

Ufkes, E., Jansen, J.H.F., Brummer, G.J.A., 1998. Living planktonic foraminifera in the eastern South Atlantic during spring: Indicators of water masses, upwelling and the Congo (Zaire) river plume. Mar. Micropale-

ontol. 33, 27–53. doi:10.1016/S0377-8398(97)00032-7

Valentin, J.L., 2001. The Cabo Frio upwelling system, Brazil, in Coastal Marine Ecosystems of Latin America, edited by U. Seeliger and B. Kjerfve, pp. 97–105, Springer, Berlin, Heidelberg.

Venancio, I.M., Belem, A.L., dos Santos, T.H.R., Zucchi, M.D.R., Azevedo, A.E.G., Capilla, R., Albuquerque, A.L.S., 2014. Influence of continental shelf processes in the water mass balance and productivity from stable isotope data on the Southeastern Brazilian coast. J. Mar. Syst. 139, 241–247. doi:10.1016/j.jmarsys.2014.06.009

Venancio, I.M., Franco, D., Belem, A.L., Mulitza, S., Siccha, M., Albuquerque, A.L.S., Schulz, M., Kucera, M., 2016a. Planktonic foraminifera shell fluxes from a weekly resolved sediment trap record in the southwestern Atlantic: Evidence for synchronized reproduction. Mar. Micropaleontol. 125, 25–35. doi:10.1016/j.marmicro.2016.03.003

Venancio, I.M., Gomes, V.P., Belem, A.L., Albuquerque, A.L.S., 2016b. Surface-to-subsurface temperature variations during the last century in a western boundary upwelling system (Southeastern, Brazil). Cont. Shelf Res. 125, 97–106.

Vicalvi, M.A., 1997. Zoneamento bioestratigráfico e paleoclimático dos sedimentos do quaternário superior do talude da bacia de Campos, RJ, Brazil. Bol. Geociênc. Petrobras 11 (K), 132–165.

Walsh, J.J., 1988. On the Nature of Continental Shelves. Academic Press, New York.

Wejnert, K.E., Thunell, R.C., Astor, Y., 2013. Comparison of species-specific oxygen isotope paleotemperature equations: Sensitivity analysis using planktonic foraminifera from the Cariaco Basin, Venezuela. Mar. Micropaleontol. 101, 76–88. doi:10.1016/j.marmicro.2013.03.001

Williams, D.F., Healy-Williams, N., 1980. Oxygen isotopic-hydrographic relationships among recent planktonic Foraminifera from Indian Ocena. Nature 283, 848–852. doi:10.1038/283848a0

Žarić, S., Donner, B., Fischer, G., Mulitza, S., Wefer, G., 2005. Sensitivity of planktic foraminifera to sea surface temperature and export production as derived from sediment trap data. Mar. Micropaleontol. 55, 75–105. doi:10.1016/j.marmicro.2005.01.002

3.10. Supplementary material

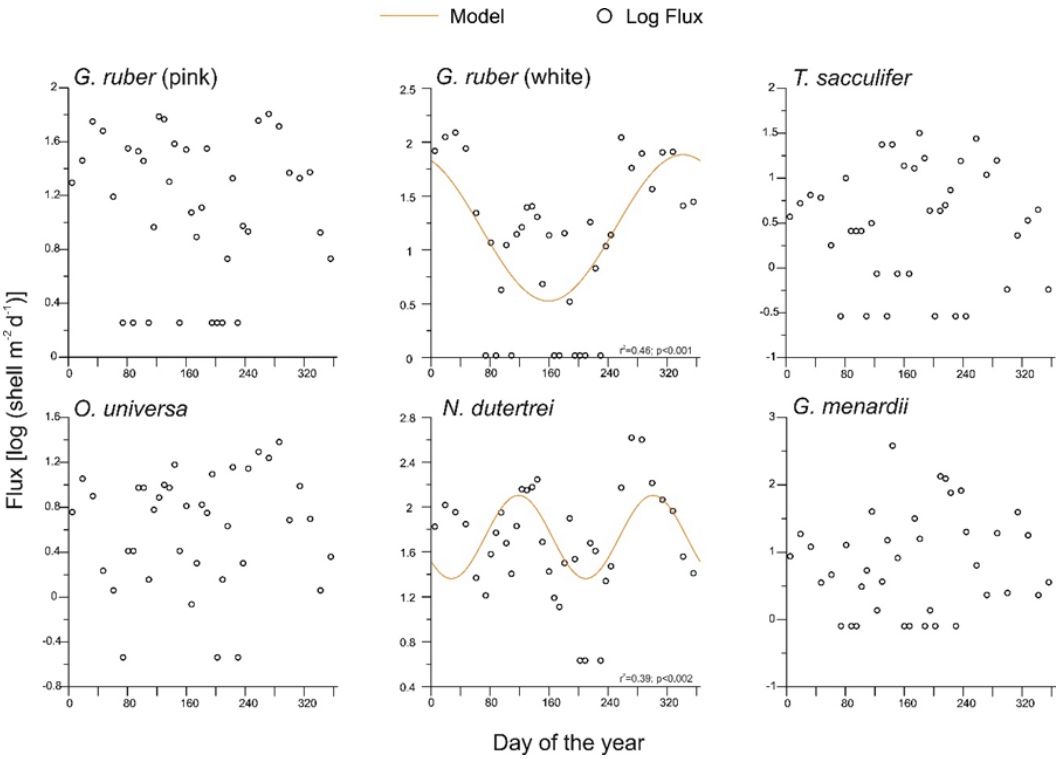

Figure S1. Periodic regression results for each planktonic foraminifer's species. The orange solid line represents significant periodic regression models. Coefficient of determination values and p-values are exhibited for each dataset. Time is represented as days of the year.

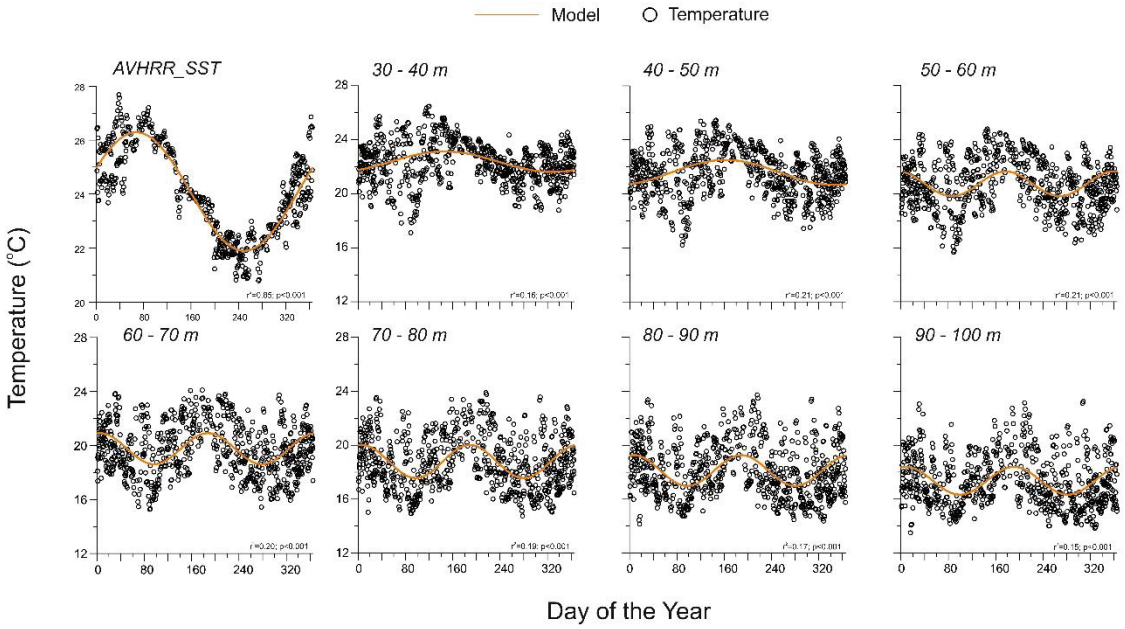

Figure S2. Periodic regression results for each temperature section and for AVHRR-SST. The orange solid line represents significant periodic regression models. Coefficient of determination values and p-values are exhibited for each dataset. Time is represented as days of the year.

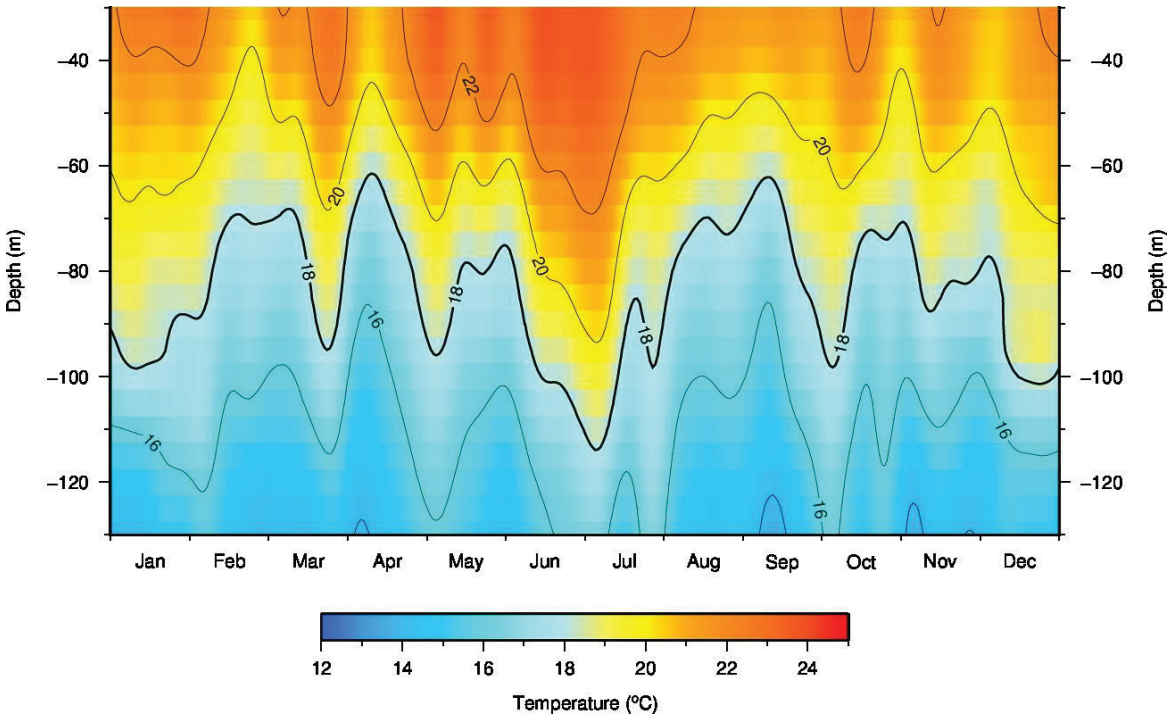

Figure S3. Interpolated monthly temperature profiles from the temperatures recorded by the mooring. Temperature data from all deployments were merged in order to generate a record that covers all months.

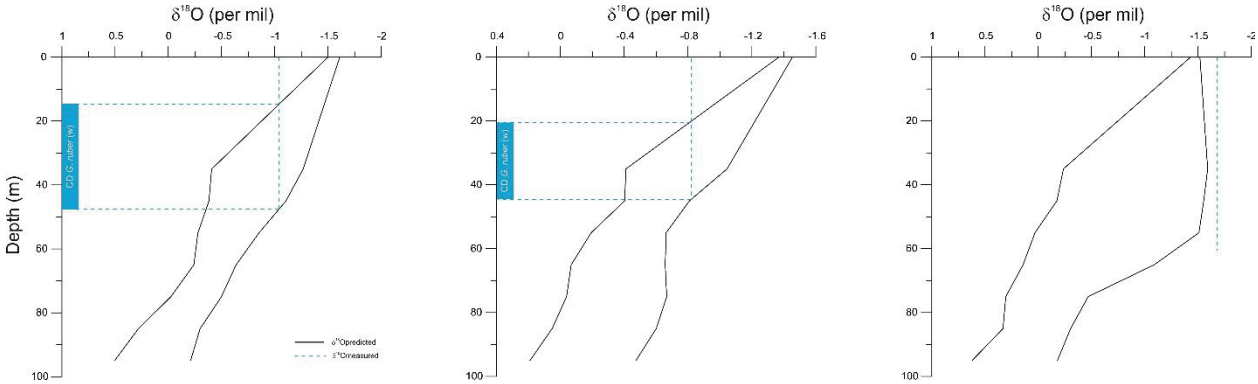

Figure S4. Examples for *G. ruber* (white) of $\delta^{18}O_{predicted}$ profiles (black solid lines) and $\delta^{18}O_{measured}$ values (blue dashed line) for generating the calcification depth estimations. Profiles demonstrate different conditions of the water column and different scenarios of calcification depth estimations. From the left to the right we have the samples 6th bottle of deployment 1 (50-m trap), 4th bottle of deployment 1 (100-m trap) and 12th bottle of deployment 2 (50-m trap). The panel in the right exemplifies the scenario where $\delta^{18}O_{measured}$ is out of the range of possibilities of the $\delta^{18}O_{predicted}$ profiles.

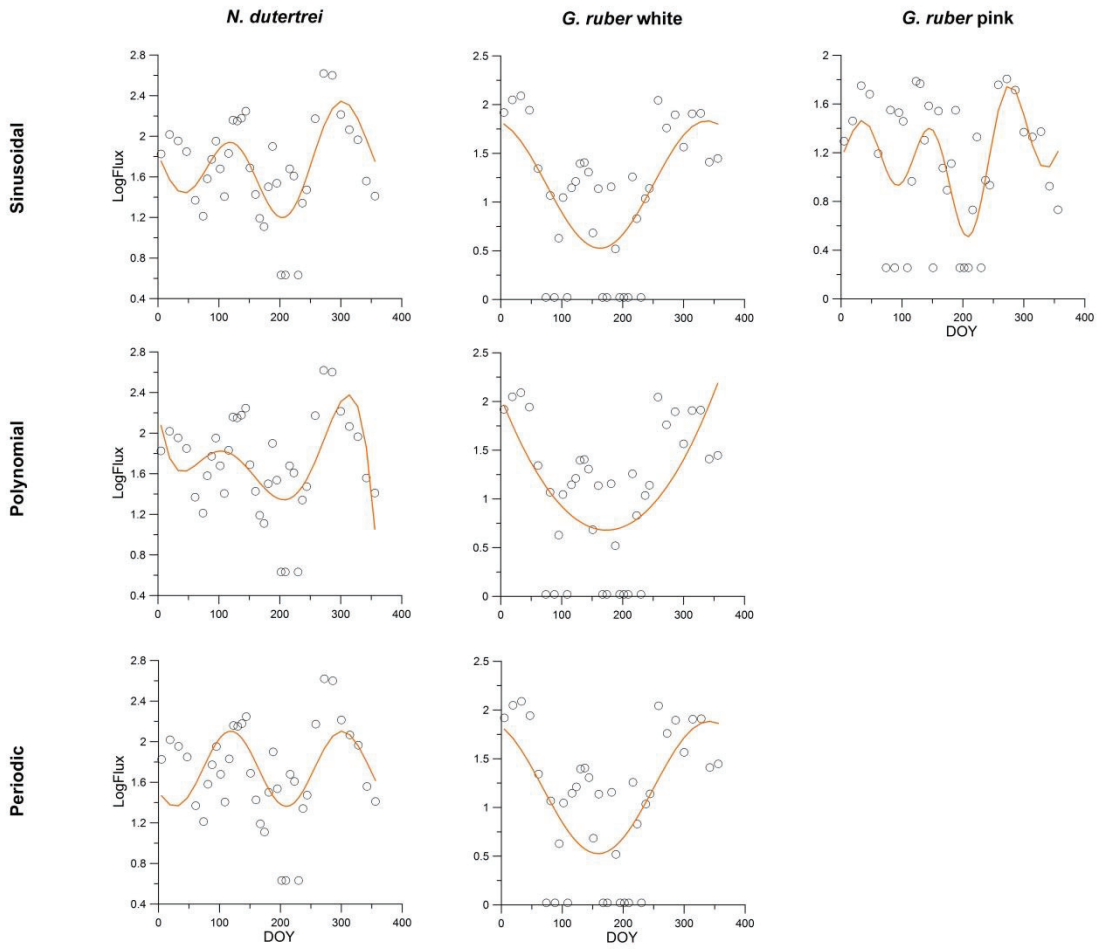

Figure S5. Statistically significant results of the regression methods (sinusoidal, polynomial and periodic). Data from deployments 2 (100-m trap), 6 and 7 for each species are represented by the open circles. The models generated by the different methods are represented by the solid orange line.

Data	Regression method	Model Peaks (DOY)	R^2	p-value
Flux *N. dutertrei*	Periodic	119/301	0.39	<0.002
Flux *N. dutertrei*	Polynomial	102/314	0.36	<0.01
Flux *N. dutertrei*	Sinusoidal	116/300	0.45	<0.001
Flux *G. ruber* w	Periodic	342	0.46	<0.001
Flux *G. ruber* w	Polynomial	356	0.36	<0.001
Flux *G. ruber* w	Sinusoidal	328	0.43	<0.001
Flux *G. ruber* p	Sinusoidal	33/144/272	0.35	0.022

Table S1. Comparison between the statistically significant results from different regression methods (periodic, polynomial and sinusoidal) for the different species.

Chapter 4. Responses of the western equatorial Atlantic to millennial-scale climatic events since the Last Interglacial

Igor M. Venancio[1,2*], Stefan Mulitza[1], Aline Govin[3], Thiago P. Santos[2], Douglas O. Lessa[2], Ana Luiza S. Albuquerque[2], Cristiano M. Chiessi[4], Ralf Tiedemann[5], Maximilian Vahlenkamp[1], Torsten Bickert[1], Michael Schulz[1]

[1]MARUM—Center for Marine Environmental Sciences and Faculty of Geosciences, University of Bremen, Bremen, Germany.

[2] Departamento de Geoquímica, Universidade Federal Fluminense, Outeiro de São João Batista, s/nº, Niterói, Rio de Janeiro, Brazil.

[3]Laboratoire des Sciences du Climat et de l´Environnement/ISPL, CEA-CNRS-UVSQ, Université Paris-Saclay, Gif-sur-Yvette, France.

[4]Escola de Artes, Ciências e Humanidades, Universidade de São Paulo, São Paulo, Brazil.

[5]Alfred Wegener Institute for Polar and Marine Research, Bremerhaven, Germany.

In preparation for *Earth and Planetary Science Letters*

4.1. Abstract

Paleoclimate archives from the equatorial Atlantic are crucial for understanding the coupling between low and high latitudes, as between hemispheres, climates during millennial and glacial-interglacial timescales. Here, we used high-resolution records of major elemental composition of bulk sediment and stable isotopic composition of two species of planktonic foraminifera (*Globigerinoides ruber* white and *Neogloboquadrina dutertrei*) from two sediment cores collected off northeastern Brazil to investigate changes in millennial-scale climate variability since the Last Interglacial. Our Ti/Ca and Fe/Ca records show the presence of Dansgaard-Oeschger (DO) cycles modulating precipitation and consequently fluvial discharge. DO stadials (interstadials) showed a positive (negative) precipitation anomaly over northeastern Brazil. In addition, our stable isotopic data reveal that changes in stratification of the upper water column in the western equatorial Atlantic are related to two modes of thermocline variability. The shoaling of the thermocline in our site during millennial-scale stadials was associated with the zonal mode, caused by a decrease in the strength of the southeast trade winds and a weakening of the South Equatorial Current (SEC)

transport. However, the shoaling of the thermocline in our site during glacial stages or cold substages of marine isotope stage 5 was linked to the meridional mode, caused by more zonal and intense trade winds with the presence of a strong and prolonged North Equatorial Countercurrent (NECC). Both modes were related to changes in the trade wind system, which are in turn modulated by the Atlantic meridional sea surface temperature gradient. Our data also allow the differentiation between Heinrich and DO stadials in terms of the magnitude of the changes in upper stratification and runoff in the western equatorial Atlantic, with stronger responses occurring during Heinrich stadials than during DO stadials.

4.2. Introduction

Greenland ice cores and North Atlantic marine sediment archives were the first to reveal the existence of millennial-scale climate events (Dansgaard et al., 1993; Bond et al., 1993). Thereafter, high-resolution tropical and subtropical records from South America (Peterson et al., 2000), Africa (Mulitza et al., 2008) and Asia (Wang et al., 2001) have also shown such climatic changes. As components of the millennial-scale climate variability, Heinrich stadials (HS) are linked to freshwater input into the North Atlantic derived from melting icebergs that caused or amplified a slowdown in the Atlantic meridional overturning circulation (AMOC) (Vidal et al., 1997; Böhm et al., 2015).Variations in the strength of the AMOC also influence the mean position of the Intertropical Convergence Zone (ITCZ) through ocean-atmosphere coupling (Broccoli et al., 2006; Clement and Peterson, 2008; Kageyama et al., 2013). Although reductions in AMOC strength are well documented for HS, the mechanisms and responses associated with Dansgaard-Oeschger (DO) events are still under debate (Menviel et al., 2014; Petersen et al., 2013). Possible mechanisms for the occurrence of DO variability may involve changes in AMOC strength (Keigwin and Boyle, 1999), fluctuations in ice-shelf growth (Petersen et al., 2013), or even changes in solar forcing (Braun et al., 2008). Despite these alternative hypotheses, evidence from marine records and model simulations has strengthen the idea of changes in AMOC strength controlling DO variability (Menviel et al., 2014; Henry et al., 2016; Bagniewski et al., 2017). Moreover, a recent study by Markle et al. (2017) provided direct evidence for a coupling between both hemispheres during DO events. However, high-resolution records able to capture DO variability are scarce in the tropics, particularly off northeastern Brazil. Speleothem records from northeastern Brazil show enhanced precipitation caused by a southward displacement of the ITCZ (Wang et al., 2004) during HS, with marine sediment cores showing a simultaneous increase in fluvial terrigenous input (Arz et al., 1998; Zhang et al., 2015). An antiphase behavior in terms of continental runoff was described based on records from the Cariaco Basin (Peterson et al., 2000; Deplazes et al., 2013). However, no record to the south of the equator in the western Atlantic provides a robust picture of the climatic responses during DO events so far.

Moreover, meridional migrations of the ITCZ may not solely be coupled to tropical rainfall, but also to upper ocean circulation in the western equatorial Atlantic (Schott et al., 1998; Rodrigues et al., 2007). Since modern seasonal changes in the ITCZ mean position are linked to changes in the trade wind regime, the seasonal variation in the wind system alters the upper water column circulation (Hastenrath and Merle,

1987). Although some marine records have pointed to shifts in the position of surface equatorial currents during glacial periods (Vink et al., 2001; Wilson et al., 2011) and to glacial-interglacial changes in thermocline depth (Bassinot et al., 1997; Wolff et al., 1999; Rühlemann et al., 2001), variations in upper ocean stratification, linked to changes in the trade wind regime during millennial-scale events have not been well documented. However, a recent study by Portilho-Ramos et al. (2017) indicates a shallow thermocline in the western equatorial Atlantic during HS1-2 and the Younger Dryas (YD) and suggested that changes in the upper stratification in this region are coupled to meridional migrations of the ITCZ. Furthermore, upper ocean stratification in the western equatorial Atlantic may influence the cross-equatorial heat transport to high latitudes, which is crucial for the maintenance of the AMOC (Zhang et al., 2011).

We present high-resolution reconstructions of terrigenous input and thermocline depth from the western equatorial Atlantic since the Last Interglacial (LIG) using two sediment cores (GL-1248 and GeoB16202-2) from the continental slope of northeastern Brazil. We use Ti/Ca and Fe/Ca ratios to reconstruct the terrigenous input (Govin et al., 2012), and the difference between the stable oxygen isotopic composition of two planktonic foraminifera species (*Globigerinoides ruber* white and *Neogloboquadrina dutertrei*; $\Delta\delta^{18}O_{dut\text{-}rub}$) as a proxy for past upper water column stratification or thermocline depth (Steph et al., 2009). Our results show a pronounced increase in terrigenous input related to shifts of the ITCZ during HS and DO stadials. Furthermore, our $\Delta\delta^{18}O_{dut\text{-}rub}$ time series revealed two modes of thermocline variability associated to changes in the trade wind system, which alter the stratification in the western equatorial Atlantic and can influence the cross-equatorial heat transport.

4.3. Materials and methods

4.3.1. Age model

Sediment core GL-1248 (0°55.2'S, 43°24.1'W, 2264 m water depth) was collected by Petrobras and sediment core GeoB16202-2 (1°54.50' S, 41°35.50' W, 2248 m water depth) was collected during the cruise MSM20/3 (Mulitza et al., 2013) from the continental slope off northeastern Brazil (Figure 1). The age model for core GeoB16202-2 is based on 13 AMS radiocarbon ages performed on two shallow-dwelling planktonic foraminifera species (*Globigerinoides ruber* and *Trilobatus sacculifer*). Radiocarbon ages were calibrated using IntCal13 (Reimer et al., 2013) with a reservoir age of 400 ± 200 years. The details regarding the age model for GeoB16202-2 are described by Mulitza et al. (submitted).

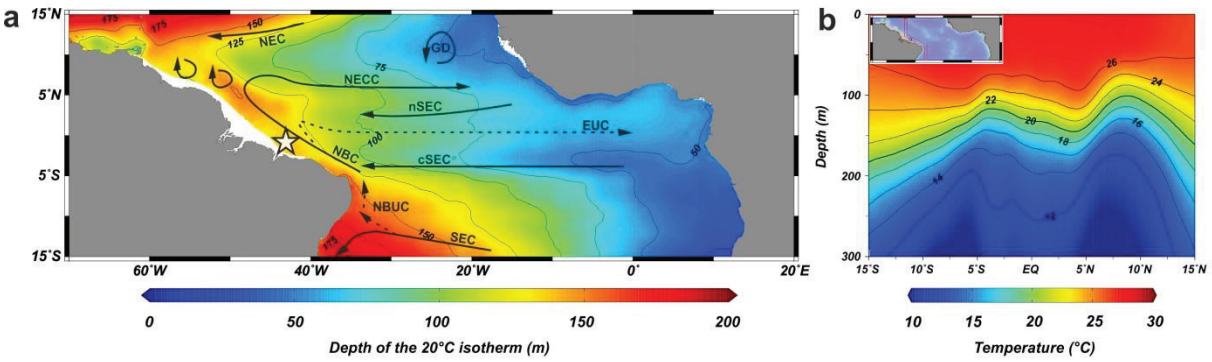

Figure 1. (a) Modern depth of the 20°C isotherm in a surface map and (b) temperature profile of a meridional section across the equator (extracted from the World Ocean Atlas 2013; Locarnini et al., 2013). (a) The main surface (solid) and thermocline (dashed lines) currents are represented: Equatorial Undercurrent (EUC), Guinea Dome (GD), North Brazil Current and Undercurrent (NBC, NBUC), North Equatorial Countercurrent (NECC), North Equatorial Current (NEC), South Equatorial Current (SEC) and its northern and central branches (nSEC, cSEC) (modified after Brandt et al., 2011). (a) The white star marks the location of cores GL-1248 and GeoB16202-2. The figures were produced using Ocean Data View (Schlitzer, 2016).

For the lower part of core GL-1248 (6.30 – 16.66 m; ≈ 44 – 129 ka), the chronology was derived from the alignment of the Ti/Ca record of core GL-1248 to the ice $\delta^{18}O$ (Figure S1) record of the North Greenland Ice Core Project (NGRIP) (NGRIP Members, 2004) using the extended Greenland Ice Core Chronology (GICC05modelext). The underlying assumption to this alignment is that Greenland stadials are associated with increased precipitation over northeastern Brazil and increased delivery of terrigenous material to the western equatorial Atlantic, as supported by speleothem and marine records of the last glacial period (e.g. Wang et al., 2004; Jaeschke et al., 2007). In addition, the beginning of the last interglacial was defined by synchronizing at approximately 129 ka the Ti/Ca record with the Antarctic methane record from EPICA Dome C (Loulergue et al., 2008) on the AICC2012 time scale (Veres et al., 2013), as it has already been done in previous studies (e.g. Govin et al., 2015). The rationale behind this alignment is that abrupt Greenland warming events occurred simultaneously with methane increases during millennial-scale events of the last glacial period and last deglaciation (Chapellaz et al., 1993; Rosen et al., 2014). We estimated the error for the defined tie-points by taking into account: (1) the mean resolution of the Ti/Ca record from GL-1248; (2) the mean resolution and dating uncertainty of the reference curves; and (3) an estimated matching error when defining a tie-point. Since, the GICC05modelext chronology does not have an intrinsic age error estimate between 60 and 123 ka, we assumed that the errors from GICC05modelext are similar to AICC2012

(Veres et al., 2013). The complete age model was constructed using linear interpolation with the software clam 2.2 (Blaauw, 2010). Then, using the same approach of Jaeschke et al. (2007), we used U/Th-dated growth intervals of Brazilian speleothems during stadials (Wang et al., 2004) to verify our age model. Since these growth intervals correspond to wet periods in northeastern Brazil, synchronous with cold events (stadials) in the North Atlantic, they should be coeval to the Ti/Ca peaks in our record. Radiocarbon ages for GL-1248 and for GeoB16202-2 and tie-points defined for GL-1248 are summarized in Table S1, with 2σ errors for the radiocarbon and tie-points ages.

4.3.2. Oxygen isotopes

Ten tests of *G. ruber* white (250–355 μm) and eight tests of *N. dutertrei* (350-415 μm) were analyzed for $\delta^{18}O$ every ca. 4 cm of core GL-1248 from the top of the core until 16.60 m. For core GeoB16202-2, five to ten tests of *G. ruber* white (350-500 μm) and a sufficient number of tests of of *N. dutertrei* (350-450 μm) were selected every ca. 10 cm (Huppertz, 2014). All tests were handpicked under a binocular microscope. Oxygen isotope analyses were performed with a Finnigan MAT 252 mass spectrometer equipped with an automatic carbonate preparation device at MARUM, University of Bremen (Germany). Isotopic results were calibrated relative to the Vienna Pee Dee Belemnite (VPDB) using the standards NBS18, 19 and 20. The standard deviation of the laboratory standard was lower than 0.07 ‰ for the measuring period. Since $\delta^{18}O$ from *G. ruber* and *N. dutertrei* were not always measured in the same samples in core GeoB16202-2, the data was interpolated before calculating the $\Delta\delta^{18}O_{dut\text{-}rub}$ record.

4.3.3. Major element composition

The Ti/Ca and Fe/Ca ratios of core GL-1248 (this study) and Fe/Ca ratios of core GeoB16202-2 (Mulitza et al., submitted) were obtained by scanning the core surfaces of the archive halves with X-ray fluorescence (XRF) Core Scanner II (AVAATECH Serial No. 2) at the MARUM, University of Bremen (Germany). The XRF data were measured downcore every 0.5 cm for GL-1248 and every 2 cm for GeoB16202-2 by irradiating a surface of about 10mm×12mm for 20 s at 10 kV.

4.3.4. Time-series analyses

A spectral analysis was performed on the oxygen isotopic difference between *G. ruber* and *N. dutertrei* ($\Delta\delta^{18}O_{dut\text{-}rub}$) using a combined dataset between GL-1248 and GeoB16202-2 in order to identify characteristic periodicities on the record. We applied the REDFIT algorithm (Schulz and Mudelsee, 2002) using the PAST software (Hammer et al., 2001). The linearly detrended record was divided in two segments and an oversampling factor of four was used. The Welch tapper type window was chosen

for the analysis and the results were compared to the autoregressive model (AR1) at two confidence levels (95 and 99%).

4.4. Results

4.4.1. Age model

Core GeoB16202-2 reaches 23.9 ka (± 0.6) close to its base at 7.63 m depth as described in Mulitza et al. (submitted). For core GL-1248, radiocarbon dating reached 44.06 ± 0.7 ka at 6.30 m depth, and the alignment between the Ti/Ca record from GL-1248 and the $\delta^{18}O$ record of NGRIP allowed us to estimate an age of 128.7 ka at 16.66 m core depth (Figure 2). The extremely low sedimentation rate (≈3 cm/ka), between 2.18 and 1.70 m core depth (29.4 and 14.4 ka, respectively) suggest the presence of a hiatus, and the data within this interval was not interpreted. The mean sedimentation rate for GL-1248 is 21 cm/ka, with high sedimentation rates up to 55 cm/ka during MIS 3 and low sedimentation rates (< 10 cm/ka) during MIS 1 and MIS 5.

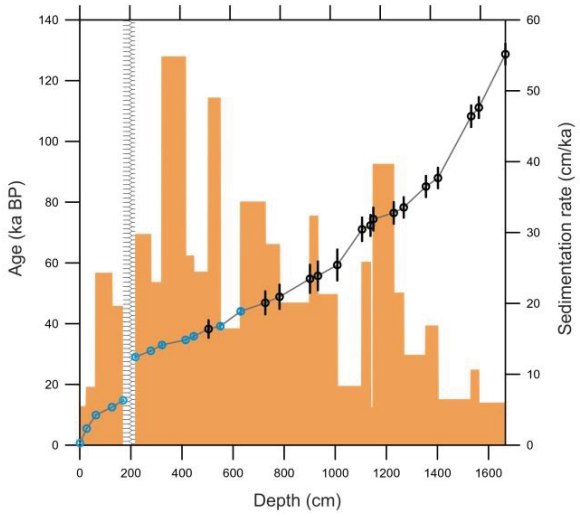

Figure 2. Age-depth model and sedimentation rates for core GL-1248. Open circles represent the calibrated radiocarbon ages (light blue) and the tie-points (black) with their respective 2 σ errors. The line (gray) represents the age-depth model constructed based on the linear interpolation between adjacent calibrated radiocarbon ages and tie-points. The step plot (light orange) shows the sedimentation rates. The hiatus in the core is represented by the white bar with black lines.

4.4.2. Oxygen isotopes

The *G. ruber* white $\delta^{18}O$ values vary between -1.74 and 0.00 ‰ in core GeoB16202-2 and between -1.80 and -0.29 ‰ in core GL-1248 (Figure 3b). *N. dutertrei* $\delta^{18}O$ values range from -0.76 to 1.37 ‰ in core GeoB16202-2, while in core GL-1248 they range from -0.77 to 1.22 ‰. Oxygen isotopic values for both cores overlap over the last 14.5 kyr with very good agreement (Figure 3b), supporting the combined use of data from both cores. In general, we observe high $\Delta\delta^{18}O_{dut\text{-}rub}$ values during HS. The exception is HS 4, where no distinct peak is

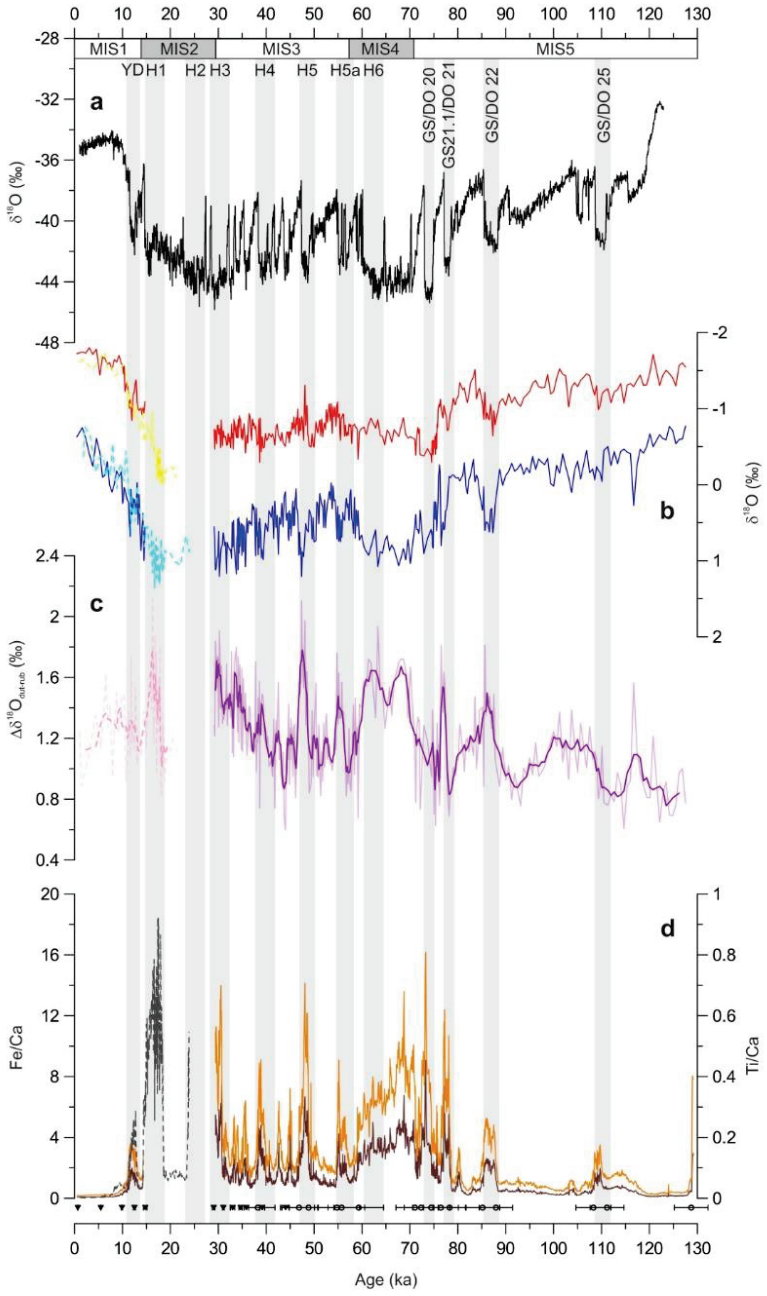

Figure 3. Records obtained on cores GeoB16202-2 and GL-1248. (a) $\delta^{18}O_{ice}$ from NGRIP on the GICC05modelext time scale (black line). (b) Oxygen isotopic composition ($\delta^{18}O$) of *Globigerinoides ruber* and *Neogloboquadrina dutertrei* from GeoB16202-2 (yellow and light blue dashed lines, respectively) and from GL-1248 (red and blue solid lines, respectively). (c) $\Delta\delta^{18}O_{dut\text{-}rub}$ record from both cores with 5-point running average, GeoB16202-2 (pink dashed line) and GL-1248 (purple solid line). (d) Fe/Ca from GeoB16202-2 (grey dashed line) and from GL-1248 (brown solid line) and Ti/Ca from GL-1248 (orange solid line). Grey bars highlight the Younger Dryas (YD), HS and some DO stadials (GS). Radiocarbon ages (black inverted triangles) and tie-points (black open circles) with their respective 2□ errors (horizontal black lines) are displayed above the lower x-axis. Marine isotope stages (MIS) are highlighted below the upper x-axis.

observed. In core GeoB16202-2, the highest $\Delta\delta^{18}O_{dut\text{-}rub}$ value (2.12 ‰) occurs during HS 1, while the highest value (2.10 ‰) in core GL-1248 is found during HS 5 (Figure 3c). In addition, high values (> 1.2 ‰) of $\Delta\delta^{18}O_{dut\text{-}rub}$ were observed for the entire MIS 4 and a steep increase can be observed from 46 to 30 ka BP (Figure 3c).

4.4.3. Major element composition

Fe/Ca from core GeoB16202-2 shows a prominent increase during HS 1 and the Younger Dryas (YD) (Figure 3d). The Ti/Ca and Fe/Ca records from core GL-1248 show peaks during the YD, HS 3-6 and several DO stadials (Figure 3d). The Ti/Ca and Fe/Ca records of core GL-1248 are low values during interglacials and comparably high during glacial periods.

4.4.4. Time series analyses

Results from REDFIT indicate the presence of characteristic periodicities in the $\Delta\delta^{18}O_{dut\text{-}rub}$ record (Figure 4). Cycles with period of 17.9, 7.9 and 4.4 ka are above the 99% confidence level, while cycles with period of 41.7, 6.5 and 0.7 ka are above the 95% confidence level. The periodicity of 18 ka is commonly associated with the precession and the 42 ka periodicity with the obliquity cycle. Besides the presence of orbital cycles, we observe millennial and multi-millennial scale cycles between 0.7 and 8 ka.

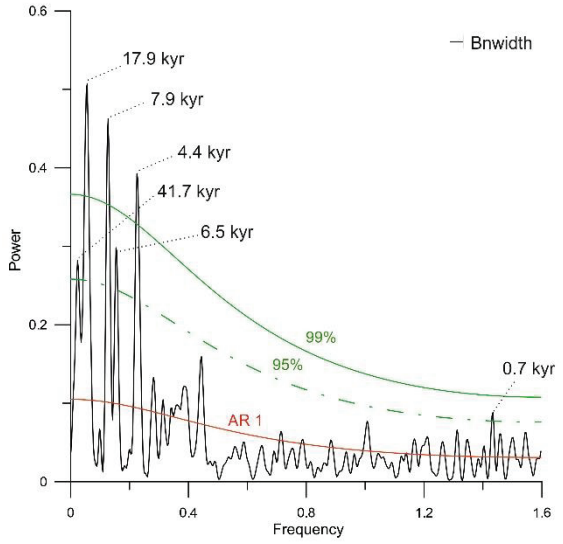

Figure 4. Time series analysis performed with REDFIT (Schulz and Mudelsee, 2002) on the $\Delta\delta^{18}O_{dut\text{-}rub}$ composite record (see section 2.5). Periodicities that excee d the 95 % (dashed green line) or 99 % (solid green line) are labeled. The AR (1) red noise model (solid red line) and the bandwidth (black line; upper right corner) are displayed.

4.5. Discussion

4.5.1. Millennial-scale changes in terrigenous input to the western equatorial Atlantic

Similarly to GL-1248, other marine sediment cores collected off northeastern Brazil (Arz et al., 1998; Jaeschke et al., 2007; Nace et al., 2014) show peaks in Ti/Ca and Fe/Ca during HS (Figure 5c-e). Multiple factors can influence the proportion of the terrigenous vs. marine biogenic fractions, such as changes in fluvial discharge of terrigenous sediments, sea level, carbonate productivity and carbonate dissolution (Govin et al., 2012). However, previous as-

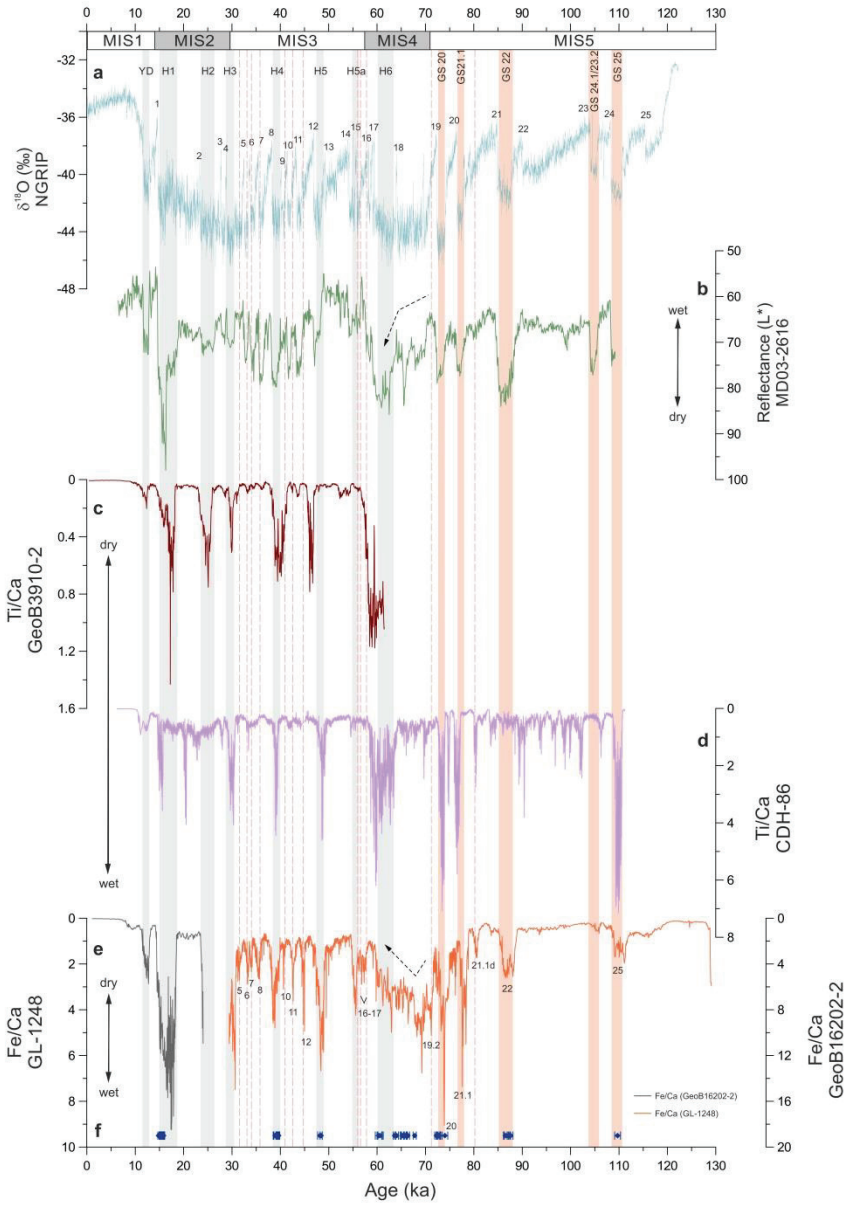

Figure 5. Comparison between the Fe/Ca records from cores GeoB16202-2 and GL-1248 to NGRIP and other tropical records. (a) $\delta^{18}O_{ice}$ from NGRIP on the GICC05modelext time scale (light blue line) with the Younger Dryas (YD), Heinrich stadials (HS) and Dansgaard-Oeschger (DO) cycles displayed. The grey bars highlight the YD and HS, while the light orange bars represent specific DO stadials (prominent North Atlantic cold events). The pink dashed lines represent other DO stadials. (b) Reflectance (L*) record from Cariaco Basin (green line) resampled with 1-ka resolution (Deplazes et al., 2013). (c) Ti/Ca record from core GeoB3910-2 (red line) collected off northeastern Brazil (Jaeschke et al., 2007). (d) Ti/Ca record from core CDH-86 (purple line) collected off northeastern Brazil (Nace et al., 2014). (e) Fe/Ca from core GeoB16202-2 (grey line) and Fe/Ca from core GL-1248 (orange line). (f) The dark blue squares in the lower part represent wet periods in northeastern Brazil derived from speleothem records (Wang et al., 2004). Black arrow in (b) and (e) highlight the opposite trends in the datasets during MIS 4. Marine isotope stages (MIS) from stage 5 to 1 are highlighted below the upper x-axis.

sessments considering these factors (Jaeschke et al., 2007; Zhang et al., 2015) have shown that sea level changes seem not to have controlled the millennial-scale increases of the terrigenous fraction registered by cores in this area. Due to minor changes in carbonate productivity in this region and carbonate dissolution above 3000 m water depth (Rühlemann et al., 1996), these two factors are likely not the main drivers of Ti/Ca and Fe/Ca changes at our study site. Consequently, increases in Ti/Ca and Fe/Ca ratios coincide with wet phases over northeastern Brazil indicated by speleothem records (Wang et al., 2004) and are a result of enhanced erosion and fluvial discharge of terrigenous material from the continent to the ocean, as suggested in previous studies (Arz et al., 1998; Jaeschke et al., 2007; Zhang et al., 2015). Studies that investigated cores collected close to the mouth of the Parnaíba River have shown increased sedimentation rates and Ti/Ca values during HS 1 and the YD (Zhang et al., 2015), as well as during other millennial-scale events covering the last 110 ka (Nace et al., 2014). The YD and HS are periods characterized by a weak AMOC (Böhm et al., 2015), probably caused (Bond et al., 1992) or potentialized (Barker et al., 2015) by freshwater input to the high latitudes of the North Atlantic. It is well documented that during these periods of AMOC slowdown the ITCZ shifted southwards (Broccoli et al., 2006; Mulitza et al., submitted), enhancing precipitation over northeastern Brazil (Wang et al., 2004).

We confirm that peaks in our Ti/Ca and Fe/Ca records reflect increased continental erosion due to wet phases over northeastern Brazil by observing the outstanding agreement with speleothem and travertine growth periods (Wang et al., 2004) along the entire time series (Figure 5e-f). Although we observe generally a good agreement between the Ti/Ca and Fe/Ca records from cores collected off northeastern Brazil (Figure 5c-e) during HS, some differences become apparent. For instance, only our records, and the record from Arz et al. (1998), register HS 5a and our peak during HS 6 seems to reflect a much longer trend encompassing the whole MIS 4 (Figure 5). The trend in terrigenous input during MIS 4 (Figure 5e) show a steep increase in Fe/Ca from 72 to 69 ka, with a subsequently long-term decrease in Fe/Ca from 69 to 58 ka, with no abrupt peak during HS 6.

Speleothem records register enhanced precipitation over northeastern Brazil during almost the entire MIS 4 (Wang et al., 2004). Moreover, reflectance data from Cariaco Basin (Deplazes et al., 2013) suggest a long-term trend towards drier conditions, with an abrupt dry period during HS 6. These findings suggest two scenarios: (1) a gradual southward displacement of the ITCZ during MIS 4, reaching its southernmost position during HS 6; or (2) a constant

southward mean position of the ITCZ during the entire MIS 4. In both scenarios, we could expect enhanced continental erosion over northeastern Brazil across MIS 4, and not only during HS 6, which partially supports our observations. A southward position of the ITCZ during the entire MIS 4 could be related to a weaker AMOC, since a decrease in benthic $\delta^{13}C$ values is observed in several records (Oppo and Lehman, 1995; Hodell et al., 2010; Lynch-Stieglitz et al., 2014), although the records of $^{231}Pa/^{230}Th$ only showed a significant decrease in AMOC strength during HS 6 (Böhm et al., 2015). An alternative trigger could be the large northern ice sheet during MIS 4 (Zweck and Huybrechts, 2005), which may have enhanced the meridional SST gradient in the Atlantic leading to a southward displacement of the ITCZ (Chiang and Bitz, 2005). Considering the above mechanisms and scenarios, our Fe/Ca record should show high Fe/Ca values during the entire MIS 4 (second scenario), as shown by others (Arz et al., 1998), or the mirrored situation to Cariaco Basin (Figure 5b). Our records suggest an antiphase behavior of precipitation to Cariaco Basin from 72 to 69 ka, but from 69 to 58 ka our records show a decrease in continental erosion and an inphase relation with Cariaco Basin, which would point to drier conditions in both sites. Therefore, we suggest that our Fe/Ca trend from 69 to 58 ka is not solely influenced by changes in precipitation. Instead, we suggest that the decrease in continental erosion form 69 to 58 ka is influenced by changes in inland vegetation. Indeed, from 67 to 58 ka the isotopic signature of the organic matter presented by Jennerjahn et al. (2004) suggests a change in terrestrial vegetation type and coverage, which could have caused a reduction in continental erosion for this period. However, we highlight that MIS 4 palynological data from northeastern Brazil would be required to further confirm our hypothesis.

Although previously published records (Arz et al., 1998; Nace et al., 2014; Zhang et al., 2015) registered HS and the YD, none of them presented robust evidence for DO variability off northeastern Brazil. Our records show several DO stadials during MIS 5 and MIS 3 (Figure 5e), which can also be referred to as Greenland stadials (GS) and correspond to intervals of depleted $\delta^{18}O$ in Greenland ice cores due to cold temperatures (Rasmussen et al., 2014). In the following discussion about the influence of DO stadials in our records, we will use the nomenclature defined by Rasmussen et al. (2014) and name the DO stadials as Greenland stadials (GS).

During MIS 5 (130-71 ka), we can associate peaks in our Fe/Ca records to DO stadials 25 (GS 25), 22 (GS 22), 21 (GS 21.1) and 20 (GS 20) (Figure 5e). In the North Atlantic, these events (GS 20-25) are related to strong SST cooling, IRD deposition and

low $\delta^{13}C$ values in benthic foraminifera (McManus et al., 1994; Oppo et al., 2006). At the same time in the tropics, most of these increases in our Fe/Ca are synchronous with dry periods over the Cariaco Basin (Figure 5b) (Desplazes et al., 2013) and wet periods over northeastern Brazil (Figure 5f) (Wang et al., 2004). However, the absence of an increase in elemental ratios during GS 24.1 is also a common feature between our records and the one from Nace et al. (2014). This absence of signal suggests no change in continental erosion (or precipitation) in northeastern Brazil, although reflectance data indicates a dry period in Cariaco Basin (Figure 5b). This would indicate that the southward shift during GS24.1 was probably minor and did not affect precipitation over northeastern Brazil. Nevertheless, we highlight that in general marine cores off northeastern Brazil (Figure 5d-e) recorded a substantial enhancement of precipitation and continental erosion due to southward migrations of the ITCZ during GS. Jacobel et al. (2016) using dust flux records from the equatorial Pacific also suggested the occurrence of southward shifts of the ITCZ during GS of the MIS 5. However, these authors also highlighted that these southward migrations were probably limited to latitudes above 0.5°N, with the possibility of a further south position of the ITCZ only during GS 22.

Even more outstanding is the presence of DO variability in the records from GL-1248 during MIS 3 (Figure 5e), a period of more frequent DO events (Dansgaard et al., 1993). Our Fe/Ca records show peaks during several DO stadials from 12 to 5 (GS 12-5) (Figure 5e). Pulses of continental erosion linked to enhanced precipitation over northeastern Brazil during these DO stadials show a strong agreement with dry periods in Cariaco Basin (Figure 5b). However, such wet phases over northeastern Brazil, as revealed by our Fe/Ca record, were apparently not registered by speleothems and travertine growth periods (Wang et al., 2004). Possibly, the short duration of GS 12-5 was not long enough to foster widespread speleothem and travertine growth. Moreover, our Fe/Ca increases during the DO stadials across MIS 3 are not reflected in other records off northeastern Brazil (Figure 5c-d). Considering the presence of DO variability in records from Cariaco Basin (Deplazes et al., 2013) and the well-known antiphased response in precipitation between Cariaco Basin and northeastern Brazil (Jaeschke et al., 2007), one would expect to find evidence of DO variability in Fe/Ca records off northeastern Brazil. The absence of DO variability in other records off northeastern Brazil could be related to a distinct provenance of terrigenous material and/or to different sizes of the catchment area of the rivers responsible for delivering terrigenous material. For example, from the terrigenous material depos-

ited in GeoB3910-2 (Jaeschke et al., 2007) have been assigned to a small drainage basin (i.e. Piranha River), while the source of terrigenous material do our records and to core CDH-86 (Nace et al., 2014) is a much larger drainage basin (i.e. Parnaíba River) (Zhang et al., 2015). Therefore, short-term changes in precipitation over northeastern Brazil may produce a signal in small drainage basins that is too small to be captured by our proxies. However, this argument cannot explain the absence of DO variability during MIS 3 in the Ti/Ca record from CDH-86 (Nace et al., 2014), since CDH-86 is also influenced by fluvial sediments from the Parnaíba River Here, the location of site GL-1248 closer to the Parnaíba River mouth than CDH-86, may have made possible the recording of short-term stadials. This highlights the outstanding value of GL-1248 as an important climate archive for northeastern Brazil.

In general, DO stadials during MIS 3 show less pronounced peaks in Fe/Ca if compared to HS, except for GS 12 and 11. Nevertheless, even if these DO stadials (GS 10, 8-5) show minor peaks in Fe/Ca, the peaks are equivalent in magnitude to the GS that occurred during MIS 5 (Figure 5e). Therefore, the increases in Fe/Ca during DO stadials across MIS 3 suggest a southward shift of the ITCZ, which causes enhanced precipitation over northeastern Brazil and more arid conditions over Cariaco Basin. However, we suggest that DO stadials during MIS 3 triggered rather minor southward displacements in the ITCZ compared to HS, with exception of DO stadials 12 and 11 (GS 12 and 11) which show values of Fe/Ca as high as for some HS (e.g. HS 4 and 5a). Recent studies using marine proxies (Henry et al., 2016) and transient climate model simulations (Bagniewski et al., 2017) show a weakening of the AMOC during DO stadials across MIS 3, but less pronounced than during HS. Model simulations estimate that during DO stadials the AMOC was approximately 30-50 % weaker than modern conditions (Bagniewski et al., 2017). We suggest that the weaker AMOC during DO stadials across MIS 3 is able to trigger changes in the interhemispheric thermal gradient, causing a southward displacement of the ITCZ.

4.5.2. Orbital and millennial-scale variability of the thermocline depth in the western equatorial Atlantic

Late Quaternary reconstructions have shown the influence of trade wind intensity changes, driven by variations in meridional thermal gradients, in modulating glacial-interglacial changes in thermocline depth in the western tropical Atlantic (Wolff

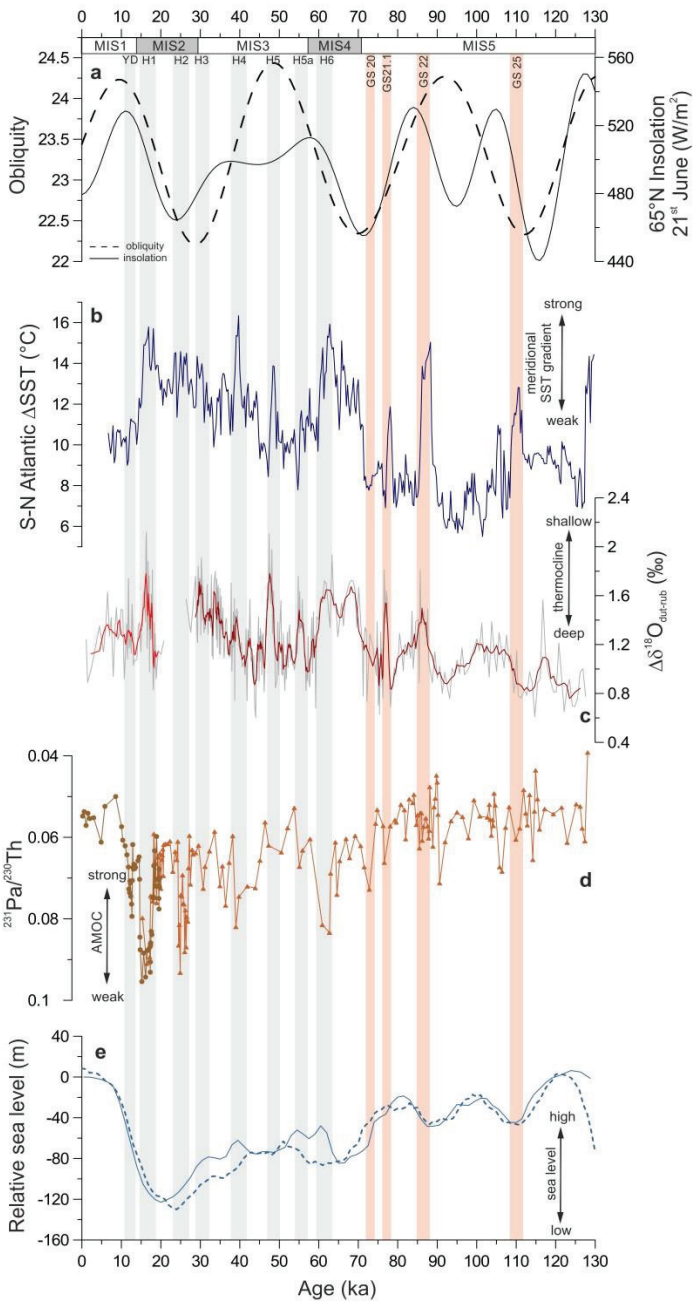

Figure 6. The interspecific stable oxygen isotopic record between *G. ruber* and *N. dutertrei* ($\Delta\delta^{18}O_{dut\text{-}rub}$) from GL-1248 and GeoB16202-2 compared to other relevant records. (a) Insolation for June 21st at 65°N (black solid line) and obliquity (black dashed line). (b) Interhemispheric thermal gradient (blue line) using the SST record from Santos et al. (2017) at 24°S subtracted by the SST from Martrat et al. (2007) at 37°N, the records where resampled every 300 kyr before subtraction. (c) $\Delta\delta^{18}O_{dut\text{-}rub}$ (‰) from GL-1248 and GeoB16202-2 (grey line) and 5-point running average (dark red line for GL-1248 and light red line for GeoB16202-2) (this study). (d) $^{231}Pa/^{230}Th$ records from McManus et al. (2004) (brown line) and from Böhm et al. (2015) (light brown line). (e) Relative sea level (m) curves (light blue) from Waelbroeck et al. (2002) (solid line) and Spratt and Lisiecki (2016) (dashed line). The grey bars highlight HS and the YD, while the light orange bars represent specific DO stadials (prominent North Atlantic cold events). Marine isotope stages (MIS) 5 to 1 are highlighted below the upper x-axis.

et al., 1999; Rühlemann et al., 2001). Our $\Delta\delta^{18}O_{dut\text{-}rub}$ records, a proxy for thermocline depth (Steph et al., 2009), are the first to show millennial-scale variability of the thermocline depth in the western equatorial during several HS and GS (Figures 4, 6). Similarly, to previously published records (Wolff et al., 1999) our thermocline depth reconstruction is also influenced by orbital-scale variability, as shown by the spectral analysis (Figure 4).

Modern changes in the thermocline depth in the western equatorial Atlantic, equivalent to the depth of the 20°C isotherm, are connected to variations in surface circulation, which in turn is influenced by the intensities of northeastern (NE) and southeastern (SE) trade winds (Hastenrath and Merle, 1987). For example, during periods of increased SE trade winds, when the ITCZ is at its northernmost position, the SEC transport is enhanced pilling up warm waters and causing a deepening of the thermocline in the western equatorial Atlantic (Hastenrath and Merle, 1987). The intensity of the trade winds is modulated by the meridional sea surface temperature gradient (Kim et al., 2003). In order to link our thermocline variations to changes in meridional temperature gradient, and consequently trade wind intensity, we compared our $\Delta\delta^{18}O_{dut\text{-}rub}$ records to the temperature difference between cores located at mid-latitudes in the southern (Santos et al., 2017) and northern hemispheres (Martrat et al., 2007). Therefore, we generated an interhemispheric temperature difference record (S-N ΔSST) by subtracting the temperature values from both records after interpolating both of them and resampling them in 300-kyr intervals (Figure 6b).

The abrupt shoaling of the thermocline observed during several HS (HS 1, 5 and 5a) as well as during some GS (GS 21.1 and GS 22) occurs simultaneously to increases in interhemispheric temperature difference, linked to a warming of the mid-latitude western South Atlantic and a cooling of the mid-latitude eastern North Atlantic (Figure 6b). Such variations in interhemispheric temperature gradient during millennial-scale events can be linked changes in AMOC strength, which generates an interhemispheric SST response known as the bipolar seesaw (Broecker et al., 1998). The resultant interhemispheric temperature gradient during these millennial-scale events would lead to stronger NE trade winds and weaker SE trade winds, together with a southward displacement of the ITCZ. Indeed, Kim et al. (2003) using temperature records from the South Atlantic have pointed to a decrease in SE trade wind intensity during HS 1, and Collins et al. (2013) using dust records from the eastern North Atlantic suggested an increase in the strength of the NE trade winds during several HS (HS 1-5). A decrease in the strength of the SE trade

winds would cause a decrease in the SEC transport and a shoaling of the thermocline in the western equatorial Atlantic, which is in agreement with our findings. Peaks in our Fe/Ca records during these periods (Figure 5e) confirm a southward position of the ITCZ. In addition, a recent study from Portilho-Ramos et al. (2017) supports our observation for HS 1 by showing a shallow mixed layer in the western equatorial Atlantic. The authors suggest that the shallow mixed layer during HS 1 is the result of enhanced precipitation over the ocean at their study site, caused by a southward position of the ITCZ. However, their coupled atmosphere-ocean model simulations indicate a shallow mixed layer along the Brazilian margin (0-20°S) and not only at the equatorial region, which would be a scenario in agreement with the mechanism here described, where weaker SE trade winds would cause a shoaling of the thermocline in the western South Atlantic.

Interestingly, during GS 20 and the YD our $\Delta\delta^{18}O_{dut\text{-}rub}$ records do not indicate a major change in thermocline depth (Figure 6c). However, during these periods (GS 20 and YD) the meridional SST gradient was weak (Figure 6b), suggesting a strong SE trade wind intensity, which would increase the SEC transport and not allow a shoaling of the thermocline. Kim et al. (2003) that also suggest the occurrence of strong SE trade winds during the YD. Moreover, these authors showed an agreement between their records and the abundance of *Florisphaera profunda* in the equatorial Atlantic, which is indicative of thermocline fluctuations driven by trade wind intensity. These findings reinforce the potential of the mechanism based in the relationship between meridional SST gradient and trade wind intensity for interpreting the thermocline variability in the western equatorial Atlantic.

Additionally to millennial-scale changes in our $\Delta\delta^{18}O_{dut\text{-}rub}$ records, long-term trends are also evident. For example, the shallow thermocline during HS 4 and HS 3 seems to compose a long-term trend towards a shallow thermocline depth from 45 to 30 ka (Figure 6c). This shoaling of the thermocline during late MIS 3 is in agreement with the decrease in relative abundance of *F. profunda* in the western equatorial Atlantic (Figure S2; Kinkel et al., 2000; Rühlemann et al. 2001), which also suggests a shoaling of the thermocline in this region. During the same interval, we observe an increase in interhemispheric temperature difference (Figure 6b). However, the trend in these curves (Figure 6b) seems to be even longer ending at HS 1. Therefore, the evidence suggests a progressive shoaling of the thermocline, as shown by our $\Delta\delta^{18}O_{dut\text{-}rub}$ records and the relative abundance of *F. profunda* (Rühlemann et al., 2001), occurring simultaneously to a progressive increase in trade wind intensity, associated to the in-

crease in interhemispheric temperature difference.

The late MIS 3 is characterized by a relatively stable boreal summer (21st of June) insolation at 65°N (Figure 6a) but a marked decrease in obliquity from 47 to 30 ka. As pointed by Pahnke and Sachs (2006), the low obliquity results in increased insolation from 43°N/S towards the equator and a decreased insolation from these mid-latitudes towards the poles, which is consistent with opposite SST trends between records from low and mid-latitudes (≤ 43°) and high latitudes (≥ 43°). This orbital configuration probably increased the meridional thermal gradient strengthening wind systems. In fact, Santos et al. (2017) showed an increase in SST during the same period in a core collected at 24°S in the western South Atlantic, supporting the suggestions from Pahnke and Sachs (2006). However, Santos et al. (2017) highlight that another mechanism is additionally necessary for sustaining this warming trend until 23 ka, as evident in their records. The authors suggested the observed warming trend is related to the state of the AMOC and showed that the warming trend is coeval with a decrease in the $\delta^{13}C$ of benthic foraminifera, which indicates a weakening in AMOC strength. This change in AMOC state and decrease in strength probably caused a general surface warming of the South Atlantic, which is opposite to the response of the SST records from the North Atlantic (Calvo et al., 2004; Martrat et al., 2007). In addition, several DO stadials (or GS) occurred from 47 to 30 ka. If the DO stadials that occurred during the MIS 3 are indeed caused by a reduction in AMOC strength (Henry et al., 2016; Bagniewski et al., 2017) and are linked to a reduction in cross-equatorial heat transport, it is plausible to expect increases in SST in the South Atlantic during these stadials. This long-term (47-30 ka) and millennial-scale warmings in South Atlantic caused by a reduction of the AMOC strength during late MIS 3 may have contributed for the increased meridional thermal gradient (Figure 6b) and to a decrease in SE trade wind intensity. Therefore, we suggest that a progressive shoaling of the thermocline from 47 to 30 ka is due to the weakening of the SE trade winds, caused by a warming in the low and mid-latitudes of the South Atlantic driven by changes in the state and strength of the AMOC.

The shoaling of the thermocline (Figure 6c) during MIS 4 and the cold substages of MIS 5 (MIS 5b and 5d) seems to be related to a different mode of thermocline variability. For millennial-scale events (e.g. HS 1) and for the trends observed during MIS 3, a "zonal" mode (east-west) of thermocline variability related to changes in the SE trade winds is able to explain the observed patterns. Thus, a shoaling of the thermocline in the entire western equatorial Atlantic would be the result of a weakening

in SE trade wind intensity, causing a decrease in the SEC transport with a subsequently reduction in the east-west equatorial thermocline tilt. However, during MIS 4 and during the cold substages of MIS 5 our data shows a shoaling of the thermocline at 0.5°S, while the records from Kinkel et al. (2000) and Rühlemann et al. (2001) show a deepening of the thermocline at 3°N in the western equatorial Atlantic. Since, the "zonal" mode assumes that variations in the thermocline for the entire western equatorial Atlantic are inphase, these contrasting results cannot be explain by this mode of thermocline variability.

The complex modern structure of the thermocline across the equatorial region (Figure 1b) is the result of the asymmetrical structure of the wind-driven surface currents (Defant et al., 1961). Between 10°S and 10°N, the thermocline is shallower than sites located at the subtropical gyres of the Atlantic at the same longitude (Figure 1b). In addition, the presence of the NECC causes a deepening of the thermocline around 5°N, which results in the asymmetrical shape of the thermocline across the equator. Thus, this pattern is enhanced during periods of an active and strong NECC, as during boreal summer in modern ocean climatology (Joyce et al., 2004; Hormann et al., 2012). Therefore, changes in the intensity of trade winds can also influence this meridional asymmetrical structure, causing changes in the thermocline depth across the equator. During MIS 4 and cold substages of MIS 5, larger northern ice sheets caused global decreases in sea level (Figure 6e) and increased the meridional SST gradient (Figure 6b). This led to a southward shift of the ITCZ (Figure 5e), more zonal and intense trade winds (NE and SE) and an equatorward compression of the climatic zones.

Several studies have suggested that the NECC, or the NBC retroflection, was active and probably shifted to the south during cold stages (Maslin et al., 1997; Rühlemann et al., 2001; Wilson et al., 2011; Govin et al., 2014). Thus, we suggest that during MIS 4 and the cold substages of MIS 5 the thermocline was more asymmetrical across the equator than modern conditions, which would result in a deepening of the thermocline around 3°N, supported by the findings of Kinkel et al. (2000) and Rühlemann et al., (2001), and a shoaling of the thermocline north and south of the NECC position. This "meridional" mode is able to conciliate our findings with the ones from Kinkel et al. (2000) and Rühlemann et al., (2001) during MIS 4 and the cold substages of MIS 5, suggesting the dominance of the "meridional" mode over the "zonal" mode during these periods (Figure S3).

Besides the glacial-interglacial and millennial-scale changes in thermocline depth in the western equatorial Atlantic, a long-term trend is also present in our $\Delta\delta^{18}O$

records (Figure 6c). The long-term trend shows a shoaling of the thermocline from MIS 5e to HS1 and then a deepening from HS1 to the present (Figure 6c). Global sea level (Figure 6e) and AMOC strength (Figure 6d) changes show a similar long-term trend, where an increase in ice volume from MIS 5e to HS 1 may be associated with a reduction in AMOC strength (Böhm et al., 2015). The long-term reduction in AMOC strength may affect the meridional thermal gradient, which also shows this long-term trend (Figure 6b). It appears that a similar long-term trend is present in the accumulation rates of terrigenous sediment in the record from Rühlemann et al. (2001). As pointed out by Rühlemann et al. (2001), the terrigenous input at their core site is controlled by the NECC and its intensity is modulated by the strength of the SE trade winds, thus it seems that the SE trade winds also varied following this long-term trend. Therefore, similar to MIS 4 and the cold substages of MIS 5, the long-term variations in ice volume may have modulated the meridional thermal gradient and the trade wind intensity, subsequently influencing the thermocline depth in the western equatorial Atlantic (meridional mode).

Despite the importance of understanding the mechanisms responsible for our $\Delta\delta^{18}O_{dut\text{-}rub}$ records, we also focus on the consequences of such thermocline fluctuations in the western equatorial Atlantic. Using several core tops across the South Atlantic, Steph et al. (2009) showed that variations of 1 ‰ in $\Delta\delta^{18}O_{dut\text{-}rub}$ of *N. dutertrei* and *G. ruber* are equivalent to approximately 100-meter variation on the depth of the 20°C isotherm, the isotherm associated to the thermocline depth in our site. Since our results show the $\Delta\delta^{18}O_{dut\text{-}rub}$ minimum values of 0.6 up to maximum values of 2.1 ‰, the thermocline depth fluctuations in our site could be up to 150 meters. During millennial-scale events (e.g. HS 1), the shoaling of the thermocline (≈ 1 ‰) might have contributed to a decrease in ocean heat content in that area, causing a reduction in cross-equatorial heat transport. A reduction in cross-equatorial heat transport was probably also a feature during glacial stages and cold substages of MIS 5, since our results together with previous studies (Rühlemann et al., 2001; Wilson et al., 2011) suggest a strengthening of the NECC and a prolongation of the NBC retroflection. Alterations of the cross-equatorial heat transport can influence the position of the ITCZ (McGee et al., 2014) and the state of the AMOC (McManus et al., 2004), subsequently influencing the formation of North Atlantic Deep Water (NADW). Thus, the observed changes in stratification (Figure 6c), during stadials and glacial stages, may have led to reductions in heat content in the western equatorial Atlantic and subsequent decrease in heat transport to the North Atlantic,

which might have contributed to setting the global climate.

4.5.3. Distinct influence of Heinrich and Dansgaard-Oeschger stadials over the upper western equatorial Atlantic circulation and discharge of fluvial sediments

Heinrich and Dansgaard-Oeschger stadials are characterized as millennial-scale changes in the global climate. However, the question whether both types of events are related to the same climatic mechanisms remains open (Alvarez-Solas et al., 2013; Petersen et al., 2013; Menviel et al., 2014; Henry et al., 2016). Although, our focus does not rely on the discussion of the causes related with both types of events, we are interested in the comparison of the tropical climate responses during HS and DO stadials.

Assuming that both types of millennial-scale events are associated to changes in AMOC strength (Henry et al., 2016; Bagniewski et al., 2017), we compared our $\Delta\delta^{18}O_{dut\text{-}rub}$ and Fe/Ca records to the Atlantic meridional temperature difference, which can be associated with SST changes due to variations in AMOC strength (Figure 7). We plotted the mean values of $\Delta\delta^{18}O_{dut\text{-}rub}$ and Fe/Ca during each HS and DO stadials, using the term GS for the DO stadials (Rasmussen et al., 2014), and during each marine isotope stage (MIS 1-5). In addition, we differentiate the substages of MIS 5 (a-e) due to the observed differences in thermocline depth and fluvial discharge during cold substages of MIS 5 (b; d). However, because our records do not cover the entire MIS 2, it does not allow us to compare with confidence the MIS 2 with other stages.

Indeed, HS show stronger impacts (i.e. higher Fe/Ca and $\Delta\delta^{18}O_{dut\text{-}rub}$) on both reconstructed parameters than DO stadials (or GS) (Figure 7c). However, GS 21.1, GS 20 and GS 19.2 show values of Fe/Ca as high as HS (Figure 7a) and GS 22 and GS 5-7 show values of $\Delta\delta^{18}O_{dut\text{-}rub}$ as high as HS (Figure 7b). The high values of Fe/Ca during GS 19.2 are due to a progressive increase in Fe/Ca in the beginning of MIS 4 (72 to 69 ka) coherent with progressively drier conditions over the Cariaco Basin (Figure 5b). For GS 20 and GS 21, the values are corroborated by increases in Ti/Ca from core CDH-86 (Nace et al., 2014) (Figure 5d). In addition, GS 20 and GS 21 occur simultaneously to strong cooling events in the North Atlantic

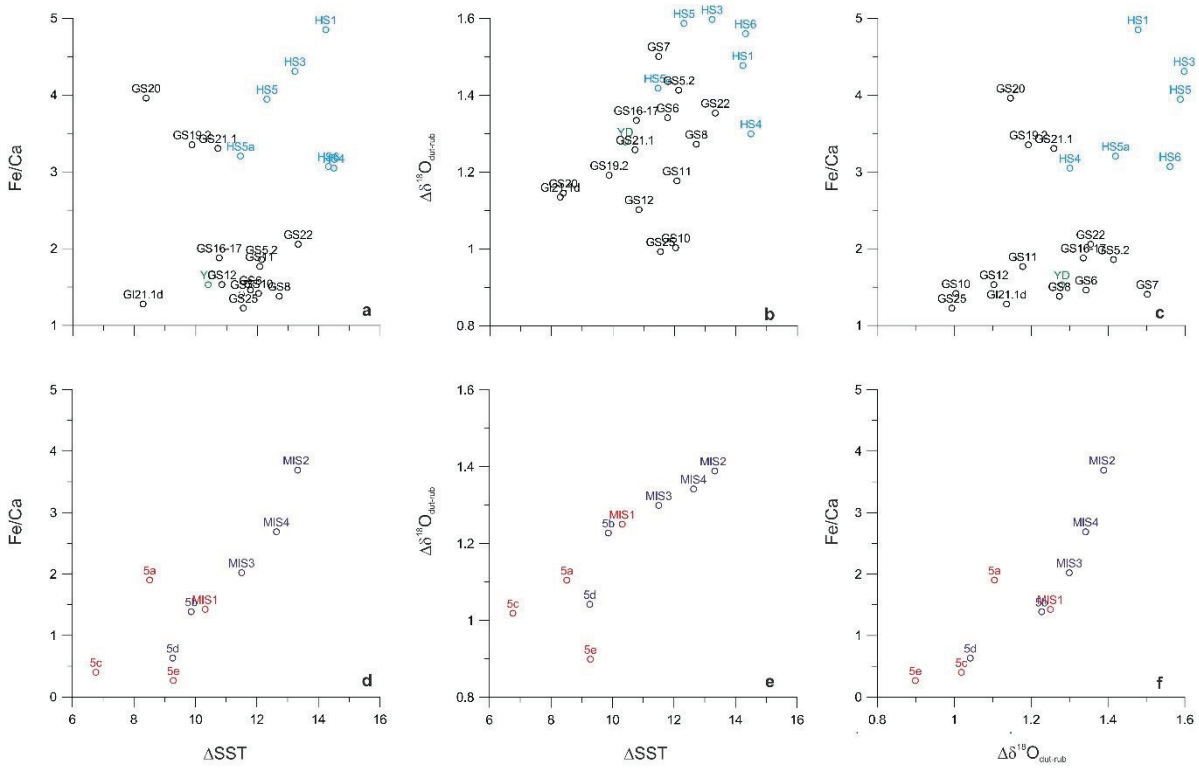

Figure 7. (a-c) Comparison between the Younger Dryas (green label), Heinrich stadials (blue labels) and Greenland stadials (or DO stadials) (black labels) responses in terms of terrigenous input (Fe/Ca), thermocline depth ($\Delta\delta^{18}O_{dut\text{-}rub}$) and interhemispheric thermal gradient (ΔSST). (d-f) Comparison between marine isotopes stages (MIS) /substages 1, 5a, 5c and 5e(red labels) and MIS / substages 2-4, 5b and 5d (blue labels) in terms of terrigenous input (Fe/Ca), thermocline depth ($\Delta\delta^{18}O_{dut\text{-}rub}$) and interhemispheric thermal gradient (ΔSST). Fe/Ca ratios from GeoB16202-2 were normalized relative to GL-1248 ratios, due to distinct intensities.

(McManus et al., 1994), C 19 and C 20 respectively, which may have contributed for a southward displacement of the ITCZ and enhanced precipitation over NE Brazil, promoting high values of Fe/Ca (and Ti/Ca) in the adjacent ocean.

In terms of thermocline variations linked to changes in trade wind intensity, GS 22 and GS 5-7 show values of $\Delta\delta^{18}O_{dut\text{-}rub}$ as high as HS (Figure 7b). GS 22 occurs during the cold substage MIS 5b and is associated with a cooling event (C 21) in the North Atlantic (McManus et al., 1994). These features may explain the increased meridional temperature gradient during this period, which may have led to changes in trade wind intensity and subsequently shoaling of the thermocline. However, we must also highlight that these strong responses may be due to the fact that some of these GS can be associated to the HS that occur between 123 and 60 ka (HS 7-10). For instance, HS 7 can be associated to GS 20, as shown by other works (e.g. Salgueiro et al., 2010) and supported by the increase in $^{231}Pa/^{230}Th$ (Figure

6d), marked by Böhm et al. (2015) as HS 7. In addition, HS 8 can be linked to GS 22 as pointed out by Jacobel et al. (2016). Therefore, the GS that occurred from 123 and 60 ka may have triggered a stronger response in the western equatorial Atlantic than other GS (DO stadials), due to their association with strong cooling events in the North Atlantic (McManus et al., 1994; Oppo et al., 2006) and/or decreases in AMOC strength (Böhm et al., 2015). For GS 5-7, the high values of $\Delta\delta^{18}O_{dut\text{-}rub}$ are linked to the trend from 47 to 30 ka, showing an increase in $\Delta\delta^{18}O_{dut\text{-}rub}$ values. Thus, the mean $\Delta\delta^{18}O_{dut\text{-}rub}$ values observed for GS 5-7 are not linked to a fast climatic response of the western equatorial Atlantic to these events, but to a long-term trend from 47 to 30 ka, which is connected to changes in orbital configuration (Pahnke and Sachs, 2006) and changes in the AMOC mode (Santos et al., 2017).

Despite these exceptions, DO stadials promoted in general minor changes in ITCZ position, as revealed by our Fe/Ca records, and trade wind intensity, as shown by our $\Delta\delta^{18}O_{dut\text{-}rub}$ records, compared to HS. If indeed both types of millennial-scale variability (HS and DO stadials) are mainly linked to changes in AMOC strength (Henry et al., 2016; Bagniewski et al. 2017), the magnitude of the climatic response in the western equatorial Atlantic and the adjacent continent may be related to the magnitude of the change in AMOC strength. This is in agreement with the recent model simulations from Bagniewski et al. (2017), which show a 30-50 % weakening of the AMOC during DO stadials, compared to a complete shutdown during HS. Reconstructions of AMOC strength using $^{231}Pa/^{230}Th$ also suggest weaker AMOC during HS compared to DO stadials (Böhm et al., 2015; Henry et al., 2016). Thus, the conclusion of Mulitza et al. (submitted) elaborated for HS 1 of a near-linear link between changes in AMOC strength and precipitation over northeastern Brazil may be valid for most of the HS and GS since the LIG.

Finally, we show a comparison of the different marine isotope stages (MIS 1-5) and substages of MIS 5 (a-e) using the same proxies (Fe/Ca, $\Delta\delta^{18}O_{dut\text{-}rub}$ and ΔSST) (Figure 7d-f). While MIS 1 and substages of MIS 5 form one group, the glacial stages (MIS 2-4) constitute another group. In general during MIS 1 and the substages of MIS 5 the terrigenous input to the ocean, the meridional thermal gradient and the thermocline depth in the western equatorial Atlantic underwent minor changes. However, during glacial stages (MIS 2-4) these parameters (Fe/Ca, $\Delta\delta^{18}O_{dut\text{-}rub}$, and ΔSST) where enhanced. Regarding the substages of MIS 5, we observe that cold substages (5b and 5d) show enhanced terrigenous input to the ocean and shallower thermocline depth than during warm substages (5c and 5e), with the exception of MIS 5a. During MIS 5a, the

occurrence of millennial-scale events (GS 21.1 and GS20) influenced the mean values, causing the observed pattern (Figure 7f). Additionally, both warm and cold stages of MIS 5 show a weaker climatic response than MIS 1 (Figure 7d-f), suggesting differences in the magnitude of climatic changes in our site between the last two interglacials. MIS 2 and MIS 4 displayed the highest values, with the high mean Fe/Ca probably linked to the lowest sea level that occurred during these stages. However, our record for MIS 2 is incomplete and substantially influenced by HS 1, which probably affects the mean values. Nevertheless, our approach provides a relevant assessment of the magnitude of the climatic changes that occurred in the western equatorial Atlantic and the adjacent continent since the LIG.

4.6. Conclusions

Our western equatorial Atlantic Fe/Ca and $\Delta\delta^{18}O_{dut\text{-}rub}$ records suggest that meridional shifts in the mean position of the ITCZ and changes in stratification of the upper water column were linked to the changes in the trade winds since the Last Interglacial. The Fe/Ca records show, for the first time in a marine sediment core collected off northeastern Brazil, the presence of Dansgaard-Oeschger cycles. The observation of these short-term climatic events highlight the presence of fast climatic teleconnections between high and low latitudes in the Atlantic Ocean, which can influence the hydroclimate over northeastern Brazil due to shifts in the ITCZ. Moreover, our reconstructions of the thermocline depth ($\Delta\delta^{18}O_{dut\text{-}rub}$) reveal the presence of two modes of variability (zonal and meridional) that can alternate in dominance through time. Anomalously shallow thermocline during millennial-scale events is linked to the zonal mode, while during glacial stages and cold substages of MIS 5 is associated to the meridional mode. We suggest that such changes in the upper stratification (0-150m) in the western equatorial Atlantic are linked to variations in the strength of the trade winds, which are turn are modulated by the Atlantic meridional temperature gradient. The observed shallow thermocline periods in our site may reduce the cross-equatorial heat transport, influencing the global climate. Furthermore, we show a comparison of changes in stratification and continental runoff in the western equatorial Atlantic between millennial-scale events (HS and DO stadials) and between glacial and interglacial periods. Our results demonstrate a stronger impact of HS than DO stadials in our study site, which can be related to the weaker AMOC during HS than during DO stadials, as proposed by paleo-records and model simulations.

4.7. Acknowledgements

The Geochemistry Network from PETROBRAS/National Petroleum Agency (ANP) of Brazil (grant 0050.004388.08.9)

financially supported this study. A.L.S. Albuquerque is senior scholar from CNPq (National Council for the Development of Science and Technology, Brazil, grant 306385/2013-9). CNPq also financially supported Igor M. Venancio with a scholarship from the CsF ("Ciencia sem Fronteiras") project (grant 248819/2013-5). This work was also funded through the DFG Research Center/Cluster of Excellence "The Ocean in the Earth System". C. M. Chiessi acknowledges the financial support from FAPESP (grant 2012/17517-3), CAPES (grants 1976/2014 and 564/2015), and CNPq (grant 302607/2016-1). This study is a contribution to the Helmholtz Initiative REKLIM, a joint research project of the Helmholtz Association of German Research Centers (HGF).

4.8. References

Alvarez-Solas, J., Robinson, A., Montoya, M., Ritz, C., 2013. Iceberg discharges of the last glacial period driven by oceanic circulation changes. Proc. Natl. Acad. Sci. U.S.A. 110, 16350–4. doi:10.1073/pnas.1306622110

Arz, H.W., Pätzold, J., Wefer, G., 1998. Correlated Millennial-Scale Changes in Surface Hydrography and Terrigenous Sediment Yield Inferred from Last-Glacial Marine Deposits off Northeastern Brazil. Quat. Res. 166, 157–166.

Bagniewski, W., Meissner, K.J., Menviel, L., 2017. Exploring the oxygen isotope fingerprint of Dansgaard-Oeschger variability and Heinrich events. Quat. Sci. Rev. 159, 1–14. doi:10.1016/j.quascirev.2017.01.007

Barker, S., Chen, J., Gong, X., Jonkers, L., Knorr, G., Thornalley, D., 2015. Icebergs not the trigger for North Atlantic cold events. Nature 520, 333–336. doi:10.1038/nature14330

Bassinot, F. C., L. Beaufort, E. Vincent, and L. Labeyrie, 1997. Changes in the dynamics of western equatorial Atlantic surface currents and biogenic productivity at the "mid-Pleistocene revolution" (930 ka), Proc. Ocean Drill. Program Sci. Results, 154, 269-284.

Blaauw, M., 2010. Methods and code for "classical" age-modelling of radiocarbon sequences. Quat. Geochronol. 5, 512–518. doi:10.1016/j.quageo.2010.01.002

Bond, G., Broecker, W., Johnsen, S., McManus, J.F., Labeyrie, L., Jouzel, J., Bonani, G., 1993. Correlations between climate records from North Atlantic sediments and Greenland ice. Nature 365, 143–147.

Bond, G., Heinrich, H., Broecker, W.S., Labeyrie, L., McManus, J.F., Andrews, J.T., Huon, S., Jantschik, R., Clasen, S., Simet, C., Tedesco, K., Klas, M., Bonani, G., Ivy, S., 1992. Evidence for massive discharges of icebergs into the North Atlantic ocean during the last glacial period. Nature 360, 245–249. doi:10.1038/360245a0

Brandt, P., Caniaux, G., Bourlès, B., Lazar, A., Dengler, M., Funk, A., Hormann, V., Giordani, H., Marin, F., 2011. Equatorial upper-ocean dynamics and their interaction with the West African monsoon. Atmos. Sci. Lett. 12, 24–30. doi:10.1002/asl.287

Braun, H., Ditlevsen, P., Chialvo, D.R., 2008. Solar forced Dansgaard-Oeschger events and their phase relation with solar proxies. Geophys. Res. Lett. 35, 1–5. doi:10.1029/2008GL033414

Broccoli, A.J., Dahl, K. A., Stouffer, R.J., 2006. Response of the ITCZ to Northern Hemisphere cooling. Geophys. Res. Lett. 33, n/a-n/a. doi:10.1029/2005GL024546

Broecker, W.S., 1998. Paleocean circulation during the Last Deglaciation: A bipolar seesaw? Paleoceanography 13, 119. doi:10.1029/97PA03707

Calvo, E., Villanueva, J., Grimalt, J.O., Boelaert, A., Labeyrie, L., 2001. New insights into the glacial latitudinal temperature gradients in the North Atlantic. Results from UK'

37 sea surface temperatures and terrigenous inputs. Earth Planet. Sci. Lett. 188, 509–519. doi:10.1016/S0012-821X(01)00316-8

Chappellaz, J., Bluniert, T., Raynaud, D., Barnola, J.-M., Schwander, J., Stauffert, B., 1993. Synchronous changes in atmospheric CH_4 and Greenland climate between 40 and 8 kyr BP. Nature 366, 443–445. doi:10.1038/366443a0

Chiang, J.C.H., Bitz, C.M., 2005. Influence of high latitude ice cover on the marine Intertropical Convergence Zone. Clim. Dyn. 25, 477–496. doi:10.1007/s00382-005-0040-5

Clement, A.C., Peterson, L.C., 2008. Mechanisms of abrupt climate change of the last glacial period. Rev. Geophys. 1–39. doi:10.1029/2006RG000204

Dansgaard, W., Johnsen, S.J., Clausen, H.B., Dahl-Jensen, D., Gundestrup, N.S., Hammer, C.U., Hvidberg, C.S., Steffensen, J.P., Sveinbjörnsdóttir, A.E., Jouzel, J., Bond, G.C., 1993. Evidence for general instability of past climate from a 250-ka ice-core record. Nature 364, 218–220. doi:10.1038/364218a0

Defant, A., 1961. Physical Oceanography, Pergamon Press, Oxford.

Deplazes, G., Lückge, A., Peterson, L.C., Timmermann, A., Hamann, Y., Hughen, K.A., Röhl, U., Laj, C., Cane, M.A., Sigman, D.M., Haug, G.H., 2013. Links between tropical rainfall and North Atlantic climate during the last glacial period. Nat. Geosci. 6, 1–5. doi:10.1038/ngeo1712

Dupont, L.M., Schlütz, F., Ewah, C.T., Jennerjahn, T.C., Paul, A., Behling, H., 2010. Two-step vegetation response to enhanced precipitation in Northeast Brazil during Heinrich event 1. Glob. Chang. Biol. 16, 1647–1660. doi:10.1111/j.1365-2486.2009.02023.x

Govin, A., Capron, E., Tzedakis, P.C., Verheyden, S., Ghaleb, B., Hillaire-Marcel, C., St-Onge, G., Stoner, J.S., Bassinot, F., Bazin, L., Blunier, T., Combourieu-Nebout, N., El Ouahabi, A., Genty, D., Gersonde, R., Jimenez-Amat, P., Landais, A., Martrat, B., Masson-Delmotte, V., Parrenin, F., Seidenkrantz, M.S., Veres, D., Waelbroeck, C., Zahn, R., 2015. Sequence of events from the onset to the demise of the Last Interglacial: Evaluating strengths and limitations of chronologies used in climatic archives. Quat. Sci. Rev. 129, 1–36. doi:10.1016/j.quascirev.2015.09.018

Govin, A., Holzwarth, U., Heslop, D., Ford Keeling, L., Zabel, M., Mulitza, S., Collins, J. a., Chiessi, C.M., 2012. Distribution of major elements in Atlantic surface sediments (36°N-49°S): Imprint of terrigenous input and continental weathering. Geochemistry, Geophys. Geosystems 13, n/a-n/a. doi:10.1029/2011GC003785

Govin, A., Chiessi, C.M., Zabel, M., Sawakuchi, A. O., Heslop, D., Hörner, T., Zhang, Y., Mulitza, S., 2014. Terrigenous input off northern South America driven by changes in Amazonian climate and the North Brazil Current retroflection during the last 250 ka. Clim. Past 10, 843–862. doi:10.5194/cp-10-843-2014

Hammer, Ø., Harper, D.A.T., T., Ryan, P.D., 2001. PAST: Paleontological Statistics Software Package for Education and Data Analysis. Palaeontol. Electron. 4(1), 1–9. doi:10.1016/j.bcp.2008.05.025

Hastenrath, S., Merle, J., 1987. Annual Cycle of Subsurface Thermal Structure in the Tropical Atlantic Ocean. J. Phys. Oceanogr. 17, 1518–1538.

Henry, L.G., McManus, J.F., Curry, W.B., Roberts, N.L., Piotrowski, A.M., Keigwin, L.D., 2016. North Atlantic ocean circulation and abrupt climate change during the last glaciation. Science (80-.). 353, 470–474. doi:10.1126/science.aaf5529

Hodell, D.A., Evans, H.F., Channell, J.E.T., Curtis, J.H., 2010. Phase relationships of North Atlantic ice-rafted debris and surface-deep climate proxies during the last glacial period. Quat. Sci. Rev. 29, 3875–3886. doi:10.1016/j.quascirev.2010.09.006

Hormann, V., Lumpkin, R., Foltz, G.R., 2012. Interannual North Equatorial Coun-

tercurrent variability and its relation to tropical Atlantic climate modes. J. Geophys. Res. Ocean. 117, 1–17. doi:10.1029/2011JC007697

Huppertz, N., 2014. Variability of surface water stratification offshore Brazil over the past 25ka. Master's Thesis, Universitiy of Bremen, pp. 30.

Jacobel, A.W., McManus, J.F., Anderson, R.F., Winckler, G., 2017. Climate-related response of dust flux to the central equatorial Pacific over the past 150 ka. Earth Planet. Sci. Lett. 457, 160–172. doi:10.1016/j.epsl.2016.09.042

Jaeschke, A., Rühlemann, C., Arz, H., Heil, G., Lohmann, G., 2007. Coupling of millennial-scale changes in sea surface temperature and precipitation off northeastern Brazil with high-latitude climate shifts during the last glacial period. Paleoceanography 22, n/a-n/a. doi:10.1029/2006PA001391

Jennerjahn, T.C., Ittekkot, V., Arz, H.W., Behling, H., Pätzold, J., Wefer, G., 2004. Asynchronous terrestrial and marine signals of climate change during Heinrich events. Science 306, 2236–9. doi:10.1126/science.1102490

Joyce, T.M., Frankignoul, C., Yang, J., Phillips, H.E., 2004. Ocean Response and Feedback to the SST Dipole in the Tropical Atlantic. J. Phys. Oceanogr. 34, 2525–2540. doi:10.1175/JPO2640.1

Kageyama, M., Merkel, U., Otto-Bliesner, B., Prange, M., Abe-Ouchi, A., Lohmann, G., Ohgaito, R., Roche, D.M., Singarayer, J., Swingedouw, D., X Zhang, 2013. Climatic impacts of fresh water hosing under Last Glacial Maximum conditions: a multi-model study. Clim. Past 9, 935–953. doi:10.5194/cp-9-935-2013

Keigwin, L.D., Boyle, E. a, 1999. Surface and deep ocean variability in the northern Sargasso Sea during marine isotope stage 3. Paleoceanography 14, 164–170. doi:10.1029/1998PA900026

Kim, J.H., Schneider, R.R., Mulitza, S., Müller, P.J., 2003. Reconstruction of SE trade-wind intensity based on sea-surface temperature gradients in the Southeast Atlantic over the last 25 kyr. Geophys. Res. Lett. 30, 3–6. doi:10.1029/2003GL017557

Kinkel, H., Baumann, K.H., Cepek, M., 2000. Coccolithophores in the equatorial Atlantic Ocean: Response to seasonal and Late Quaternary surface water variability, in: Marine Micropaleontology. pp. 87–112. doi:10.1016/S0377-8398(00)00016-5

Loulergue, L., Schilt, A., Spahni, R., Masson-Delmotte, V., Blunier, T., Lemieux, B., Barnola, J.-M., Raynaud, D., Stocker, T.F., Chappellaz, J., 2008. Orbital and millennial-scale features of atmospheric CH4 over the past 800,000 years. Nature 453, 383–386. doi:10.1038/nature06950

Lynch-Stieglitz, J., Schmidt, M.W., Gene Henry, L., Curry, W.B., Skinner, L.C., Mulitza, S., Zhang, R., Chang, P., 2014. Muted change in Atlantic overturning circulation over some glacial-aged Heinrich events. Nat. Geosci. 7, 1–7. doi:10.1038/ngeo2045

Martrat, B., Grimalt, J.O., Shackleton, N.J., de Abreu, L., Hutterli, M. a, Stocker, T.F., 2007. Four climate cycles of recurring deep and surface water destabilizations on the Iberian margin. Science 317, 502–507. doi:10.1126/science.1139994

Markle, B.R., Steig, E.J., Buizert, C., Schoenemann, S.W., Bitz, C.M., Fudge, T.J., Pedro, J.B., Ding, Q., Jones, T.R., White, J.W.C., Sowers, T., 2016. Global atmospheric teleconnections during Dansgaard–Oeschger events. Nat. Geosci. 10. doi:10.1038/NGEO2848

McGee, D., Donohoe, A., Marshall, J., Ferreira, D., 2014. Changes in ITCZ location and cross-equatorial heat transport at the Last Glacial Maximum, Heinrich Stadial 1, and the mid-Holocene. Earth Planet. Sci. Lett. 390, 69–79. doi:10.1016/j.epsl.2013.12.043

McManus, J.F., Bond, G.C., Broecker, W.S., Johnsen, S., Labeyrie, L., Higgins, S., 1994. High-resolution climate records from the North Atlantic during the last interglacial. Nature. doi:10.1038/371326a0

McManus, J.F., Francois, R., Gherardi, J.-M., Keigwin, L.D., Brown-Leger, S., 2004. Collapse and rapid resumption of Atlantic meridional circulation linked to deglacial climate changes. Nature 428, 834–7. doi:10.1038/nature02494

Menviel, L., Timmermann, A., Friedrich, T., England, M.H., 2014. Hindcasting the continuum of Dansgaard-Oeschger variability: Mechanisms, patterns and timing. Clim. Past 10, 63–77. doi:10.5194/cp-10-63-2014

Mulitza, S., Chiessi, C.M., Schefuß, E., Lippold, J., Wichmann, D., Antz, B., Mackensen, A., Paul, A., Prange, M., Rehfeld, K., Werner, M., Bickert, T., Frank, N., Kuhnert, H., Lynch-Stieglitz, J., Portilho-Ramos., R.C., Sawakuchi, A.O., Schulz, M., Schwenk, T., Tiedemann, R., Vahlenkamp, M., Zhang, Y., submitted. Synchronous and proportional deglacial changes in Atlantic Meridional Overturning Circulation and northeast Brazilian precipitation. Paleoceanography.

Mulitza, S., Prange, M., Stuut, J.B., Zabel, M., Von Dobeneck, T., Itambi, A.C., Nizou, J., Schulz, M., Wefer, G., 2008. Sahel megadroughts triggered by glacial slowdowns of Atlantic meridional overturning. Paleoceanography 23, 1–11. doi:10.1029/2008PA001637

Mulitza, S., Chiessi, C.M., Cruz, A.P.S., Frederichs, T.W., Gomes, J.G., Gurgel, M.H.C., Haberkern, J., Huang, E., Jovane, L., Kuhnert, H., Pittauerová, D., Reiners, S.J., Roud, S.C., Schefuß, E., Schewe, F., Schwenk, T.A., Sicoli-Seoane, J.C., Sousa, S.H.M., Wangner, D.J., Wiers, S., 2013. Response of Amazon sedimen-tation to deforestation, land use and climate variability. Cruise No. MSM20/3 (February 19–March 11, 2012), Recife (Brazil)–Bridgetown (Barbados). MARIA S. MERIAN-Berichte, MSM20/3. DFG Senatskommission für Ozeanographie. 86pp.

Nace, T.E., Baker, P.A., Dwyer, G.S., Silva, C.G., Rigsby, C.A., Burns, S.J., Giosan, L., Otto-Bliesner, B., Liu, Z., Zhu, J., 2014. The role of North Brazil Current transport in the paleoclimate of the Brazilian Nordeste margin and paleoceanography of the western tropical Atlantic during the late Quaternary. Palaeogeogr. Palaeoclimatol. Palaeoecol. doi:10.1016/j.palaeo.2014.05.030

North Greenland Ice Core Project members, 2004. High-resolution record of Northern Hemisphere climate extending into the last interglacial period. Nature 431, 147-151.

Oppo, D.W., Lehman, S.J., 1995. Suborbital timescale variability of North Atlantic Deep Water during the past 200,000 years. Paleoceanography 10, 901–910. doi:10.1029/95pa02089

Oppo, D.W., McManus, J.F., Cullen, J.L., 2006. Evolution and demise of the Last Interglacial warmth in the subpolar North Atlantic. Quat. Sci. Rev. 25, 3268–3277. doi:10.1016/j.quascirev.2006.07.006

Pahnke, K., Sachs, J.P., 2006. Sea surface temperatures of southern midlatitudes 0-160 ka B.P. Paleoceanography 21, 1–17. doi:10.1029/2005PA001191

Petersen, S. V., Schrag, D.P., Clark, P.U., 2013. A new mechanism for Dansgaard-Oeschger cycles. Paleoceanography 28, 24–30. doi:10.1029/2012PA002364

Peterson, L.C., 2000. Rapid Changes in the Hydrologic Cycle of the Tropical Atlantic During the Last Glacial. Science (80-.). 290, 1947–1951. doi:10.1126/science.290.5498.1947

Portilho-Ramos, R.C., Chiessi, C.M., Zhang, Y., Mulitza, S., Kucera, M., Siccha, M., Prange, M., Paul, A., accepted. Coupling of equatorial Atlantic surface stratification to glacial shifts in the tropical rainbelt. Sci. Rep. 7, 1-8. doi:10.1038/s41598-017-01629-z

Rasmussen, S.O., Bigler, M., Blockley, S.P., Blunier, T., Buchardt, S.L., Clausen, H.B., Cvijanovic, I., Dahl-Jensen, D., Johnsen, S.J., Fischer, H., Gkinis, V., Guillevic, M., Hoek, W.Z., Lowe, J.J., Pedro, J.B., Popp, T., Seierstad, I.K., Steffensen, J.P., Svensson, A.M., Vallelonga, P., Vinther, B.M., Walker, M.J.C., Wheatley, J.J., Winstrup, M., 2014. A stratigraphic framework for abrupt climatic changes during the Last Glacial period based on three synchronized Greenland ice-core

records: Refining and extending the INTIMATE event stratigraphy. Quat. Sci. Rev. 106, 14–28. doi:10.1016/j.quascirev.2014.09.007

Reimer, P.J., Bard, E., Bayliss, A., Beck, J.W., Blackwell, P.G., Bronk Ramsey, C., Buck, C.E., Cheng, H., Edwards, R.L., Friedrich, M., Grootes, P.M., Guilderson, T.P., Haflidason, H., Hajdas, I., Hatté, C., Heaton, T.J., Hoffmann, D.L., Hogg, A.G., Hughen, K.A., Kaiser, K.F., Kromer, B., Manning, S.W., Niu, M., Reimer, R.W., Richards, D.A., Scott, E.M., Southon, J.R., Staff, R.A., Turney, C.S.M., van der Plicht, J., 2013. IntCal13 and Marine13 Radiocarbon Age Calibration Curves 0–50,000 Years cal BP. Radiocarbon 55, 1869–1887. doi:10.2458/azu_js_rc.55.16947

Rodrigues, R.R., Rothstein, L.M., Wimbush, M., 2007. Seasonal Variability of the South Equatorial Current Bifurcation in the Atlantic Ocean: A Numerical Study. J. Phys. Oceanogr. 37, 16–30. doi:10.1175/JPO2983.1

Rosen, J.L., Brook, E.J., Severinghaus, J.P., Blunier, T., Mitchell, L.E., Lee, J.E., Edwards, J.S., Gkinis, V., 2014. An ice core record of near-synchronous global climate changes at the Bølling transition. Nat. Geosci. 7, 459–463. doi:10.1038/ngeo2147

Rühlemann, C., Frank, M., Hale, W., Mangini, A., Mulitza, S., Müller, P.J., Wefer, G., 1996. Late Quaternary productivity changes in the western equatorial Atlantic: Evidence from 230Th-normalized carbonate and organic carbon accumulation rates. Mar. Geol. 135, 127–152. doi:10.1016/S0025-3227(96)00048-5

Rühlemann, C., Diekmann, B., Mulitza, S., Frank, M., 2001. Late Quaternary changes of western equatorial Atlantic surface circulation and Amazon lowland climate recorded in Ceara Rise deep-sea sediments. Paleoceanography 16 (3), 293–305. doi:10.1029/1999PA000474.

Salgueiro, E., Voelker, A.H.L., de Abreu, L., Abrantes, F., Meggers, H., Wefer, G., 2010. Temperature and productivity changes off the western Iberian margin during the last 150 ky. Quat. Sci. Rev. 29, 680–695. doi:10.1016/j.quascirev.2009.11.013

Santos, T.P., Lessa, D.O., Venancio, I.M., Chiessi, C.M., Mulitza, S., Kuhnert, H., Govin, A., Machado, T., Costa, K.B., Toledo, F., Dias, B.B., Albuquerque, A.L.S., 2017. Prolonged warming of the Brazil Current precedes deglaciations. Earth Planet. Sci. Lett. 463, 1–12. doi:10.1016/j.epsl.2017.01.014

Schott, F.A., Fischer, J., Stramma, L., 1998. Transports and Pathways of the Upper-Layer Circulation in the Western Tropical Atlantic. J. Phys. Oceanogr. 28, 1904–1928.

Schulz, M., Mudelsee, M., 2002. REDFIT: Estimating red-noise spectra directly from unevenly spaced paleoclimatic time series. Comput. Geosci. 28, 421–426. doi:10.1016/S0098-3004(01)00044-9

Spratt, R.M., Lisiecki, L.E., 2016. A Late Pleistocene sea level stack. Clim. Past 12, 1079–1092. doi:10.5194/cp-12-1079-2016

Steph, S., Regenberg, M., Tiedemann, R., Mulitza, S., Nürnberg, D., 2009. Stable isotopes of planktonic foraminifera from tropical Atlantic / Caribbean core- tops : Implications for reconstructing upper ocean stratification. Mar. Micropaleontol. 71, 1–19. doi:10.1016/j.marmicro.2008.12.004

Veres, D., Bazin, L., Landais, A., Toyé Mahamadou Kele, H., Lemieux-Dudon, B., Parrenin, F., Martinerie, P., Blayo, E., Blunier, T., Capron, E., Chappellaz, J., Rasmussen, S.O., Severi, M., Svensson, A., Vinther, B., Wolff, E.W., 2013. The Antarctic ice core chronology (AICC2012): An optimized multi-parameter and multi-site dating approach for the last 120 thousand years. Clim. Past 9, 1733–1748. doi:10.5194/cp-9-1733-2013

Vidal, L., Labeyrie, L., Cortijo, E., Arnold, M., Duplessy, J.C.J.-C., Michel, E., Becqué, S., van Weering, T.C.E., 1997. Evidence for changes in the North Atlantic Deep Water linked to meltwater surges during the Heinrich events. Earth Planet. Sci. Lett. 146, 13–27. doi:10.1016/S0012-821X(96)00192-6

Vink, A., Rühlemann, C., Zonneveld, K.A.F., Mulitza, S., Hüls, M., Willems, H., 2001. Shifts in the position of the North Equatorial Current and rapid productivity changes in the western Tropical Atlantic during the last glacial. Paleoceanography 16, 479–490. doi:10.1029/2000PA000582

Waelbroeck, C., Labeyrie, L., Michel, E., Duplessy, J.C., McManus, J.F., Lambeck, K., Balbon, E., Labracherie, M., 2002. Sea-level and deep water temperature changes derived from benthic foraminifera isotopic records. Quat. Sci. Rev. 21, 295–305. doi:10.1016/S0277-3791(01)00101-9

Wang, X., Auler, A.S., Edwards, R.L., Cheng, H., Cristalli, P.S., Smart, P.L., Richards, D. a, Shen, C.-C., 2004. Wet periods in northeastern Brazil over the past 210 ka linked to distant climate anomalies. Nature 432, 740–3. doi:10.1038/nature03067

Wang, Y.J., Cheng, H., Edwards, R.L., An, Z.S., Wu, J.Y., Shen, C.-C., Dorale, J.A., 2001. A High-Resolution Absolute-Dated Late Pleistocene Monsoon Record from Hulu Cave, China. Science (80-.). 294, 2345–2348. doi:10.1126/science.1064618

Wilson, K.E., Maslin, M.A., Burns, S.J., 2011. Evidence for a prolonged retroflection of the North Brazil Current during glacial stages. Palaeogeogr. Palaeoclimatol. Palaeoecol. 301, 86–96. doi:10.1016/j.palaeo.2011.01.003

Wolff, T., Mulitza, S., Rühlemann, C., Wefer, G., 1999. Response of the tropical Atlantic thermocline to Late Quaternary Trade Wind changes. Paleoceanography 14, 374–383.

Zhang, D., Msadek, R., McPhaden, M.J., Delworth, T., 2011. Multidecadal variability of the North Brazil Current and its connection to the Atlantic meridional overturning circulation. J. Geophys. Res. 116, C04012. doi:10.1029/2010JC006812

Zhang, Y., Chiessi, C.M., Mulitza, S., Zabel, M., Trindade, R.I.F., Hollanda, M.H.B.M., Dantas, E.L., Govin, A., Tiedemann, R., Wefer, G., 2015. Origin of increased terrigenous supply to the NE South American continental margin during Heinrich Stadial 1 and the Younger Dryas. Earth Planet. Sci. Lett. 432, 493–500. doi:10.1016/j.epsl.2015.09.054

Zweck, C., Huybrechts, P., 2005. Modeling of the northern hemisphere ice sheets during the last glacial cycle and glaciological sensitivity. J. Geophys. Res. Atmos. 110, 1–24. doi:10.1029/2004JD005489

4.9. Supplementary material

Table 1. Radiocarbon ages and tie-points of core GL-1248 with their respective 2σ errors

Sediment core	Depth (cm)	Sample type	Lab. No.	Alignment to reference curve	Calibrated ages (ka BP)	Tie-point ages (ka)
GL-1248	0-2	*G. ruber; T. sacculifer*	Beta 423071		675 (643-752)	
GL-1248	26-28	*G. ruber; T. sacculifer*	Beta 423082		5475 (5378-5561)	
GL-1248	62-64	*G. ruber; T. sacculifer*	Beta 423072		9900 (9765-10097)	
GL-1248	125-127	*G. ruber; T. sacculifer*	Beta 423073		12500 (12249-12581)	
GL-1248	169-171	*G. ruber; T. sacculifer*	Beta 423074		14750 (14356-15041)	
GL-1248	217-219	*G. ruber; T. sacculifer*	Beta 423075		29040 (28777-29429)	
GL-1248	277-279	*G. ruber; T. sacculifer*	Beta 423076		31060 (30867-31250)	
GL-1248	321-323	*G. ruber; T. sacculifer*	Beta 423083		32980 (32493-33462)	
GL-1248	413-415	*G. ruber; T. sacculifer*	Beta 423078		34660 (34289-35011)	
GL-1248	445-447	*G. ruber; T. sacculifer*	Beta 423084		35860 (35370-36260)	
GL-1248	549-551	*G. ruber; T. sacculifer*	Beta 423079		39160 (38682-39860)	
GL-1248	629-631	*G. ruber; T. sacculifer*	Beta 423080		44060 (43355-44836)	
GL-1248	504	Ti/Ca		*to NGRIP-GICC05δ¹⁸Oice*		38240/±2962
GL-1248	726	Ti/Ca		*to NGRIP-GICC05δ¹⁸Oice*		46860/±3872
GL-1248	782	Ti/Ca		*to NGRIP-GICC05δ¹⁸Oice*		48840/±4072
GL-1248	901	Ti/Ca		*to NGRIP-GICC05δ¹⁸Oice*		54780/±4700
GL-1248	932	Ti/Ca		*to NGRIP-GICC05δ¹⁸Oice*		55740/±4816
GL-1248	1008	Ti/Ca		*to NGRIP-GICC05δ¹⁸Oice*		59320/±5176
GL-1248	1105	Ti/Ca		*to NGRIP-GICC05modelext δ¹⁸Oice*		71060/±3966
GL-1248	1138	Ti/Ca		*to NGRIP-GICC05modelext δ¹⁸Oice*		72340/±3550
GL-1248	1149	Ti/Ca		*to NGRIP-GICC05modelext δ¹⁸Oice*		74440/±3862
GL-1248	1229	Ti/Ca		*to NGRIP-GICC05modelext δ¹⁸Oice*		76460/±3636
GL-1248	1268	Ti/Ca		*to NGRIP-GICC05modelext δ¹⁸Oice*		78280/±3452
GL-1248	1355	Ti/Ca		*to NGRIP-GICC05modelext δ¹⁸Oice*		85160/±3572
GL-1248	1402	Ti/Ca		*to NGRIP-GICC05modelext δ¹⁸Oice*		87960/±3466
GL-1248	1532	Ti/Ca		*to NGRIP-GICC05modelext δ¹⁸Oice*		108300/±3646
GL-1248	1562	Ti/Ca		*to NGRIP-GICC05modelext δ¹⁸Oice*		111140/±3528
GL-1248	1666	Ti/Ca		*to EDC-AICC2012 CH4*		128726/±3504

Figure S1. Alignment (black dashed line) of the Ti/Ca record (orange line) from core GL-1248 with the references curves: δ^{18}Oice from NGRIP-GICC05modelext (blue line) and with methane from EDC-AICC2012 (black solid line). Radiocarbon ages (red symbols) and tie-points (green symbols) are plotted with their 2σ errors.

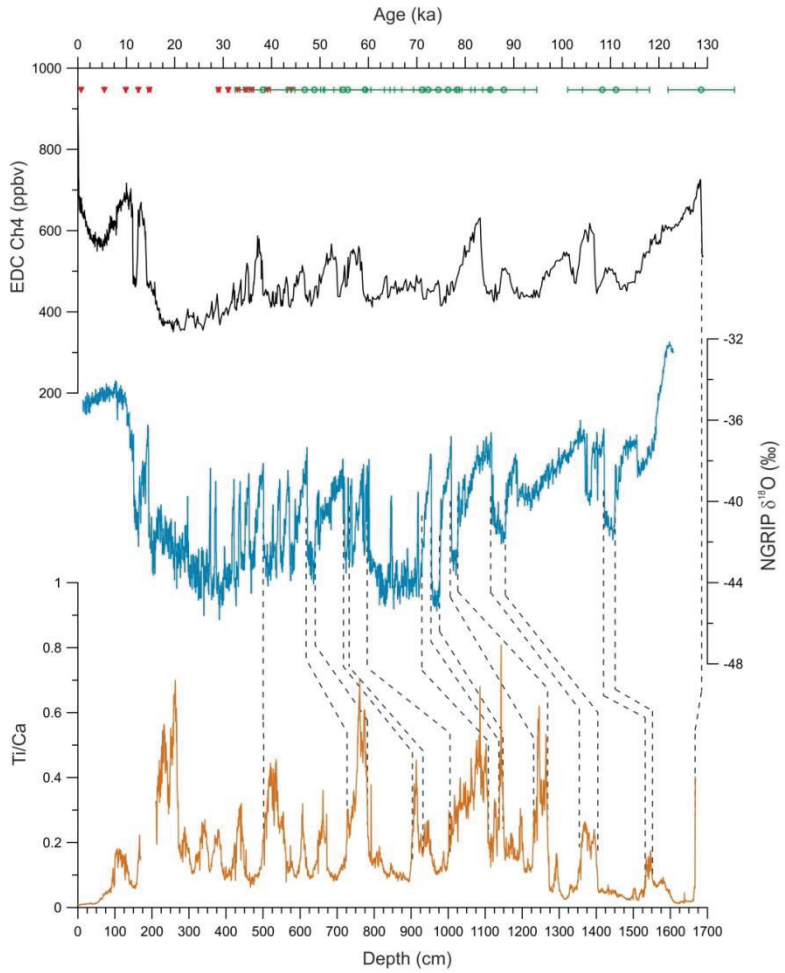

Figure S2. Comparison between the $\Delta\delta^{18}O_{dut\text{-}rub}$ record from core GL-1248, with 5-point running average (red line), and the relative abundance of *F. profunda* in core GeoB1523 (blue line). The grey bars highlight periods of shallow thermocline depth at the GL-1248 site and deep thermocline at the GeoB1523 site. The black arrows indicate the similar trends of both datasets during late MIS 3.

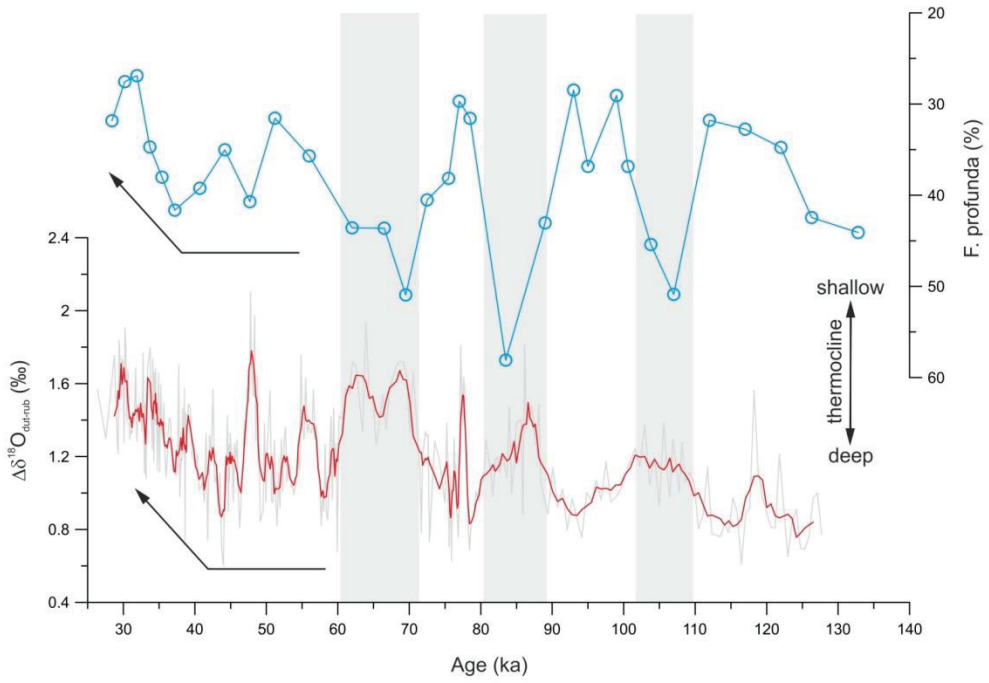

Figure S3. Conceptual figures of the modes of thermocline variability. In the left panel (meridional mode), the black dashed line represent modern depth of the thermocline (18° isotherm), the red line the scenario during interglacial periods and the blue line the scenario during MIS 4 and cold substages of MIS 5. In the right panel (zonal mode), the black dashed line represent modern depth of the thermocline, the red line the scenario during interstadials and the blue line the scenario during stadials.

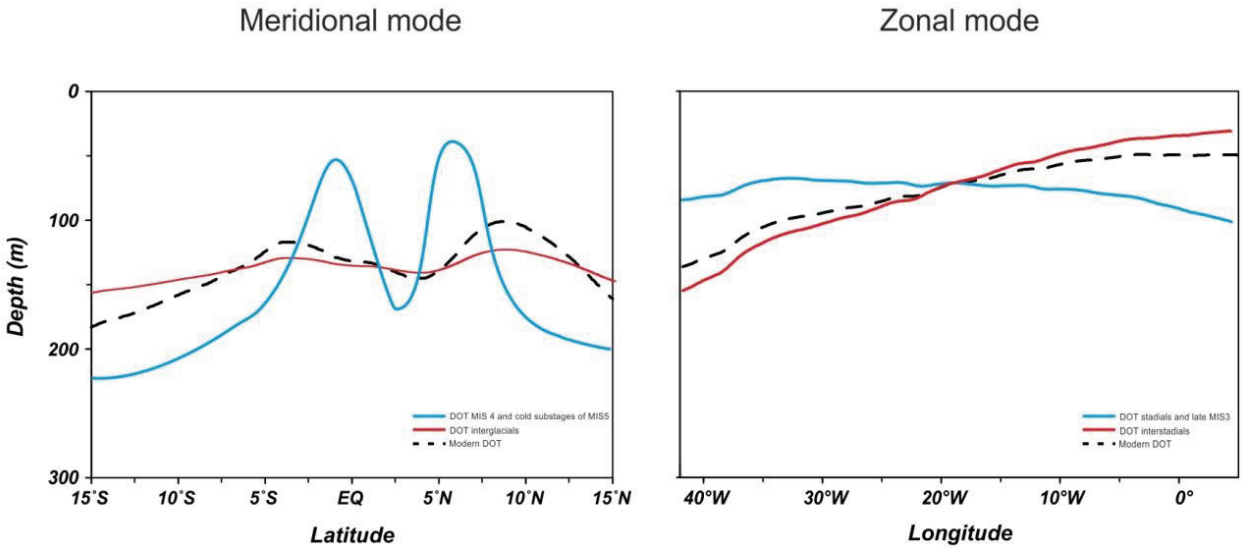

Chapter 5. Synthesis and Outlook

5.1. Synthesis

The objectives of this thesis were achieved by analyzing new high-resolution data from sediment traps and marine sediment cores located at the western South Atlantic. Our analysis of the planktonic foraminiferal fluxes at the southwestern Atlantic revealed the presence of lunar synchronized reproduction (chapter 2) and provided an objective assessment of the magnitude of the seasonal component on the shell fluxes of several planktonic foraminifera species (chapter 3). First, we showed that although a significant signal of lunar periodicity was observed for shell fluxes of several planktonic foraminifera species for the first deployment (3-day sampling resolution), with the maximum shell fluxes occurring during the last quarter, data from the other deployments suggests that the period of reproductive cycle is not strictly synchronous with the phases of the moon during each month (chapter 2). Despite the fact that our observations are restricted to the southwestern Atlantic, if synchronized cycles exist in planktonic foraminifera reproduction it should be a general feature that can be globally detected. In addition, our observation corroborates the recent findings from Jonkers et al. (2015), which show that lunar synchronized reproduction is a common feature of several planktonic foraminifera species. However, both studies could not resolve the nature of the mechanisms (endogenous or exogenous) and only suggest that an exogenous trigger would be more likely, based on the observed patterns.

In a second step, planktonic foraminiferal shell fluxes at the southwestern Atlantic were also analyzed regarding the influence of seasonal cycle (chapter 3). Our analysis revealed that most of the analyzed surface-dwelling species (*G. ruber* pink, *T. sacculifer*, *O. universa* and *G. menardii*) do not present a significant seasonal cycle in their shell fluxes, which is an expected pattern for the low latitudes (Fraile et al., 2009). However, the fluxes of two species (*G. ruber* white and *N. dutertrei*) showed a significant seasonal component, which highlights the influence of seasonal changes in hydrography, even at low latitudes, in modulating foraminiferal fluxes. The seasonal variability of the fluxes of these species was mainly attributed to changes in stratification, with *G. ruber* white showing an increase in the shell fluxes during summer, when we observe high sea surface temperatures com-

bined with a deep mixed layer, while *N. dutretrei* presented increases in the shell fluxes during spring and autumn, which are periods characterized by a shoaling of the thermocline. However, our explanations for the observed seasonal signals of these species are restricted to vertical changes in temperature, since no other parameter was continuously recorded (e.g. chlorophyll). Summarizing, our case studies on the short-term (lunar and seasonal) dynamics of the foraminiferal fluxes in the southwestern Atlantic provided new insights on planktonic foraminifera biology and indicates that the carbonate export to the seafloor in this region can be influenced by either periodicities in the lunar and/or in the seasonal band.

Another important achievement of this thesis was the new estimations of calcification depths for several planktonic foraminifera species in the southwestern Atlantic (chapter 3). Using stable oxygen isotopic composition of foraminiferal tests and the in situ vertical temperature profiles, we were able to estimate the calcification depths for several species and determine the seasonal variation of their calcification depths through the time series. We showed that the depth of calcification may vary seasonally for some species (*G. ruber* pink, *G. ruber* white, *G. menardii* and *N. dutertrei*), being linked to the mixed layer dynamics in the region. Further, we use this information (multi-species calcification depths) to propose the use of interspecific isotopic composition between *G. ruber* pink and *N. dutertrei* ($\Delta\delta^{18}O_{dut\text{-}rub}$) as a proxy for water column stratification at the southwestern Atlantic. Moreover, we applied this proxy, using *G. ruber* white instead of *G. ruber* pink, in cores located at the western equatorial Atlantic (chapter 4). Although we applied the $\Delta\delta^{18}O_{dut\text{-}rub}$ in cores in a different location, $\Delta\delta^{18}O_{dut\text{-}rub}$ was already suggested as a proxy for surface-to-thermocline stratification in the western equatorial Atlantic (Steph et al., 2009). Our $\Delta\delta^{18}O_{dut\text{-}rub}$ results indicated large millennial and orbital-scale changes in the thermocline depth since the Last Interglacial (chapter 4). The observed changes were explained by two different modes (zonal and meridional) of thermocline variability in the South Atlantic, which were linked to changes in the trade wind system and surface circulation in the equatorial region. In addition to the $\Delta\delta^{18}O_{dut\text{-}rub}$, Fe/Ca records from the same cores were used to reconstruct past variations in continental runoff, which were associated with changes in rainfall over northeastern Brazil due to migrations of the ITCZ. By coupling these proxies ($\Delta\delta^{18}O_{dut\text{-}rub}$ and Fe/Ca), we compared the magnitude of the climatic responses of Heinrich and Dansgaard-Oeschger stadials and showed that, in general, Heinrich stadials display a stronger impact over the climate of our study site.

5.2. Outlook

Future developments regarding planktonic foraminifera biology may be achieved by using different sampling designs. For example, sediment trap studies using high-resolution sampling temporal integration (< 7-days), similar to our study (chapter 2) and others (Lin, 2014), may be more suitable for the detection of lunar synchronized reproduction. Furthermore, mooring lines with a double (or multiple) set of traps can provide a continuous record of the extent of vertical migration through the water column of planktonic foraminifera species during their life cycle. In addition, since it remains unresolved if the mechanism of reproduction is connected to an endogenous or exogenous trigger (Lončarić et al., 2005; Jonkers et al., 2015), future works should focus on this topic. A possible way to answer this question is to compile the available records with adequate temporal resolution and to make a global analysis of the reproductive behavior of each planktonic foraminifera species. However, such global approach would be highly dependent on existing sediment trap observations, which are still spatially sparse and with most of them lacking appropriate temporal resolution for resolving lunar cycles.

Another relevant assessment for studies focusing on planktonic foraminifera biology, as for paleoceanographic studies, is to evaluate the influence of hydrography changes in planktonic foraminifera abundances and calcification depths. Similar to our mooring setting (chapter 3), future sediment traps studies may improve the interpretation of their results by also recording environmental parameters (e.g. temperature, salinity, chlorophyll, oxygen concentration and others) in a continuous way, using sensors distributed through the mooring line. Recording other parameters besides temperature may also improve our own future observations in the southwestern Atlantic. The current setting of our mooring line also does not allow us to acquire data on deep-dwelling planktonic foraminifera species, thus changing the location of the mooring, as well as the depth of the traps, would provide new information on this group of species. Less ecological information is currently available for the deep-dwelling species, which is unfortunate since chemical composition of their calcite shells can give paleoceanographers relevant information about subsurface changes in the water column properties that can help to unravel oceanic teleconnections (e.g. Schmidt et al., 2012).

In this context of subsurface ocean conditions, our interspecific oxygen isotopic composition ($\Delta\delta^{18}O_{dut\text{-}rub}$) from cores located in the western equatorial Atlantic (chapter 4) is an example of the sort of information that can be derived from a multi-species approach. Our data revealed the presence of millennial and orbital-scale variations in

stratification in the western equatorial Atlantic, which was interpreted as the result of different modes of thermocline variability related to changes in the trade wind system. Further, our ideas (chapter 4) provided new insights that differ from previous interpretations (Rühlemann et al., 2001) for the region. Interestingly, in a recent study by Portilho-Ramos et al. (2017) the authors used planktonic foraminifera assemblages from cores in the western equatorial Atlantic and also reported a shoaling of the thermocline during Heinrich stadial 1, which supports our findings. However, the authors propose a different explanation for the observed pattern, focusing on changes in the hydrological cycle as the main forcing for changes in stratification. Although the observations of both studies are equivalent, the climatic processes highlighted are different, which is due to the lack of appropriate spatial coverage and temporal resolution to build a more complete scenario of climatic changes in the tropics for the late Quaternary. Another way to tackle this issue would be to use ocean-atmosphere model simulations that can deal with different depth levels in the ocean, in order to understand what could be the dominant factors modulating the ocean thermal gradient in this region.

5.3. References

Fraile, I., Schulz, M., Mulitza, S., Merkel, U., Prange, M., Paul, A., 2009. Modeling the seasonal distribution of planktonic foraminifera during the last glacial maximum. Paleoceanography 24, 1–15.

Jonkers, L., Reynolds, C.E., Richey, J., Hall, I.R., 2015. Lunar periodicity in the shell flux of planktonic foraminifera in the Gulf of Mexico. Biogeosciences 12, 3061–3070.

Lin, H.-L., 2014. The seasonal succession of modern planktonic foraminifera: Sediment traps observations from southwest Taiwan waters. Cont. Shelf Res. 84, 13–22.

Lončarić, N., Brummer, G.-J. a., Kroon, D., 2005. Lunar cycles and seasonal variations in deposition fluxes of planktic foraminiferal shell carbonate to the deep South Atlantic (central Walvis Ridge). Deep Sea Res. Part I Oceanogr. Res. Pap. 52, 1178–1188.

Portilho-Ramos, R.C., Chiessi, C.M., Zhang, Y., Mulitza, S., Kucera, M., Siccha, M., Prange, M., Paul, A., accepted. Coupling of equatorial Atlantic surface stratification to glacial shifts in the tropical rainbelt. Sci. Rep. 7, 1-8. doi:10.1038/s41598-017-01629-z

Rühlemann, C., Diekmann, B., Mulitza, S., Frank, M., 2001. Late Quaternary changes of western equatorial Atlantic surface circulation and Amazon lowland climate recorded in Ceara Rise deep-sea sediments. Paleoceanography 16, 293–305.

Schmidt, M.W., Chang, P., Hertzberg, J.E., Them II, T.R., Ji, L., Otto-Bliesner, B., 2012. Impact of abrupt deglacial climate change on tropical Atlantic subsurface temperatures. Pnas 109, 1–5.

Steph, S., Regenberg, M., Tiedemann, R., Mulitza, S., Nürnberg, D., 2009. Stable isotopes of planktonic foraminifera from tropical Atlantic/Caribbean core-tops: Implications for reconstructing upper ocean stratification. Mar. Micropaleontol. 71, 1–19.

Appendix 1. Holocene oscillations of Southwest Atlantic shelf circulation based on planktonic foraminifera from a upwelling system (off Cabo Frio, Southeastern Brazil)

Douglas VO Lessa[1], Igor M Venancio[1,2], Thiago P dos Santos[1], André L Belem[3], Bruno J Turcq[4], Abdelfetah Sifeddine[1,4] and Ana Luiza S Albuquerque[1]

[1]Programa de Pós-Graduação em Geoquímica Ambiental, Universidade Federal Fluminense, Brazil

[2]MARUM – Center for Marine Environmental Sciences and Faculty of Geosciences, University of Bremen, Germany

[3]Departamento de Engenharia Agrícola e Meio Ambiente, Universidade Federal Fluminense, Brazil

[4]LMI PALEOTRACES, Institut de Recherche pour le Développement, France

Published in *The Holocene*

Abstract

The Brazil Current (BC) is a relevant feature in the Atlantic Meridional Overturning Circulation (AMOC). Its behavior during slowdown or intense AMOC remains poorly known because of the lack of paleoceanographic records, especially for the Holocene. Here, we investigate changes in a western boundary upwelling system (Cabo Frio, off Southeastern Brazil) that are driven by variations in the BC and NE winds during the last 9 kyr. To assess the variability of the BC, we used δ18O, Mg/Ca and assemblages of planktonic foraminifera. Our results indicate five oceanographic phases during the last 9 kyr. During Phase I (from 9.0 to 7.0 cal kyr BP), the BC diverged offshore from the modern upwelling area because of the low sea level, increasing the influence of shelf waters and coastal upwelling plumes on foraminifera assemblages. Phase II (7.0 to5.0 kyr BP) was marked by the approach of the internal front in the BC with low intensity and episodes of strong productivity that were linked primarily to the upwelling of the South Atlantic Central Water (SACW) and/or subpolar shelf waters (cold). Phase III (5.0 to 3.5 kyr BP) was a transition, marking a large oceanographic and climatic change from the weakening of the AMOC. The internal front of the BC became warm and subsurface SACW upwelling was stronger. In Phase IV

(3.5 to 2.5 kyr BP), the BC acquired its modern dynamics, but weak NE winds weakened the SACW's contribution to upwelling events. Finally, in Phase V (last 2.5 kyr BP), the NE winds reintensified, promoting frequent episodes of upwelling and intrusion by subpolar shelf waters during the Medieval Climate Anomaly.

Appendix 2. Prolonged warming of the Brazil Current precedes deglaciations

Thiago P. Santos[1], Douglas O. Lessa[1], Igor M. Venancio[2], Cristiano M. Chiessi[3], Stefan Mulitza[2], Henning Kuhnert[2], Aline Govin[4], Thiago Machado[1], Karen B. Costa[5], Felipe Toledo[5], Bruna B. Dias[1], Ana Luiza S. Albuquerque[1]

[1]Departamento de Geoquímica, Universidade Federal Fluminense, Niterói, Brazil.

[2]MARUM-Center for Marine Environmental Sciences, University of Bremen, Bremen, Germany.

[3]Escola de Artes, Ciências e Humanidades, Universidade de São Paulo, São Paulo, Brazil.

[4]Institut Pierre-Simon Laplace/Laboratoire des Sciences du Climat et de l'Environnement, (CEA-CNRS-UVSQ), Université Paris Saclay, Gif-sur-Yvette, France.

[5]Laboratório de Paleoceanografia do Atlântico Sul, Instituto Oceanográfico, Universidade de São Paulo, Brazil.

Published in *Earth and Planetary Science Letters*

Abstract

Paleoceanographic reconstructions from the Brazil Current are scarce and lack the required temporal resolution to appropriately represent its variability during key periods of the last glacial-interglacial cycles. Here, we present the first high-temporal resolution multiproxy reconstruction of the Brazil Current at 24 ºS covering the last 185 ka. During the last and penultimate glacial periods, our Mg/Ca-derived sea surface temperature (SST) record shows a strong cooling at ca. 47 and ca. 156 ka, respectively, that is followed by a warming trend from late-Marine Isotope Stage (MIS) 3 to MIS 1 and from late-MIS 6 to MIS5e, respectively. Importantly, the Brazil Current warmed uninterruptedly towards Termination I (II) after the low SST at ca. 47 and ca. 156 ka, with no SST minima during the Last Glacial Maximum or penultimate glacial maximum. The reason for the strong cooling and the warming trend during late-MIS 3 and late-MIS 6 could reside in the favorable obliquity configuration. However, this mechanism is not sufficient to sustain the warming observed for the rest of the last and penultimate glacial periods. We propose that

the change in the Atlantic meridional overturning circulation (AMOC), as described in the literature, from a "warm" to a "cold mode" for MIS 2 and MIS 6 is responsible for the accumulation of warm waters in the subtropical western South Atlantic, preventing SST minima during the last and penultimate glacial maxima in the region. Change in benthic $\delta^{13}C$ corroborates that a fundamental modification in the AMOC mode might have triggered the heat accumulation. Our data also show a sudden increase in SST and surface salinity during the last glacial descent (MIS 4), indicating that the western portion of the subtropical gyres may have acted as a heat and salt reservoir, while higher latitude climates transited to a glacial background. Our findings imply that the AMOC “cold mode” induces heat storage in the subtropical western South Atlantic and, because of that, the last two regional SST minima occurred out-of-phase with the glacial maxima of higher latitudes.